

# TRUSS STRUT TRADE STUDY

**Borell, G.J.**  
**Daubendiek, A. W.**  
**Updike, C. A.**  
**Dupper, J.K.**  
**Gierow, P.**

**Harris Corporation**  
**Government Aerospace Systems Division**  
**Melbourne, Florida 32902**

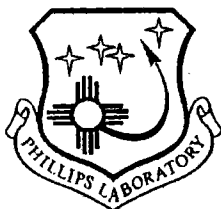
**May 1993**

## Final Report

Distribution authorized to U.S. Government agencies and their contractors; Critical Technology May 1993. Other requests for this document must be referred to OL-AC PL/TSTR, Edwards AFB, CA 93524-7015.

**WARNING** - This document contains technical data whose export is restricted by the Arms Export Control Act (Title 22, U.S.C., Sec 2751 et seq.) or the Export Administration Act of 1979, as amended (Title 50, U.S.C., App. 2401, et seq.) Violations of these export laws are subject to severe criminal penalties. Disseminate in accordance with the provisions of AFR 80-34.

**DESTRUCTION NOTICE** - Destroy by any method that will prevent disclosure of contents or reconstruction of the document.



**PHILLIPS LABORATORY**  
**Propulsion Directorate**  
**AIR FORCE MATERIEL COMMAND**  
**EDWARDS AIR FORCE BASE CA 93524-7001**

## **GOVERNMENT PURPOSE LICENSE RIGHTS (SBIR PROGRAM)**

**CONTRACT NO: F29601-91-C-0009**

For a period of four (4) years after delivery and acceptance of the last deliverable item under the above contract, this technical data shall be subject to the restrictions contained in the definitions of the "Limited Rights" in DFARS clause at 252.227-7013. After the two-year period, the data shall be subject to the restrictions contained in the definition of "Government Purpose License Rights" in DFARS clause at 252.227-7013. The Government assumes no liability for the unauthorized use or disclosure by others. This legend, together with the indications of the portions of the data which are subject to such limitations, shall be included on any reproductions hereof which contains any portions subject to such limitations and shall be honored only as long as the data continues to meet the definition on Government purpose license rights.

### **NOTICE TO ACCOMPANY THE DISSEMINATION OF EXPORT-CONTROLLED TECHNICAL DATA**

1. Export of information contained herein, which includes, in some circumstances, release to foreign nationals within the United States, without first obtaining approval or license from the Department of State for items controlled by the International Traffic in Arms Regulations (ITAR), or the Department of Commerce for items controlled by the Export Administration Regulations (EAR), may constitute a violation of law.
2. Under 22 U.S.C.2778 the penalty for unlawful export of items or information controlled under the ITAR is up to 2 years imprisonment, or a fine of \$100,000, or both. Under 50 U.S.C., Appendix 2410, the penalty for unlawful export of items or information controlled under the EAR is a fine of up to \$1,000,000, or five times the value of the exports, whichever is greater; or for an individual, imprisonment of up to 10 years, or a fine of up to \$250,000, or both.
3. In accordance with your certification that establishes you as a "qualified U.S. contractor," unauthorized dissemination of this information is prohibited and may result in disqualification as a qualified U.S. contractor, and may be considered in determining your eligibility for future contracts with the Department of Defense.
4. The U.S. Government assumes no liability for direct patent infringement, or contributory patent infringement or misuse of technical data.
5. The U.S. Government does not warrant the adequacy, accuracy, currency, of completeness of the technical data.
6. The U.S. Government assumes no liability for loss, damage, or injury resulting from manufacture or use for any purpose of any product, article, system, or material involving reliance upon any or all technical data furnished in response to the request for technical data.
7. If the technical data furnished by the Government will be used for commercial manufacturing of other profit potential, a license for such use may be necessary. Any payments made in support of the request for data do not include or involve any license rights.
8. A copy of this notice shall be provided with any partial or complete reproduction of these data that are provided to qualified U.S. contractors.

## GOVERNMENT PURPOSE LICENSE RIGHTS (SBIR PROGRAM)

CONTRACT NO: F29601-91-C-0009

For a period of four (4) years after delivery and acceptance of the last deliverable item under the above contract, this technical data shall be subject to the restrictions contained in the definitions of the "Limited Rights" in DFARS clause at 252.227-7013. After the four-year period, the data shall be subject to the restrictions contained in the definition of "Government Purpose License Rights" in DFARS clause at 252.227-7013. The Government assumes no liability for the unauthorized use or disclosure by others. This legend, together with the indications of the portions of the data which are subject to such limitations, shall be included on any reproductions hereof which contains any portions subject to such limitations and shall be honored only as long as the data continues to meet the definition on Government purpose license rights.

### FOREWORD

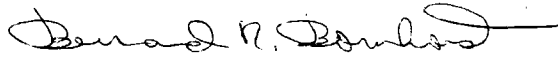
This final report was submitted by Harris Corporation, Government Aerospace Systems Division, Melbourne Florida, under SBIR Contract F29601-91-C-0009 with the OLAC, Phillips Laboratory, Edwards AFB CA 93524-7001. SBIR funding provided by the Small Business Innovative Research Program. OLAC PL Project Manager was Kristi Laug

This report has been reviewed and is approved for release and distribution in accordance with the distribution statement on the cover and on the SF Form 298.



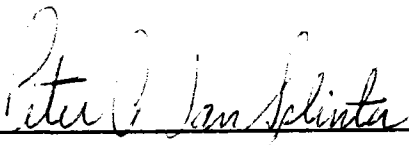
---

KRISTI K. LAUG  
Project Manager



---

BERNARD R. BORNHORST  
Chief, Space Propulsion Branch



---

PETER A. VAN SPLINTER  
Director,  
Applications Engineering Division

# REPORT DOCUMENTATION PAGE

Form Approved  
OMB No 0704-0188

Public reporting burden for this collection of information is estimated to average 1 hour per response, including the time for reviewing instructions searching existing data sources gathering and maintaining the data needed, and completing and reviewing the collection of information. Send comments regarding this burden estimate or any other aspect of this collection of information, including suggestions for reducing this burden to Washington Headquarters Services, Directorate for Information Operations and Reports, 1215 Jefferson Davis Highway, Suite 1204, Arlington, VA 22202-4302, and to the Office of Management and Budget, Paperwork Reduction Project (0740-0188), Washington DC 20503.

|   |  |   |   |  |
|---|--|---|---|--|
| 1. AGENCY USE ONLY (LEAVE BLANK)  |  | 2. REPORT DATE<br>May 1993                              | 3. REPORT TYPE AND DTAES COVERED<br>Final Nov 1991 - Jan 1993                   |  |
| 4. TITLE AND SUBTITLE<br>Truss Strut Trade Study  |  |   | 5. FUNDING NUMBERS<br>C: F29601-91-C-0009<br>PE: 62302F<br>PR: 3058<br>TA: 00DJ |  |
| 6. AUTHOR(S)<br>G. J. Borell; C.A. Updike; P. Gierow<br>A. W. Daubendiek; J. K. Dupper  |  |   | 8. PERFORMING ORGANIZATION REPORT NUMBER<br>1710-024                            |  |
| 7. PERFORMING ORGANIZATION NAME(S) AND ADDRESS(ES)<br>Harris Corporation<br>Government Aerospace Systems Division<br>Melbourne, Florida 32902   |  |   | 10. SPONSORING/MONITORING AGENCY REPORT NUMBER<br>PL-TR-93-3008                 |  |
| 9. SPONSORING/MONITORING AGENCY NAME(S) AND ADDRESS(ES)<br>Phillips Laboratory<br>OLAC-PL/RKAS<br>Edwards AFB California 93524-7690   |  |   | 11. SUPPLEMENTARY NOTES<br>COSATI CODE(S): 22/02                                |  |
| 12a. DISTRIBUTION/AVAILABILITY STATEMENT<br>Distribution authorized to U. S. Government Agencies and their contractors; Critical Technology; May 1993. All other requests for this document shall be referred to OLAC-PL/TSTR, Edwards AFB, CA 93524-7015   |  |   | 12b. DISTRIBUTION CODE  |  |
| 13. ABSTRACT (MAXIMUM 200 WORDS)<br>A deployable support structure for thin film solar concentrators has been designed. The support structure design takes advantage of lightweight composite structures and reliable mechanical deployment schemes to support a large film inflatable concentrator (7m x 9m ellipse). Large concentrators are an important component of Solar Thermal Propulsion systems proposed for future space missions. This report describes the support structure, the driving requirements and constraints, packaging and deployment schemes, and the analysis of the interrelated optical, static, and dynamic system behavior. The reflector of the concentrator is an off-axis paraboloid whose rim is a 7m x 9m ellipse. The principal components of the support structure are three deployable telescoping struts and a 9.2 m circular hoop, all fabricated from graphite-epoxy composites. Graphite cords and tapes are used to tension the tubes to provide structural stiffness beyond that required to maintain the shape of the inflatable concentrator. This design generally has slightly higher weight and slightly larger stowed volume than competing inflatable support structure design. However, this design has two significant advantages over competing inflatable support structure designs. First, the mechanical design has a significant maturity advantage in materials and fabrication complexity. Second, the mechanical design has a large advantage in ground testability. |  |   |   |  |
| 14. SUBJECT TERMS<br>Concentrators; Truss; Solar Thermal Propulsion; Solar Rocket Deployable Truss  |  |   | 15. NUMBER OF PAGES   |  |
|   |  |   | 16. PRICE CODE  |  |
| 17. SECURITY CLASSIFICATION OF REPORT<br>Unclassified   | 18. SECURITY CLASSIFICATION OF THIS PAGE<br>Unclassified | 19. SECURITY CLASSIFICATION OF ABSTRACT<br>Unclassified | 20. LIMITATION OF ABSTRACT<br>SAR   |  |

## Table of Contents

|       |                                  |     |
|-------|----------------------------------|-----|
| 1.0   | Introduction                     | 1   |
| 1.1   | Background                       | 1   |
| 1.2   | Summary                          | 3   |
| 2.0   | Support Structure Requirements   | 7   |
| 2.1   | Weight                           | 7   |
| 2.2   | Performance                      | 8   |
| 2.3   | Stowed Package                   | 9   |
| 2.4   | Testability                      | 9   |
| 2.5   | Environments                     | 11  |
| 2.6   | Scalability                      | 12  |
| 3.0   | Support Structure Designs        | 13  |
| 3.1   | Conventional Concentrator/Canopy | 13  |
| 3.1.1 | Torus Design                     | 16  |
| 3.1.2 | Strut Design                     | 28  |
| 3.1.3 | Strut Deployment System Design   | 38  |
| 3.1.4 | Strut End Fittings               | 45  |
| 3.1.5 | Torus to Concentrator Attachment | 46  |
| 3.1.6 | Stowed Package                   | 50  |
| 3.1.7 | System Deployment                | 54  |
| 3.1.8 | Weight Summary                   | 64  |
| 3.1.9 | System Performance               | 67  |
| 3.2   | Single Chamber Concentrator      | 99  |
| 4.0   | Conclusions                      | 124 |
|       | References                       | 126 |

## List of Figures

| Figure |   | Page |
|--------|---|------|
| 1      | Two 30 x 40 meter offset concentrators gather energy to power the solar rocket 2  |      |
| 2      | The solar rocket flight experiment utilizes a single 7 x 9 meter concentrator to verify deployment and initial operating characteristics                                  | 2    |
| 3      | A deployable solid segment hoop and telescoping struts enable a compact stowed package and a reliable deployment (thin film concentrator and canopy not shown for clarity | 5    |
| 4      | The Single Chamber Concentrator offers an alternative to the conventional concentrator and support structure design   | 6    |
| 5      | The Get Away Special canister also provides a challenging stowed volume goal for the flight experiment  | 10   |
| 6      | Conventional Inflatable Concentrator/Canopy   | 14   |
| 7      | The Single Chamber Inflatable Concentrator  | 15   |
| 8      | The 15 meter diameter hoop-column antenna was developed with NASA-Langley on the LSST Program   | 17   |
| 9      | The hoop designs deploy from fully vertical to fully horizontal yielding a segmented circular hoop  | 18   |
| 10     | The circular hoop supports an elliptical concentrator   | 19   |
| 11     | In the cable-pulley design, a cable is continuously wrapped through a series of pulleys at the ends of each hoop segment. As the cable is retracted, the hoop deploys.    | 21   |
| 12     | A view of the partially deployed and fully deployed cable-pulley hoop design  | 22   |

## List of Figures

|    |   |    |
|----|---|----|
| 13 | The Sliding Linkage Design uses a motor to turn a ballscrew which deploys the hoop  | 24 |
| 14 | The LSST hoop in the stowed configuration   | 24 |
| 15 | The LSST hoop partially deployed  | 26 |
| 16 | The fully deployed LSST hoop measures 15 meters in diameter   | 27 |
| 17 | A hinge redesign, pictured in the stowed configuration, reduces the LSST hoop hinge weight by 50%   | 27 |
| 18 | The split ring latch is the basic design concept for the strut latch  | 31 |
| 19 | The two piece retractable radial latch adds radial guidance to the split ring design  | 34 |
| 20 | The two piece retractable radial latch requires 0.125 inch separation between adjacent tube faces   | 34 |
| 21 | The circumferential latch design has improved performance in bending but requires internal guides along the tube walls to assure deployment   | 36 |
| 22 | The bladder concept uses pressurized gas to inflate a bladder which drives the strut tubes to deploy  | 40 |
| 23 | The Sealed Tubes concept uses pressurized gas to force the strut tubes to deploy and relies on a seal to maintain the pressure differential   | 41 |
| 24 | A ballscrew transports a tube which drives the individual strut tube segments to deployment in a synchronized fashion in the push-pull design | 42 |
| 25 | A rotating spool takes up a cable which pulls the tube segments to deployment in the cable-pulley concept                                     | 43 |

## List of Figures

|    |  |    |
|----|--|----|
| 26 | A motor turns gears which engage lengthwise tracks on each tube segment and deploys the segments sequentially                                  | 44 |
| 27 | A spherical ball joint at each end of the three struts allows the struts to rotate about three axes, a requirement for system deployment       | 46 |
| 28 | Individual stringers could be used to transfer loads from the hoop to the concentrator   | 48 |
| 29 | A mesh material could be used to evenly distribute load to the concentrator  | 48 |
| 30 | A hybrid design capitalizes on the strong points of the mesh attachment method (even loads) and the stringer attachment method (adjustability) | 49 |
| 31 | The entire concentrator and support structure stows within the stowed hoop   | 51 |
| 32 | The system designer is able to choose stowed length and stowed diameter by simply adjusting the number of hoop segments                        | 51 |
| 33 | Stowed volume of the hoop increases as the number of segments increases  | 52 |
| 34 | Hoop weight increases as the number of hoop segments increases   | 52 |
| 35 | Stowed dimensions of the full scale system are also a function of the number of hoop segments  | 53 |
| 36 | The support structure and concentrator begin the deployment from the stowed position   | 55 |
| 37 | The first deployment motion is the deploying of the three struts which moves the hoop and concentrator away from the spacecraft                | 56 |
| 38 | Activation of the deployment motors begins the articulation of the hoop. In this view the hinges of the hoop have deployed 30°.                | 57 |

## List of Figures

|    |  |    |
|----|--|----|
| 39 | As the hoop deploys the long struts extend also, further deploying the structure.  | 58 |
| 40 | The hoop is fully deployed when the hinges lock out. Motors are automatically shut off upon lockout.                     | 59 |
| 41 | Deployment of the long struts to their full length sets the concentrator in the offset position.                         | 60 |
| 42 | Fully deployed torus attached to a 16 foot membrane.   | 62 |
| 43 | Membrane and torus after three folding pattern. Diameter is approximately 9 feet.  | 62 |
| 44 | Top view of the membrane and torus after three folding steps.  | 63 |
| 45 | Membrane and torus at 4-6 foot diameter. Notice the film is between some of the torus segments.                          | 63 |
| 46 | Membrane and torus fully packaged for deployment.  | 64 |
| 47 | A finite element model of the support structure is the primary evaluation tool.  | 68 |
| 48 | The reaction forces at the rim nodes agree well with continuous media predictions by Grossman <sup>8</sup> (solid line). | 70 |
| 49 | A deformation of an elliptical torus FEM similar to "potato chipping".   | 72 |
| 50 | Case 1: 0.03g acceleration applied in the +x direction.  | 73 |
| 51 | Case 2: 0.03g acceleration applied in the -x direction.  | 74 |
| 52 | Case 3: 0.03g acceleration applied in the +y direction.  | 75 |

## List of Figures

|    |  |    |
|----|--|----|
| 53 | Case 4: 0.03g acceleration applied in the -y direction.  | 76 |
| 54 | Case 5: 0.03g acceleration applied in the +z direction.  | 78 |
| 55 | The 1g static load case causes a maximum deflection of 1.6 at node 135, a point on the hoop opposite the short strut attachment point. | 81 |
| 56 | A 2.5 inch aperture radius enables a 95% intercept factor in a 1g distorted case.  | 82 |
| 57 | A flux peak of 13100 suns is developed at the aperture by an undistorted concentrator.   | 82 |
| 58 | The 1g static load causes the center of the concentrated energy to shift 1.12 inches on the aperture plane.                            | 83 |
| 59 | Fixed base mode 7 is a localized stringer motion at 3.74 Hertz.  | 88 |
| 60 | Free-free mode 7 is a defocus/drum motion at 1.55 Hertz.   | 88 |
| 61 | Free-free mode 8 is a hoop twist motion at 1.62 Hertz.   | 89 |
| 62 | Free-free mode 13 involves many substructures at 3.65 Hertz.   | 89 |
| 63 | Free-free mode 16 is a hoop bending/mispointing motion at 4.99 Hertz.  | 90 |
| 64 | Fixed-base mode 1 (torsion, 0.84 Hertz) viewed from a point perpendicular to y-z plane.  | 90 |
| 65 | Fixed-base mode 2 (1.1 Hertz) causes mispointing about the z axis.   | 91 |
| 66 | Fixed-base mode 3 (1.2 Hertz) is hoop twist with mispointing.  | 91 |

## List of Figures

|    |  |     |
|----|--|-----|
| 67 | Fixed-base mode 4 (1.57 Hertz) is defocus/<br>drum shape.  | 92  |
| 68 | Fixed-base mode 5 (2.73 Hertz) is hoop twist<br>with strut motion.   | 92  |
| 69 | Fixed-base mode 6 (3.29 Hertz) is defocus, drum<br>and hoop bending.   | 93  |
| 70 | Fixed-base mode 9 (4.96 Hertz) corresponds<br>directly to free-free mode 16 at same frequency.   | 93  |
| 71 | The theta-z (solid line) and theta-x (dashed<br>line) components of line-of-sight error due to<br>a 1 pound thrust are less than 1.5 millidegrees.                   | 98  |
| 72 | The trajectory of the focal point of the system<br>due to a 1 pound thrust. This trajectory<br>translates into focal point movement of<br>approximately 0.01 inches. | 98  |
| 73 | The Single Chamber Concentrator design provides<br>a radical alternative to the conventional<br>concentrator and torus design.                                       | 100 |
| 74 | The preferred attachment concept uses a composite<br>cone and a ball and socket to connect the strut<br>to the concentrator.   | 102 |
| 75 | An alternative attachment concept utilizes<br>composite elements and a universal joint to<br>connect the strut to the concentrator.                                  | 102 |
| 76 | The undeformed SCC finite element model as<br>viewed along the x axis.   | 107 |
| 77 | The undeformed SCC finite element model as<br>viewed along the y axis.   | 108 |
| 78 | The undeformed SCC finite element model as<br>viewed along the z axis.   | 109 |
| 79 | Mode shape 1 identified by the SCC finite<br>element model.  | 111 |

## List of Figures

|    |   |     |
|----|---|-----|
| 80 | Mode shape 2 identified by the SCC finite element model.  | 112 |
| 81 | Mode shape 3 identified by the SCC finite element model.  | 113 |
| 82 | Mode shape 4 identified by the SCC finite element model.  | 114 |
| 83 | Mode shape 5 identified by the SCC finite element model.  | 115 |
| 84 | Mode shape 6 identified by the SCC finite element model.  | 116 |
| 85 | Mode shape 7 identified by the SCC finite element model.  | 117 |
| 86 | Mode shape 8 identified by the SCC finite element model.  | 118 |
| 87 | Mode shape 9 identified by the SCC finite element model.  | 119 |
| 88 | Mode shape 10 identified by the SCC finite element model. | 120 |

## List of Tables

| Table |   | Page |
|-------|---|------|
| 1     | An aggressive weight goal is established for the flight experiment support structure to enable a launch in a Get Away Special container | 7    |
| 2     | Summary of Typical Results  | 12   |
| 3     | Attributes of the Barrel Concept  | 20   |
| 4     | Attributes of the Cable/Pulley Concept  | 20   |
| 5     | Attributes of the Sliding Linkage   | 23   |
| 6     | Attributes of the LSST Hoop Concept   | 25   |
| 7     | Preliminary strut tube layup and material properties  | 29   |
| 8     | Latch Design Requirements and Goals   | 31   |
| 9     | Latch concept trade matrix  | 37   |
| 10    | A trade matrix identifies the Push-Pull design as the most advantageous to the Solar Thermal Propulsion system                          | 45   |
| 11    | Qualitative requirements for the attachment between the hoop and concentrator   | 47   |
| 12    | Flight Experiment Concentrator/Support Structure Weight Budget  | 65   |
| 13    | Full Scale Concentrator/Support Structure Weight Budget   | 66   |
| 14    | The node numbering scheme for the principal nodes of the support structure finite element model   | 69   |
| 15    | Static load summary with translational degrees of freedom restrained at strut/SC interface nodes (316, 348, 380)                        | 77   |

## List of Tables

|    |   |     |
|----|---|-----|
| 16 | The first 20 nodes of the "free-free" configuration are listed below. The first mode of significance is at frequency of 1.55 Hz well above the 0.4 Hz requirement | 84  |
| 17 | The first 20 nodes of the "fixed-base" case are greater than the 0.4 Hz requirement   | 85  |
| 18 | The modes excited by the thruster are also above the 0.4 Hz requirement   | 86  |
| 19 | A mode shape summary for the ground test and orbital configurations   | 94  |
| 20 | The flight experiment sized single chamber concentrator weighs approximately 40% of the conventional weight   | 105 |
| 21 | Film properties for the polyimide film of the single chamber concentrator   | 106 |
| 22 | Single Chamber Concentrator modelling assumptions and their effects on results  | 106 |
| 23 | Single Chamber Concentrator (SCC) Pressurized Eigenvalues   | 121 |
| 24 | The sensitivity of the eigenvalues to strut weight is demonstrated in this table  | 122 |
| 25 | The sensitivity of the eigenvalues to the strut stiffness is demonstrated in this table   | 122 |
| 26 | The effect of inflation pressure on the SCC pressurized eigenvalues is shown to be small in this table  | 123 |

## **1.0 Introduction**

This report is a summary of the work conducted by Harris Corporation of Melbourne, Florida and SRS Technologies of Huntsville, Alabama under contract F29601-91-C-0009 with the Phillips Lab (AFMC) for the period from November 1991 through January 1993. George Borell served as the Harris program manager. Kristi Laug of the Phillips Lab served as the Air Force program manager.

### **1.1 Background**

The Air Force is developing a Solar Thermal Propulsion system as a potential alternative to chemical rockets which transport satellites from low earth orbit (LEO) to geosynchronous orbit (GEO). The Solar Thermal Propulsion system offers increased specific impulse (on the order of 1000 seconds) at low thrust levels. The system also offers an improvement to conventional engines in that only one propellant gas is needed. The propellant gas, hydrogen, is not burned with an oxidizer but expanded using solar energy. The main disadvantage of Solar Thermal Propulsion systems is slightly longer flight times from LEO to GEO. Current projections indicate orbit transfer periods on the order of 10 days, as compared to a few hours for chemical systems. The success of the system is dependent upon an effective concentrator and support structure.

The solar concentrators of the Solar Thermal Propulsion system, shown in Figure 1, concentrate energy at the aperture of a propulsion engine. At the time of this contract award, two symmetric, offset, elliptic concentrators, each 30 meters (minor axis) by 40 meters (major axis) were required. The concentrators and engine are connected via a support structure. The support structure torus provides a rigid interface to react the loads of the concentrator while the support structure truss connects the concentrator to the propulsion engine.

The Air Force is considering a flight experiment to prove the operation of the concentrator system. The flight experiment, shown in Figure 2, would include a single 7 meter x 9 meter concentrator, a support structure, and an instrumentation package. The objectives of this flight experiment may include: a verification of deployment of the concentrator, simple dynamics experiments, pointing experiments, and concentrated flux measurements.

The purpose of this study was to design a support structure to meet the requirements of the flight experiment. This support structure is also required to be compatible with the full scale Solar Thermal Propulsion system.

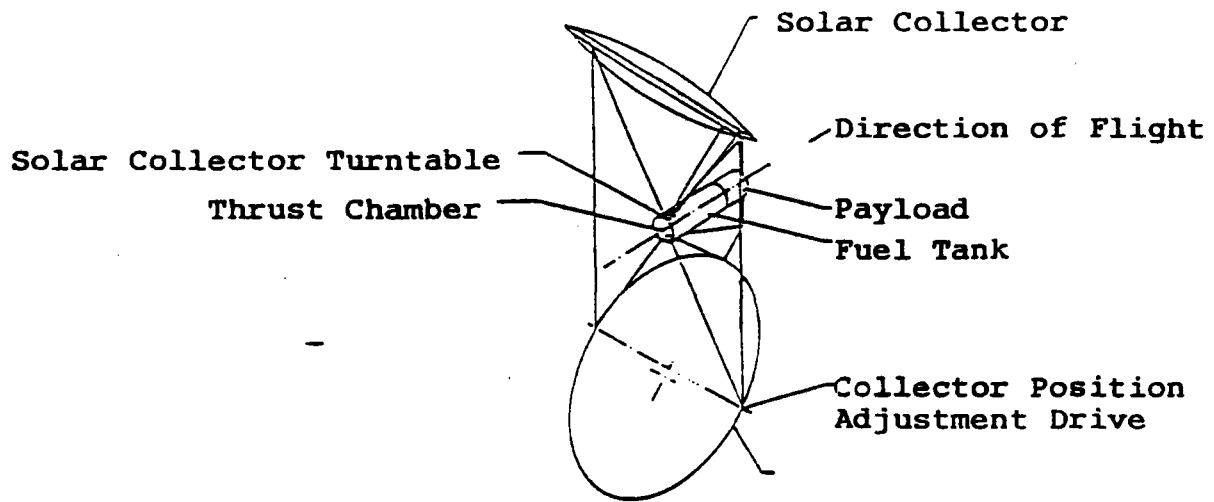


**Figure 1**  
 Two 30 x 40 meter offset concentrators gather energy to power the solar rocket

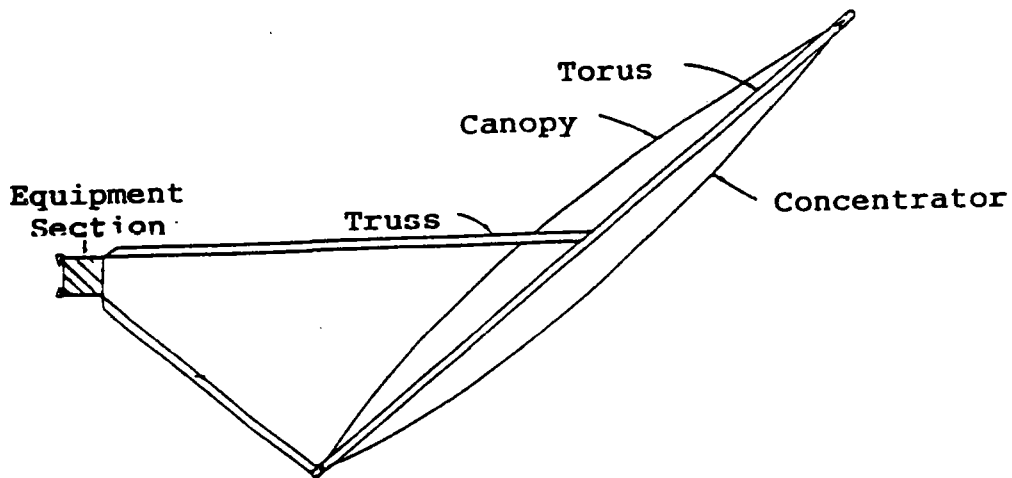


**Figure 2**  
 The solar rocket flight experiment utilizes a single 7 x 9 meter concentrator to verify deployment and initial operating characteristics

## 1.2 Summary

The Harris/SRS team has developed two potential solutions to the support structure design.

The first solution, shown in Figure 3, consists of a deployable solid segment hoop which reacts the concentrator loads, and a truss, formed by three telescoping struts and nine tension cords. The truss connects the concentrator to the engine.

The hoop is based on Harris' deployable hoop developed in the mid-1980's for NASA. The hoop consists of 44 segments of 2.5 inch diameter graphite-epoxy tubes with a hinge at each segment interface. The hoop is deployed using synchronized motors connected to each hinge. A working breadboard of this hoop (15 meter diameter) was fabricated for NASA-Langley.

The three struts of the truss deploy via a telescoping motion driven by a motor and ballscrew. Each of the struts consists of graphite epoxy tubes (3 inch outer diameter minimum, 0.015 inch wall thickness) with individual latches at each tube end. As the strut deploys, the tubes latch together to stiffen the structure. The tension cords connect the ends of the struts together and add stiffness to the truss. The cords are 0.010 inch diameter graphite bundles for high strength and high stability over wide temperature ranges.

The hoop and truss solution implements mechanical deployment systems to create a mature design which results in a reliable, lightweight, compact support structure. Mechanical systems of this type have been designed, fabricated and flown in space for many years. Technology exists today to implement a system of this type. Total weight of a 7 meter by 9 meter concentrator and support structure is 123.8 pounds. The system packages into a cylinder 28 inches diameter and 28 inches in height.

The second solution, shown in Figure 4, utilizes a novel Single Chamber Concentrator design, developed by SRS Technologies. The Single Chamber concentrator is a statically stable inflatable concentrator and canopy. The stability of the concentrator eliminates the need for a membrane-supporting torus, thereby reducing weight and stowed volume significantly. A simple three legged truss was designed to attach the concentrator to the engine. The truss is a similar design, although different in size, to the truss described above. This Single Chamber system, when

sized for a 7 meter by 9 meter concentrator, weighs 50.1 pounds and stows easily into a NASA Get Away Special container for small payloads. Although this design is not as mature as the mechanical structure design, it warrants close observation as concentrator technology matures due to it's tremendous advantages.

Both of the support structure designs generated under this contract are capable of near term use in a flight system. Future work in this technology should focus on system performance analysis and fabrication of breadboard models.

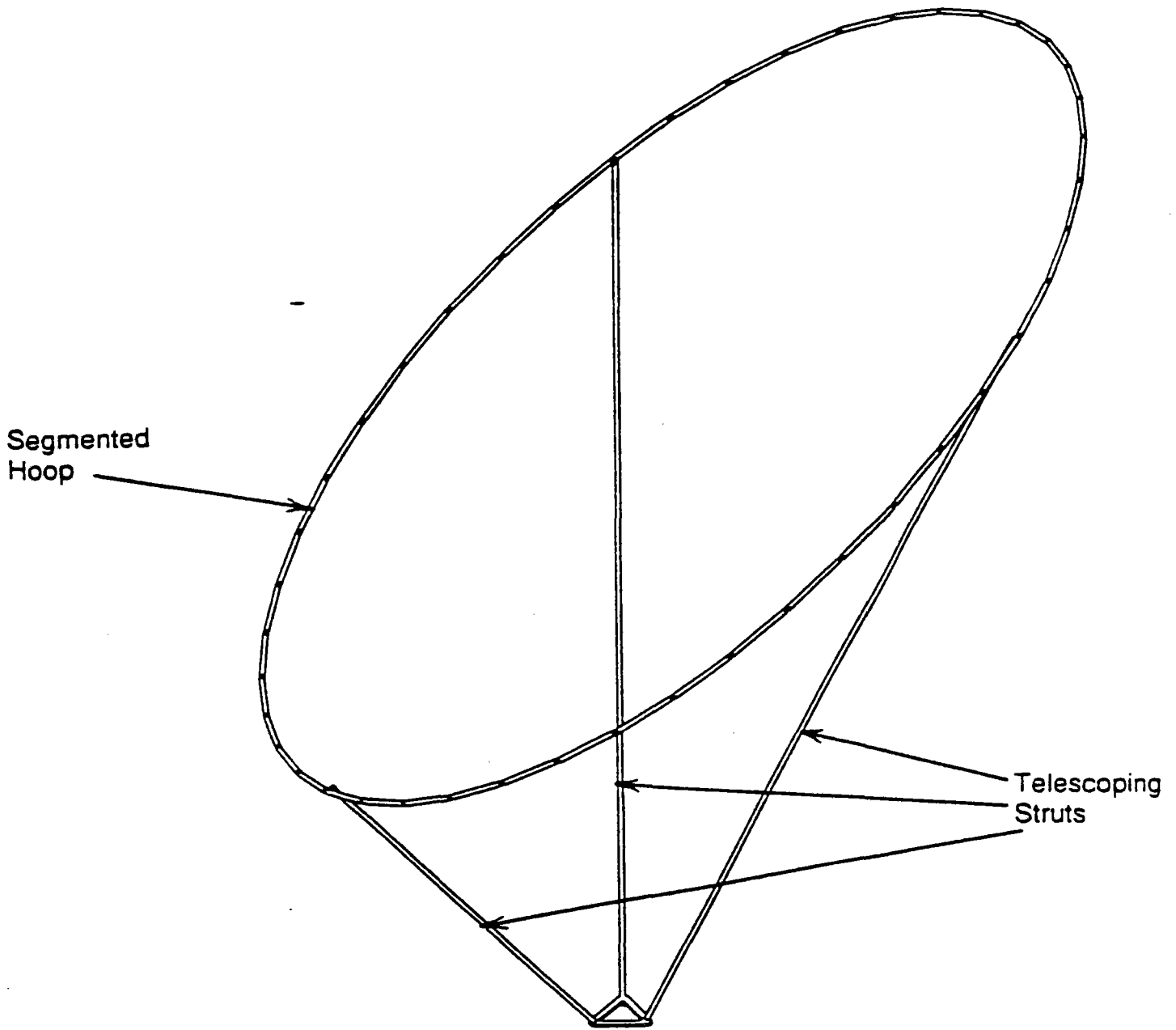


**Figure 3**  
A deployable solid segment hoop and telescoping struts enable a compact stowed package and a reliable deployment (thin film concentrator and canopy not shown for clarity)

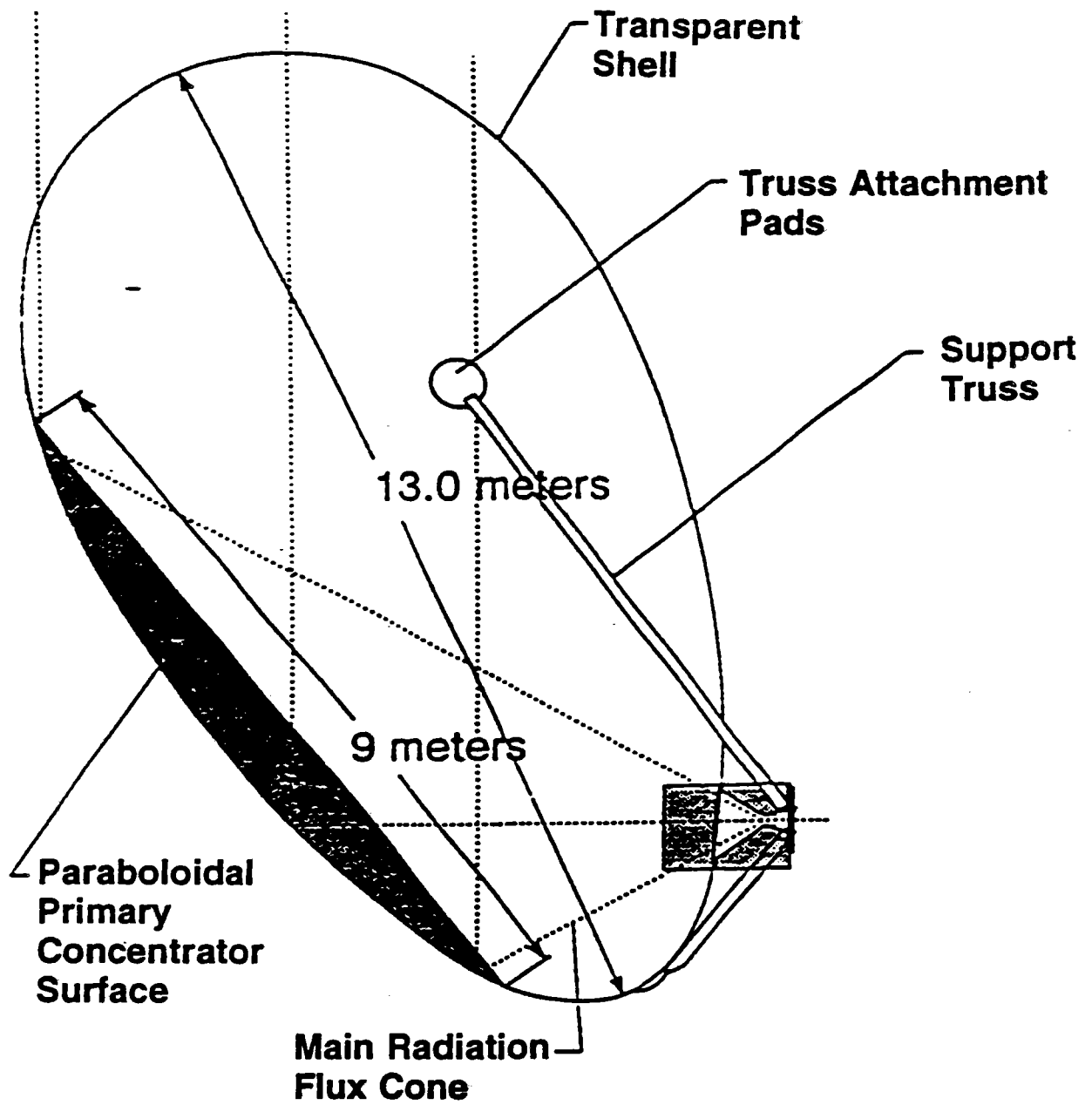


**Figure 4**  
**The Single Chamber Concentrator offers an alternative to the conventional concentrator and support structure design**

## 2.0 Support Structure Requirements

The support structure requirements for the flight experiment and the full scale concentrator systems are described below.

The flight experiment has the goal of flying on NASA's Get Away Special (GAS) program. This establishes a goal for the flight experiment designs in terms of the weight and stowed package of the design. Additionally, performance requirements exist for the optical accuracy tests and the dynamics tests from the flight experiments. Other requirements include testability, environmental stability, and scalability.

### 2.1 Weight

Since the flight experiment intends to utilize the GAS program to minimize cost, the weight goal for the support structure is defined by limits for the GAS canister. The maximum experiment weight to be packaged within the GAS can is 200 pounds, 50 pounds of which will be required for the motorized ejector door<sup>1</sup>. This leaves a total of 150 pounds for the complete flight experiment. The weight of the test support equipment is 64.5 pounds as defined in Reference 2. Therefore, a total of 85.5 pounds (see Table 1) can be allocated to the support structure and concentrator.

**Table 1. An aggressive weight goal is established for the flight experiment support structure to enable a launch in a Get Away Special container**

| ITEM   | WEIGHT<br>( pounds) | SOURCE                        |
|--|---------------------|-------------------------------|
| GAS CAN LIMIT  | + 200               | GAS EXPERIMENTERS<br>HANDBOOK |
| MOTORIZED DOOR<br>EJECTOR  | - 50                | GAS EXPERIMENTERS<br>HANDBOOK |
| SATELLITE MASS<br>(excluding<br>concentrator and<br>support structure) | - 64.47             | AL-TR-90-066                  |
| MASS LEFT FOR<br>CONCENTRATOR AND<br>SUPPORT STRUCTURE                 | 85.53               |                               |

As the complexity of the flight experiment increases from that established in Reference 2, the weight of the test support equipment will likely increase. This evolution places increasingly stringent weight requirements on the support structure and concentrator. Therefore, the likelihood of packaging an advanced flight experiment in a GAS decreases.

There are other low cost methods of obtaining launch services. Both the expendable launch vehicles and the Space Shuttle offer launch services for small payloads. These services are generally used to fill excess capacity and are generally the second or third priority of the mission. Often, these services are more flexible with weight and stowed volume constraints than the GAS program.

The weight of a full scale system is an important parameter. The objective is to minimize the weight of the solar thermal propulsion system, including the concentrator and support structure, in order to maximize the mass of the payload to be transported. Since there are no specific missions planned, there are no specific weight budgets available.

## **2.2 Performance**

The performance requirements for the support structure and the concentrator are identical for the flight experiment and the full scale system. The success of the mission hinges on the ability of the concentrator to provide energy to the aperture to enable the engine to produce thrust.

To deliver the concentrated flux to the aperture, the overall system pointing must be accurate to within  $0.5^\circ$  on-orbit<sup>3</sup>. This alignment is generally a combination of dimensional tolerance errors and alignment measurement uncertainties during fabrication, and on-orbit effects (such as thermoelastic distortion).

The concentrator and support structure must maintain the concentrator-to-receiver alignment during the various on-orbit disturbances (mainly due to pointing and thrusting of the system). Preliminary analysis<sup>4</sup> of the full scale system indicates the support structure and concentrator together must have a deployed resonance frequency greater than 0.1 Hertz to minimize misalignment and Attitude Control System interactions. This 0.1 Hertz requirement for the full scale system roughly translates to a requirement of 0.4 Hertz for the flight experiment.

The size and shape of the concentrated flux field is largely a function of the sun shape and the specular error of the concentrator. To assure the concentrated flux field can be largely contained by the aperture, and to minimize aperture size, the specular error of the concentrator must be less than  $2.0 \text{ mrad}^3$  rms.

### **2.3 Stowed Package**

Since the initial flight experiment is intended to be flown on the GAS program, the goal is to design a stowed package which can fit in the GAS envelope. The GAS envelope is pictured in Figure 5. The nominal volume available is a cylinder approximately 19 inches high and 33 inches in diameter. However, NASA reserved volume and room for the ejector mechanism reduce the usable height of the cylinder to approximately 18.5 inches. An additional 6 inches of height have been designated for electrical, pneumatic and mechanical equipment for the initial flight experiment<sup>2</sup>. Therefore, the final volume available for the support structure and concentrator is approximately a cylinder 19 inches in diameter by 12.5 inches high (3544 cubic inches).

As previously mentioned (with respect to weight), as the complexity of the flight experiment increases, the volume of the support equipment will likely increase. Therefore, the available volume within a GAS for the support structure and concentrator will decrease. An evolution of this manner decreases the likelihood of packaging an advanced flight experiment in a GAS.

The stowed volume of the full scale system is also an important attribute. The full scale system must be able to be packaged, with the rocket and payload, on a conventional expendable rocket or the Space Shuttle. Therefore, the minimum stowed volume is desired to preserve volume for the payload.

### **2.4 Testability**

The complexity of the large deployable structures envisioned for Solar Thermal Propulsion applications is such that customers will demand verification of proper operation of the system on the ground prior to launch. The requirement for testability of the support structure is enacted to facilitate this effort to assure high reliability of the systems.

The requirement of deployment of the large lightweight structure on the ground (a 1-G environment) adds a significant structural load case to the design. Often, the structural loads caused by the 1-G case, even after offloading or counterbalancing, are the design drivers for the structure. The addition of this load case (via enactment of the ground testability requirement) cause the system designer to increase the mass of the structure which would otherwise meet all on-orbit requirements. However, a ground test is the only acceptable means of verification of a flight system (since a flight test of each solar rocket is not feasible) and is therefore a worthwhile design tradeoff.

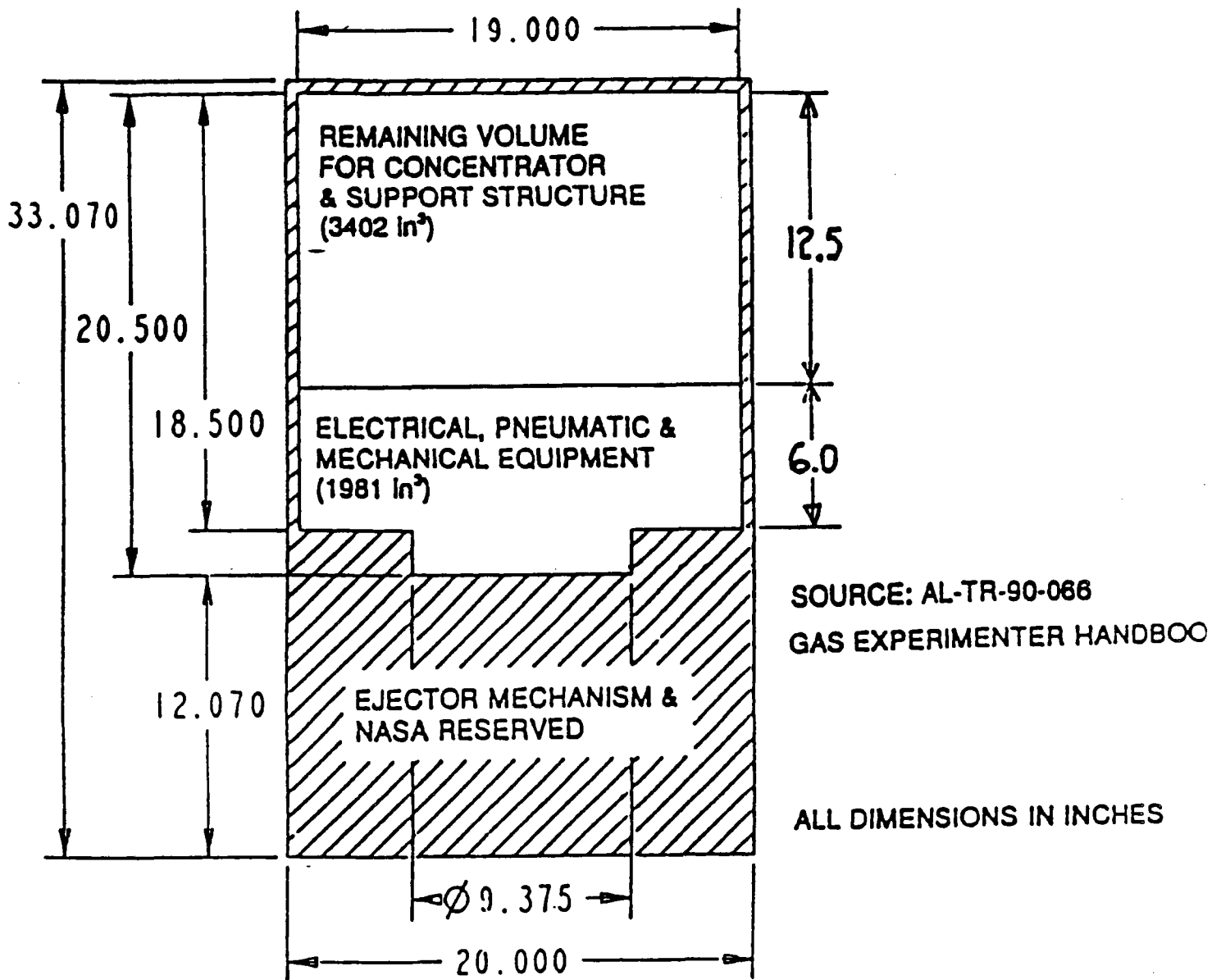


**Figure 5**  
The Get Away Special canister also provides a challenging stowed volume goal for the flight experiment

## 2.5 Environments

The flight experiment must operate in a LEO for approximately 24 hours. In the LEO, the flight experiment will be exposed to direct solar, albedo, infrared and ultraviolet irradiance, atomic oxygen, and particle radiation.

Solar, albedo and infrared irradiance impact the temperature and therefore the thermoelastic distortions of the support structure and concentrator. Thermal control coatings and/or insulation are typically used to mitigate any such effects.

Ultraviolet radiation affects the mechanical properties of organic materials such as graphite/epoxy used for a deploying strut or hoop and thin films from which the concentrator is made. With proper material selection (especially for the thin film), and judicious use of coatings and insulation, protection against UV damage can be achieved.

Atomic oxygen affects many organic materials and some metals. These effects range from film thickness degradation to degradation of mechanical and optical properties. Again, proper material selection, coatings and insulation are typically used to withstand environments with high atomic oxygen fluxes. The short flight time of the flight experiment minimizes the amount of atomic oxygen exposure.

Regions of LEO that lie outside of the Van Allen belt experience high energy particle fluxes of protons, alpha particles and some heavier nuclei. These particles are generally non-penetrating. However, they can affect optical properties. Coatings and/or insulation can be used to limit damage due to these particles. Again, the short flight time of the flight experiment minimizes the particle flux dose.

It is also required that the flight experiment use materials and designs which can be applied to the full scale system. Since the full scale system traverses from LEO to GEO, the materials and designs must withstand these environments. Table 2 summarizes the natural environment for both LEO and GEO. The GEO has higher levels of particle radiation (including protons, electrons and ionizing radiation).

**Table 2. Summary of Typical Natural Environments**

| ENVIRONMENT             | ORBIT                        |                            | EFFECTS  |
|-------------------------|------------------------------|----------------------------|--|
|                         | LEO                          | GEO                        |  |
| SOLAR                   | 1.35 kW/m <sup>2</sup>       |                            | THERMOELASTIC<br>ORGANIC MATERIALS<br>(MECHANICAL) |
| UV<br>(SOLAR COMPONENT) | 0.09 kW/m <sup>2</sup>       |                            | THERMOELASTIC                                      |
| EARTH INFRARED          | 0.210<br>kW/m <sup>2</sup>   | 0.004<br>kW/m <sup>2</sup> | THERMOELASTIC                                      |
| ALBEDO                  | 0.195<br>kW/m <sup>2</sup>   | 0.004<br>kW/m <sup>2</sup> | ORGANIC MATERIALS<br>(EROSION)                     |
| ATOMIC OXYGEN           | 726<br>atoms/cm <sup>2</sup> | 0<br>atoms/cm <sup>2</sup> | ORGANIC MATERIALS<br>(MECHANICAL &<br>OPTICAL)     |

In addition to the natural environments, the full scale system also has induced environments. The induced environments include plume impingement and concentrated solar radiation due to mispointing. Plume impingement induces heating and applies pressure to the surfaces which are impinged. These effects must be accounted for in the design of the support structure and concentrator. Mispointing of the concentrator can cause high solar concentrations on the support structure and the spacecraft in the vicinity of the aperture. Proper design of the support structure will limit the severity of the mispointing environment. For less severe mispointing environments within tolerances, the effects can be minimized by proper material selection.

## **2.6 Scalability**

The flight experiment support structure and concentrator must utilize materials and designs which can be scaled to the full scale design. This means that the flight experiment designs must be capable of scaling by a factor of approximately four for length and sixteen in area (i.e. from 7 by 9 meters to 30 by 40 meters).

### **3.0 Support Structure Designs**

The goal of this design effort was to develop a support structure which meets the requirements established in Section 2.0. Two different inflatable concentrator designs were studied in this effort.

A torus and support structure were designed for the conventional inflatable concentrator/canopy similar to that shown in Figure 6 and described in Reference 2. The torus and support structure design is described in Section 3.1.

A second support structure was designed to accommodate the Single Chamber Concentrator (SCC) design. The Single Chamber Concentrator is shown in Figure 7 and is described further in Reference 5. This support structure is described in Section 3.2.

#### **3.1 Conventional Concentrator/Canopy Support Structure Design**

This section describes the design and performance of a support structure for a conventional solar thermal propulsion system concentrator design. The word conventional, in this context, refers to the use of an inflatable reflector/canopy (a double curved lens) assembly connected to a torus support structure as shown in Figure 6.

The goal of this design effort was to develop a support structure which meets the requirements defined in Section 2.0. The concentrator technology is assumed to be equivalent to that described in Reference 6.

The basic design configuration of the system, shown in Figure 6, consists of the inflatable concentrator supported by a deployable torus. The torus is rigidly attached to the equipment section via a truss consisting of three deployable struts and nine tension stringers.

Five component designs are described in Section 3.1; the torus(3.1.1), the struts(3.1.2), the strut deployment system(3.1.3), the strut end fittings(3.1.4) and the torus-to-concentrator attachment(3.1.5). In addition, the stowed package design(3.1.6), system deployment design(3.1.7), weight budget (3.1.8), and system performance (3.1.9) are described.

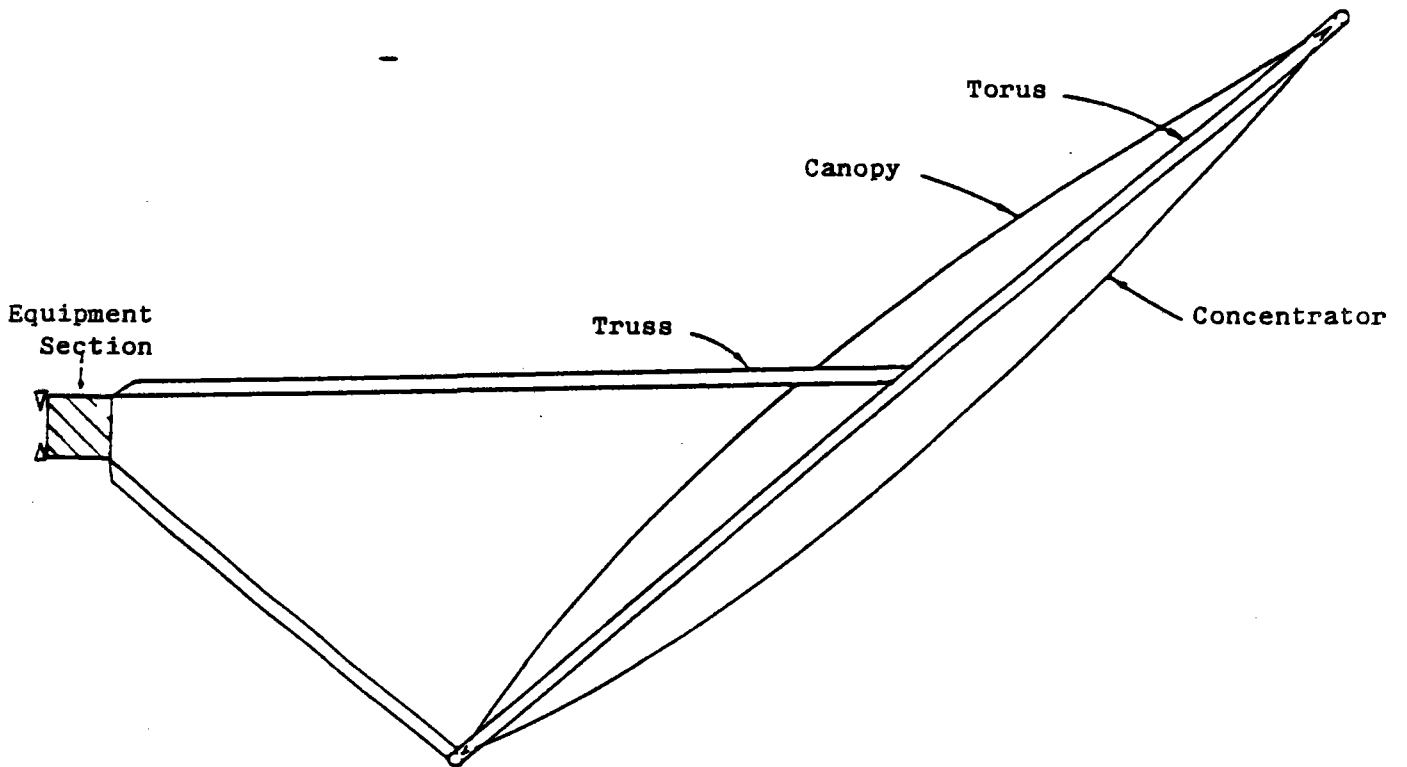


**Figure 6**  
**Conventional Inflatable Concentrator/Canopy**

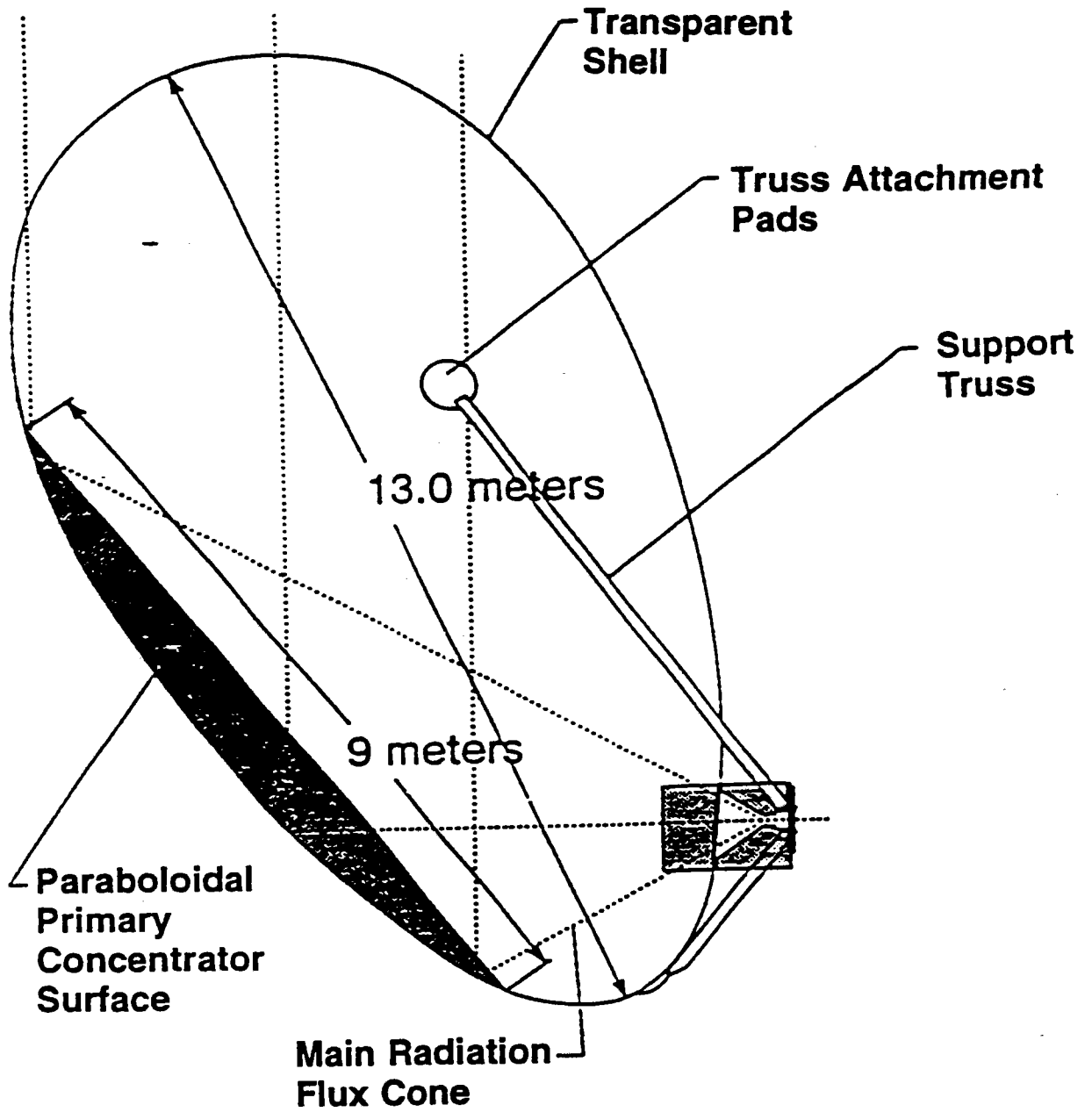


**Figure 7**  
**The Single Chamber Inflatable Concentrator (Reference 5)**

### 3.1.1 Torus Design

The difficult stowed packaging requirement necessitates the use of a deployable torus structure which provides a means of support for the inflatable concentrator. This section describes the concepts considered for the torus design and the selection process used to choose the most promising design.

Mechanically deploying hoops and inflatable design concepts were considered for the torus design. There is a large maturity gap between the two design options. Harris has significant experience with mechanically deploying hoops, such as that shown in Figure 8, and considers the technology mature and ready for immediate implementation into flight hardware. Harris has previously built a 15 meter diameter ground model of a deploying hoop for NASA-Langley under the Large Space Structures Technology program. Inflatable torus designs, on the other hand, are still in the technology development stage and are not ready for implementation into a flight experiment.

The main disadvantage to any mechanical system in comparison to an inflatable design is that mechanical systems are inherently heavier. However, the advantages that the mechanical systems offer over an inflatable structure in terms of strength, stiffness, testability, analysis, and maturity transcend the weight disadvantage. For this reason, a decision was made to focus on mechanical systems.

To preserve the maturity advantage, mechanical system concepts were limited to those similar to the Large Space Structure Technology hoop design (Figure 8). Each of the design options contains rigid tubular segments that deploy from fully vertical to fully horizontal, yielding a segmented circle as the final configuration (see Figure 9). This segmented circle supports the elliptic concentrator tensioned inside the hoop as shown in Figure 10.

The materials within the hoop are patterned after the LSST design. The rigid tube segments which create the hoop are graphite/epoxy composite tubes 2 inches in diameter with wall thickness of 0.015 inches. The hinges and end fittings of each tube are fabricated of aluminum. This combination of graphite/epoxy and aluminum fittings has a long history of use in space due to its low coefficient of thermal expansion and high strength/weight ratio. These materials, with minimal coating work, are capable of operation in the LEO environment of the flight experiment or the various environments of the full-scale rocket.

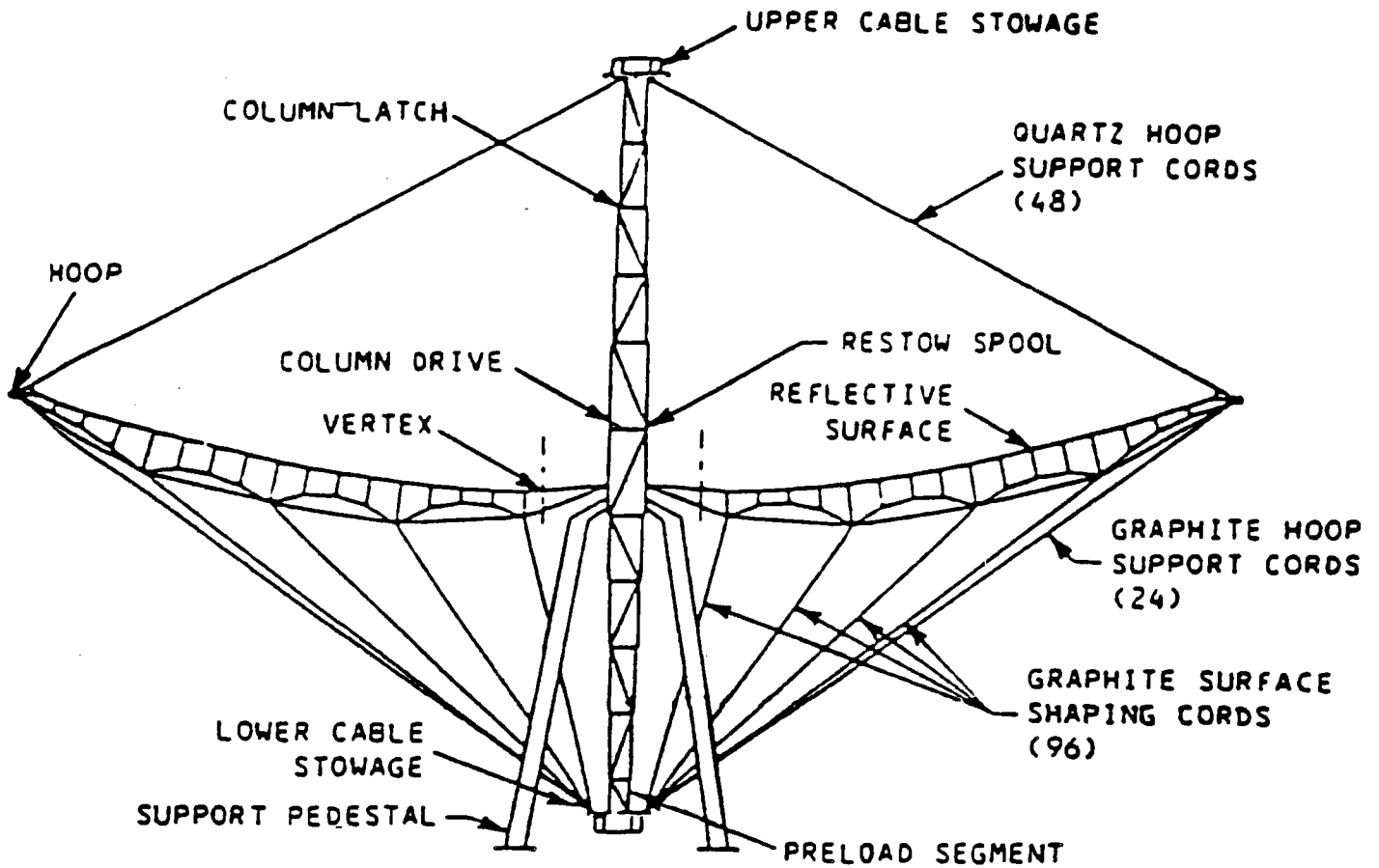


**Figure 8**  
**The 15 meter diameter hoop-column antenna was developed with**  
**NASA-Langley on the LSST Program**

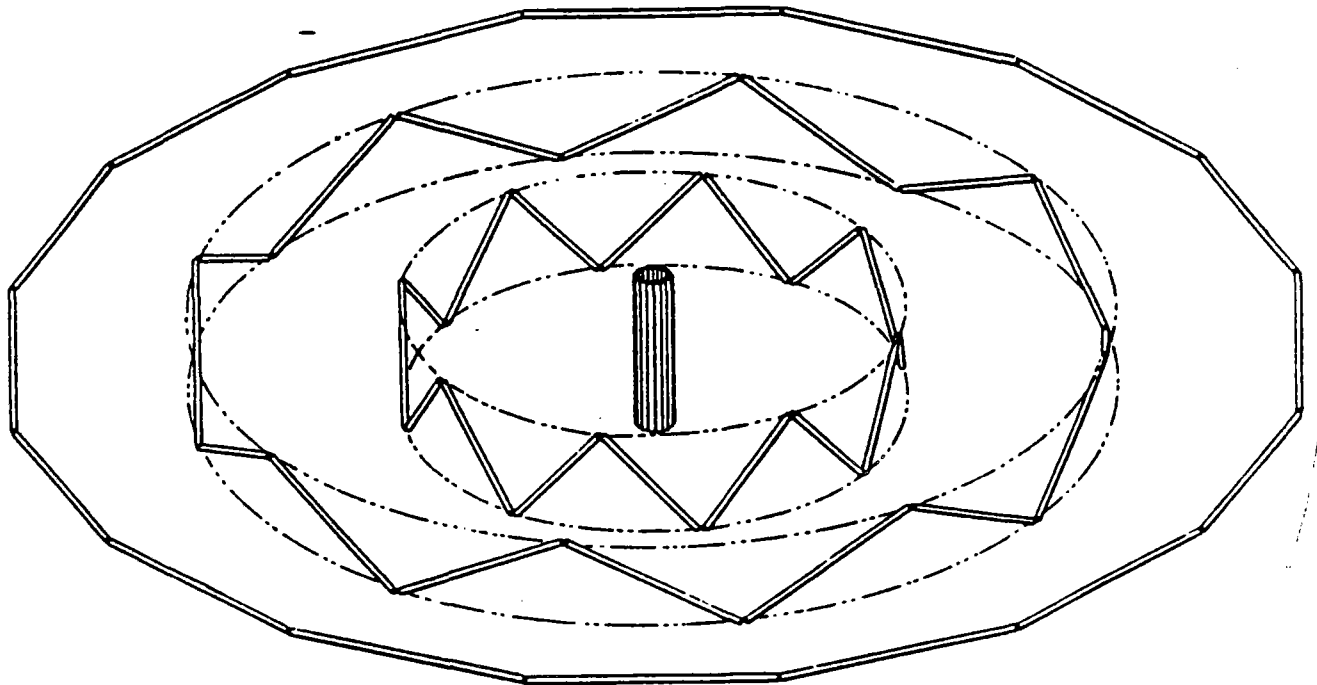


**Figure 9**  
**The hoop designs deploy from fully vertical to fully horizontal yielding a segmented circular hoop**

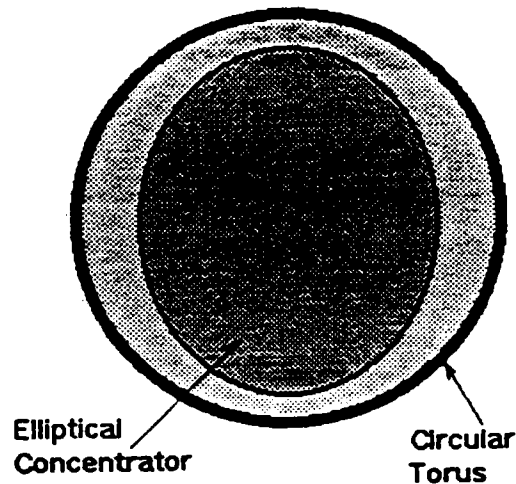


**Figure 10**  
**The circular hoop supports an elliptical concentrator**

Four mechanical systems were evaluated; the Cable Concept, the Cable/Pulley Concept, the Sliding Linkage Concept, and the LSST Hoop Concept. A conceptual design and table of advantages and disadvantages were made for each concept and a preferred design was chosen based on applicability to the Solar Thermal Propulsion mission.

Of the mechanical systems considered, the LSST concept with the modifications described in paragraph 3.1.1.4 is recommended.

#### **3.1.1.1 Cable Concept**

The Cable Concept uses the inflation energy of the deploying concentrator to deploy the segments. A cable is guided through each of the segments and is loose when the tubes are fully stowed (vertical). As the concentrator inflates, the tubes are free to follow the edges of the inflated concentrator where they are attached. When the concentrator is fully inflated, a motor tightens the cable strung through the hoop segments. The tightened cable forces latches, located at each segment-to-segment interface, to lock which stiffens the structure. The tightened cable has a secondary purpose of adding stiffness to the hoop.

Table 3 lists the advantages and disadvantages of the Cable Concept.

**Table 3. Attributes of the Cable Concept**

| Advantages  | Disadvantages  |
|---|--|
| Simple Design   | No synchronization of segments is provided (random deployment) |
| The cable is an efficient means of alignment and latch engagement | Deployment is dependent on the concentrator deployment energy  |
| The cable provides stiffness to the deployed structure            | The system is difficult to analyze                             |
|   | The system is difficult to test                                |

**3.1.1.2 Cable/Pulley Concept**

In the Cable/Pulley hoop design, a cable is continuously wrapped through a series of pulleys located at the ends of each of the hoop segments as shown in Figure 11. One end of the cable is attached to a motor which drives the structure to deployment (tubes rotate to horizontal) by pulling on the cable. Two stages of deployment are shown in Figure 12.

Gears are used to maintain a constant angle between segments during deployment, and synchronization rods keep the deployment of the different segments synchronized (controlled). Table 4 lists the advantages and disadvantages of the Cable/Pulley Concept.

**Table 4. Attributes of the Cable/Pulley Concept**

| Advantages   | Disadvantages   |
|--|---|
| When deployed, the cable can be used to help provide stiffness                 | The cable is not an efficient means of deploying the torus since the tension provides only a small moment at any time |
| This design provides a positive and synchronized deployment                    | The moment is variable with the deployment angle  |
| This design uses low friction elements (rolling friction vs. sliding friction) | The number of parts tends to make this system undesirable from a weight standpoint                                    |

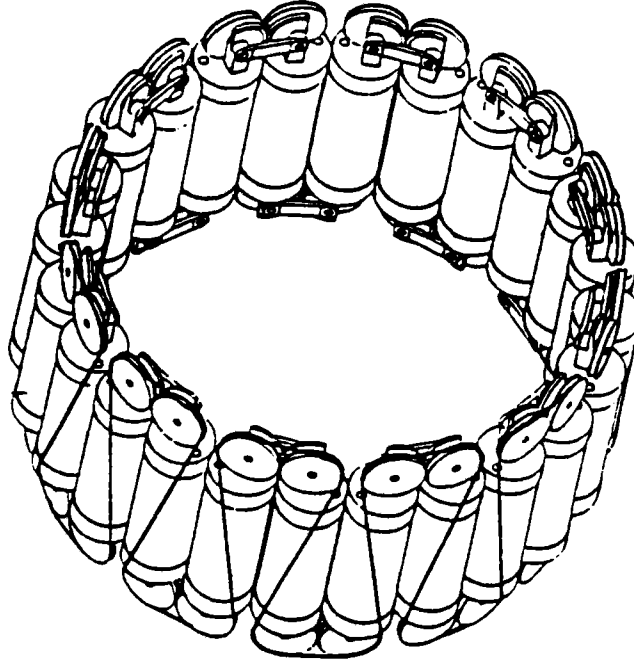


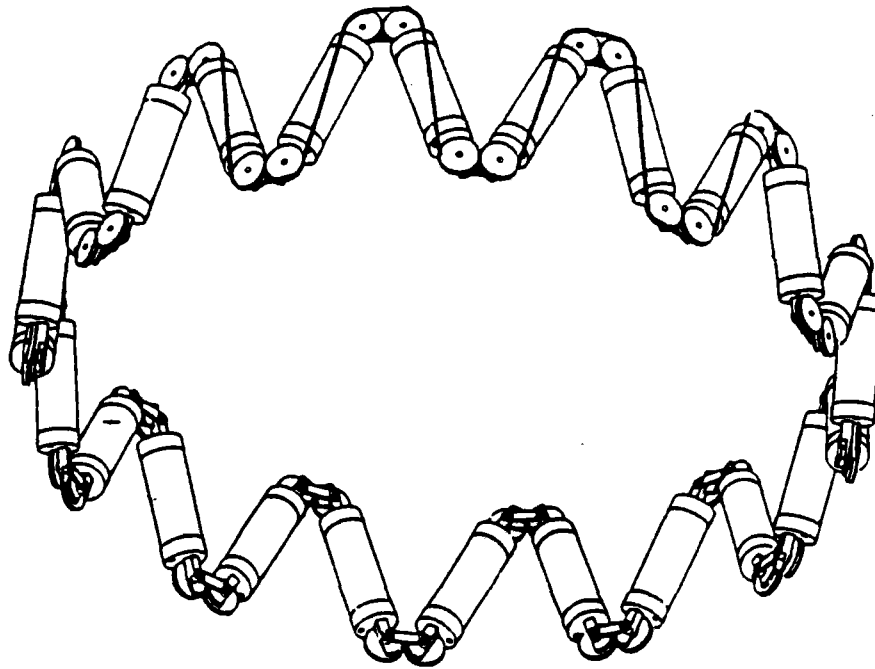
**Figure 11**  
In the cable-pulley design, a cable is continuously wrapped through a series of pulleys at the ends of each hoop segment. As the cable is retracted the hoop deploys

### **3.1.1.3 Sliding Linkage Concept**

In the Sliding Linkage Concept, a ball screw, attached to each hinge, is used to drive a linkage. The linkage is attached on both ends to a segment through another linkage. As the linkage translates, the segments are rotated to the fully deployed position. Synchronization rods would be required in this design to ensure a controlled deployment between segments.

Figure 13 illustrates the Sliding Linkage Concept. Note that the figure does not show the synchronization rods, or the hoop segments attached to the hinge. Table 5 lists the advantages and disadvantages of the Sliding Linkage Concept.

Partially Deployed Hoop



Fully Deployed Hoop

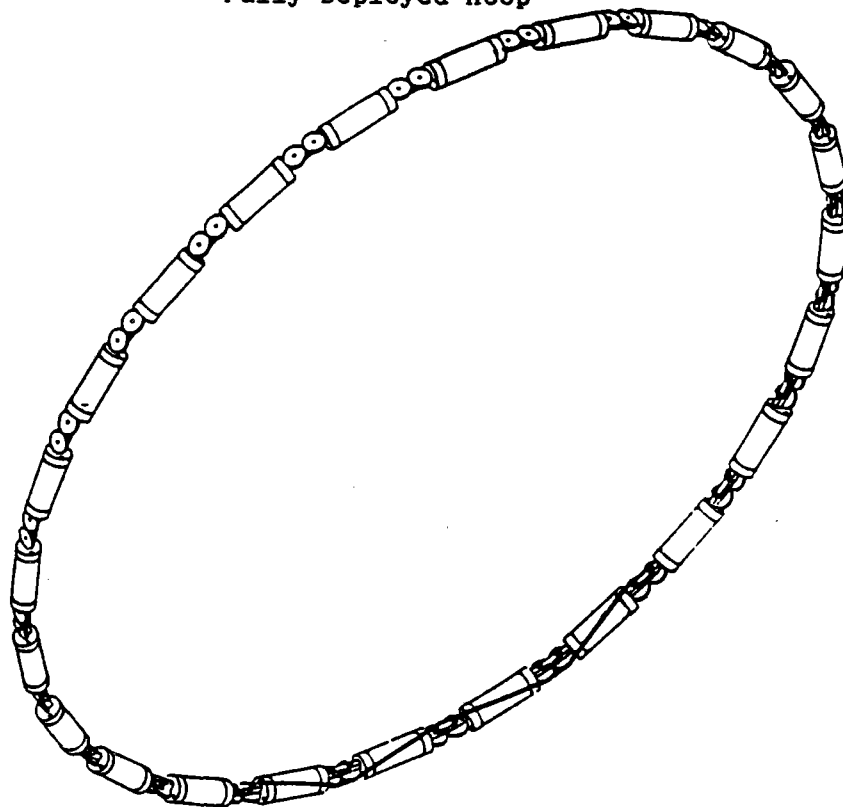
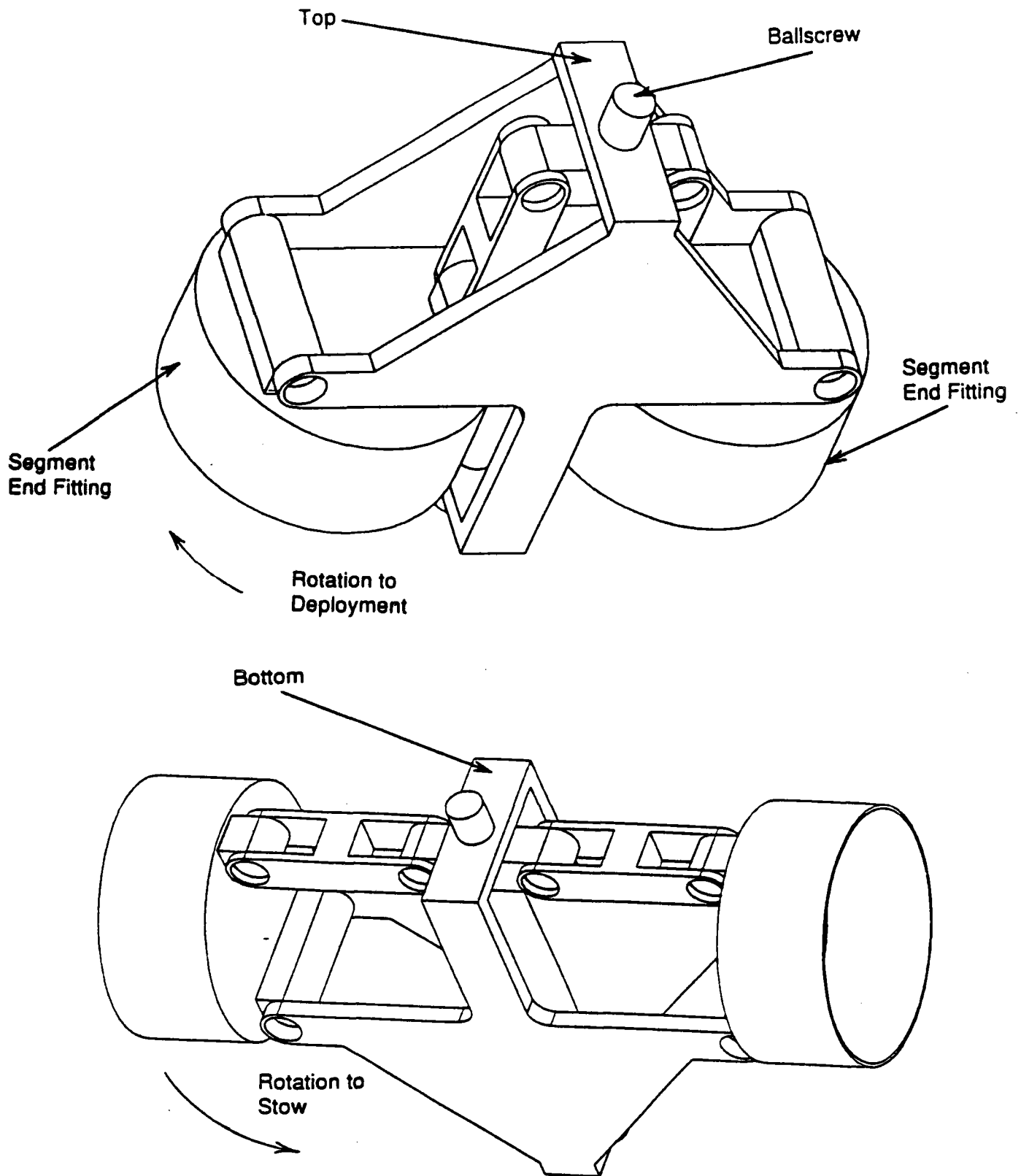


Figure 12  
A view of the partially deployed and fully deployed cable-pulley hoop design

**Table 5. Attributes of the Sliding Linkage Concept**

| <b>Advantages</b>  | <b>Disadvantages</b>  |
|--|---|
| Provides a positive synchronized deployment                                      | The design contains sliding surfaces (instead of rolling) in the slots and the ball screw which increases friction. |
| The design is relatively lightweight (no gears, pulleys, or cables are required) | The moment applied during deployment is variable  |



**Figure 13**  
The Sliding Linkage Design uses a motor to turn a ballscrew which deploys the hoop

### 3.1.1.4 LSST Hoop Concept

The Large Space Systems Technology (LSST) reflector, Figures 14, 15, and 16, was designed by Harris Corporation for NASA Langley Research Center, Hampton, Virginia.<sup>6</sup> A working 15 meter diameter, 24 segment, model was built and tested. The hoop portion of the LSST reflector utilized bevel gears at each hinge to maintain the proper angle between segments during deployment. Synchronization rods (4 per segment) were used to maintain a controlled deployment. Motors placed at selected hinges supplied the deployment energy.

Several improvements were incorporated into the LSST hoop design to adapt it to the Solar Thermal Propulsion application.

The motor drive was changed from a worm gear to a spur gear to increase reliability. Since a worm gear operates with sliding friction and a spur gear operates with rolling friction, a change to a spur gear increases reliability.

The synchronization rods of the LSST hoop were replaced with thin graphite tapes to reduce weight and volume.

The hinge assembly was redesigned to reduce weight and stowed volume. The LSST hinge assembly was never optimized for weight or stowed volume. This redesign reduces hoop weight by approximately 30% and stowed volume by approximately 20%. In addition, a mechanical stop was added to the hinge to prevent over-deployment. The new hinge is shown in Figure 17.

Table 6 lists the advantages and disadvantages of the LSST concept.

**Table 6. Attributes of the LSST Hoop Concept**

| <b>Advantages</b>   | <b>Disadvantages</b>   |
|---|--|
| This design provides synchronized deployment of the segments                                      | The hinge motors will need to be synchronized to prevent binding |
| The concept was proven via engineering model on the LSST program                                  |  |
| The design has low friction   |  |
| Because the motors are located at the point of rotation, the moment during deployment is constant |  |



**Figure 14**  
**The LSST hoop in the stowed configuration**

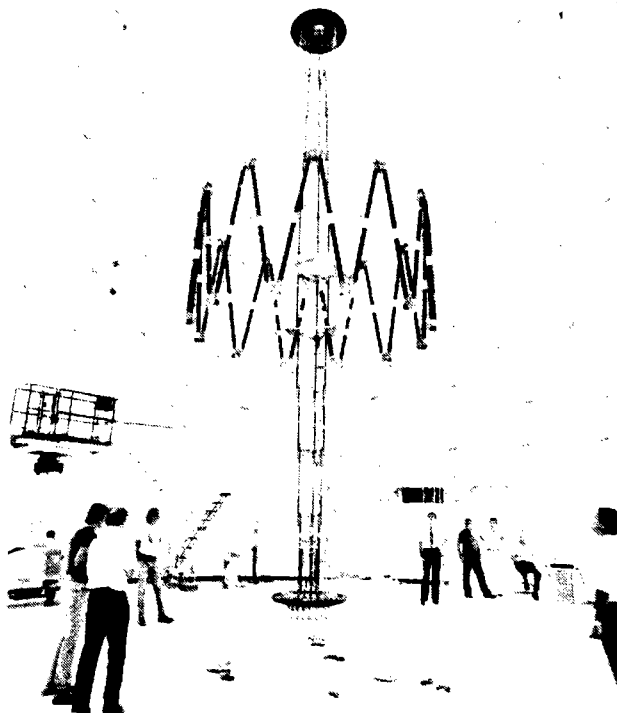


**Figure 15**  
**The LSST hoop partially deployed**

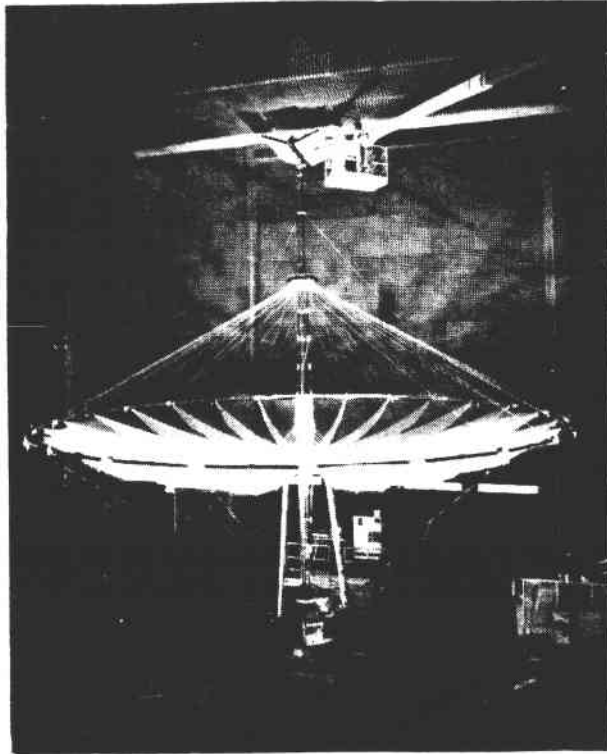


**Figure 16**  
The fully deployed LSST hoop measures 15 meters in diameter

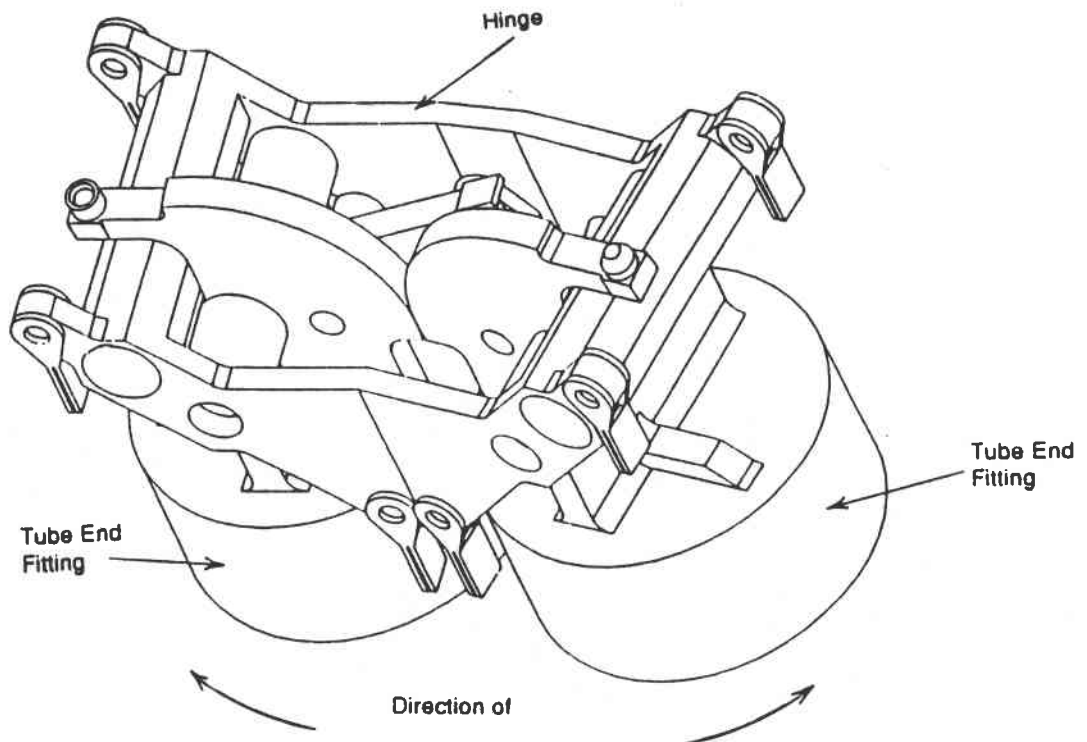


**Figure 17**  
A hinge redesign, pictured in the stowed configuration, reduces the LSST hoop hinge weight by 50%

### **3.1.1.5 Hoop Design Selection**

The proposed hoop designs were compared and contrasted. The weight and stowed volume of the systems were approximately equivalent. Therefore, the overriding factor in the design selection was reliability.

The LSST design is deemed the most desirable of the designs because it offers a proven concept with synchronized deployment, low friction components, and a constant moment throughout deployment. These attributes generally lead to high deployment reliability.

The reliability of the Cable concept is least desirable since the deployment of the hoop segments is not controlled and successful deployment relies on energy provided by the inflation of the concentrator.

The reliability of the cable-pulley concept is suspect due to the availability of only a small moment to deploy the system. The available deployment moment is actually zero near fully stowed condition necessitating a secondary startup deployment system which adds weight and complexity.

The sliding linkage concept has a variable deployment moment and sliding friction (instead of rolling friction) which makes this design relatively low in reliability.

### **3.1.2 Strut Design**

Four different strut designs were identified for use in the support structure; a telescoping design, a deploying mast, an articulating four-bar linkage and an inflatable concept.

The main requirement of the struts is to provide structural stability to the hoop and concentrator. Each of the design options can provide adequate structural stability for the system. The struts must also be lightweight, compact in the stowed position, and reliable in operation to optimize the effectiveness of the solar thermal propulsion system. The inflatable design provides the minimum stowed volume and minimum mass, two large advantages. However, the reliability of this design is suspect due to the immaturity of the technology. A deploying mast provides reliable strut operation but the weight is significantly larger than the other options. A four bar linkage provides reliable operation at a low weight. However, this design requires substantially more stowed volume than is available. The telescoping design, in a qualitative comparison, provides good reliability, a reasonable stowed volume and an acceptable weight. Therefore, the telescoping design was

identified early in the program as the preferred strut design.

The telescoping strut design consists of two major components; the strut tubes and the strut latches. The strut tubes (Section 3.1.2.1) are the individual structural members that are connected to form the full strut. The strut latches (Section 3.1.2.2) are located at each end of the strut tubes and create a stiff interface between strut tubes upon deployment. The strut deployment system (Section 3.1.3) is the method by which the struts are extended from the nested position to the deployed position. The strut fittings (Section 3.1.4) are located at each end of the strut and interface the strut to the hoop at one end and to the spacecraft at the other.

### 3.1.2.1 Strut Tube Design

A graphite/epoxy composite was chosen as the material for the strut tubes due to its high strength/weight and high stiffness/weight ratios and low coefficient of thermal expansion(CTE). The composite consists of Hercules 3501-6 epoxy reinforced with Ultra-High Modulus (UHMS) fibers, a fairly common graphite/epoxy material for aerospace structures. This material easily survives the flight experiment environments and could be coated to survive the full scale system environments. A preliminary zero-CTE layup was designed and is described in Table 3.1.2.1-1.

**Table 7 Preliminary strut tube layup and material properties**

| <b>Ply</b>   | <b>Thickness<br/>(inches)</b> | <b>Orientation<br/>(degrees)</b> |
|--------------|-------------------------------|----------------------------------|
| 1            | 0.0030                        | 69                               |
| 2            | 0.0045                        | 0                                |
| 3            | 0.0045                        | 0                                |
| 4            | 0.0030                        | -69                              |
| <b>TOTAL</b> | 0.0150                        |                                  |

| <b>Properties<br/>(UHMS/3501-6)</b> | <b>Lamina</b> | <b>Laminate</b> |
|-------------------------------------|---------------|-----------------|
| E11 (Msi)                           | 36.45         | 22.47           |
| E22 (Msi)                           | 13.80         | 11.96           |
| CTE11 (min/in°F)                    | -0.430        | -0.045          |
| CTE22 (min/in°F)                    | 14.9          | 0.815           |

The desired deployed strut lengths were determined to be 365.4 inches and 148.8 inches for the long struts and the short strut, respectively. It was assumed that 14 segments would be used to form the long struts to allow the struts to package within the stowed length of the hoop. A segment overlap of 2 inches was assumed. Therefore, the segment lengths are calculated as:

$$L = ( SL + ( N - 1 ) * OL ) / N$$

$$L = 27.96 \text{ inches}$$

where

|    |   |  |
|----|---|--|
| L  | = | segment length   |
| SL | = | desired deployed strut length of the long struts = 365.4 |
| N  | = | number of strut segments = 14                            |
| OL | = | overlap of segments when deployed = 2.0                  |

It is desirable to minimize the number of different strut segment lengths to minimize cost. Therefore, the short strut was designed to use the same segment length as the long struts. The integral number of segments, IN, smaller than the desired deployed short strut length, SS, was calculated and a final partial segment length, PS, was calculated to make up the remaining length. For this case, IN=5 and the length of the integral number of segments, IL, when deployed, is calculated as follows:

$$IL = IN * L - ( N - 1 ) * OL$$

$$IL = 131.8 \text{ inches}$$

The partial segment length is the difference between the desired deployed strut length and the length of the integral number of segments just smaller than the desired strut length plus the overlap:

$$PS = SS - IL + OL$$

$$PS = 19.0 \text{ inches}$$

The diameter of the strut segments is defined by the stiffness required of the deployed strut, the packaging design, and the latch design. A 3 inch outer diameter tube was selected as the minimum tube size. Each successive tube is stacked around the original tube thus requiring a slightly larger diameter for each successive tube. The outer diameter increases by 0.28 inch to accommodate latch thickness and wall thickness. The latch thickness is 0.125 inch as described in Section 3.1.2.2. The tube wall thickness is 0.015 inch as shown in Table 3.1.2.1-1.

### 3.1.2.2 Latch Design Concepts

Two latch designs were initially considered for the telescoping strut; a regenerative latch/pawl design and a split ring design. The split ring design, shown in Figure 18, was selected for further refinement due to its higher packaging efficiency, lower weight and simplicity. The requirements and goals for the split ring latch are listed in Table 3.1.2.2-1 and are discussed in the next two paragraphs.

**Table 8. Latch Design Requirements and Goals**

| Requirements             | Goals                                       |
|--------------------------|---|
| Retractability           | Simplicity                                  |
| Metal-to-metal stiffness | Robustness                                  |
| Radially guided          | Minimal staggering                          |
|                          | Thin  |
|                          | Amenable to different deployment techniques |

The retractability requirement is necessary for ground testing and prevents the use of designs such as a locking taper. Metal-to-metal stiffness means that the mating surfaces of the latches must have metal contacting metal to provide adequate stiffness and to minimize backlash or play of mated latches. The latches must also guide the tubes radially during deployment so that one tube cannot become misaligned relative to neighboring tubes. A latch that does

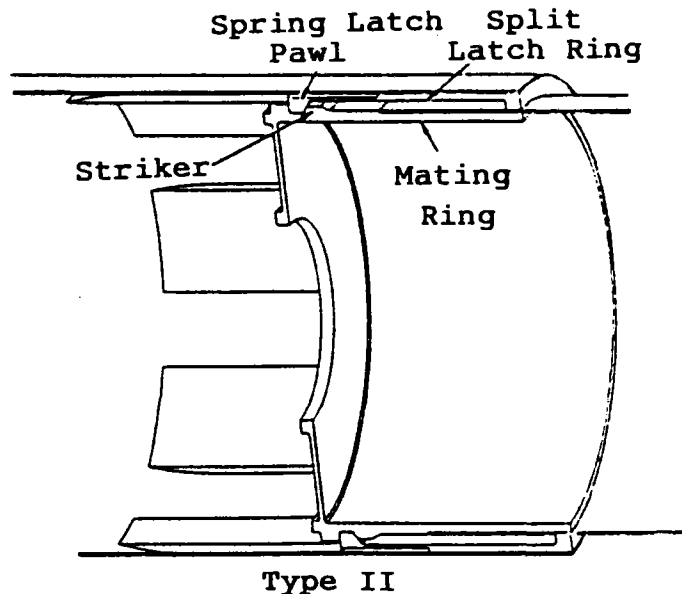


**Figure 18**  
The split ring latch is the basic design concept for the strut latch

not guide the tubes radially during deployment could generate large frictional forces (and bind), especially just before the latch engages. To radially guide the tubes, the female half of the latch on the inner diameter of the outer tube must just allow the outer diameter of the inner tube to clear.

The simplicity goal implies that a latch with fewer parts or mechanisms is less expensive and easier to fabricate and generally lighter in weight. A robust latch design is tolerant of less than ideal situations such as misalignment during deployment or bending moments on a deployed strut. Staggering is the difference in length between neighboring tube ends in a stowed configuration (i.e. the step height from the top of one tube to the top of the next tube in a stowed configuration). Latches that require more staggering package less efficiently than latches with less staggering. Thin latch designs also have packaging advantages over thicker latch designs. Thin latches allow more tube segments to fit within a given diameter. Additionally, when all other variables are held constant, increasing the latch thickness can increase strut weight in a non-linear manner. This occurs since latch weight increases roughly proportional to the square of the latch diameter which is strongly influenced by the latch thickness. A latch design should be selected which is amenable to as many deployment techniques as possible, since some strut deployment techniques cannot be used with certain latch designs without greatly increasing the complexity of the design.

Three variations on the split ring latch were considered; the baseline split ring latch (henceforth referred to as latch concept 1), the two piece retractable radial latch (latch concept 2) and the circumferential latch (latch concept 3). The three concepts have several features in common. They all are metallic (aluminum), split ring designs and would have to be machined to tight tolerances to eliminate the need for shimming or fine tuning (although it might be more efficient to relax the tolerances and use a shimming and fine tuning procedure). All three of these designs require only minimal staggering and roughly the same amount of overlap which means that they all will occupy about the same height when stowed. The concept 1 latch and concept 2 latch both require about the same amount of tube separation (which determines stowed radius) but concept 3 probably requires the most tube separation. All three designs become more difficult to realize as the tube diameter decreases below 1.5 inches OD. Concept 1 and concept 2 are probably more suitable for small tube diameters than concept 3.

The baseline split ring latch (Figure 18) uses multiple wedge pieces to align the halves of the latch just before they engage. These wedges are undesirable since they would have to be aligned and bonded into the tube thus increasing costs. Additionally, these wedges only guide the tubes radially at the very end of the stroke. The baseline split ring latch also uses the pawl to restrain axial motion in both directions. This could lead to a buckling problem in the flexure if the latch is loaded in compression. This concept also has somewhat limited deployment options. For example, it would be very difficult to implement a cable-pulley deployment mechanism with this concept. This latch will also be difficult to retract since access to the pawl is limited once the latch is engaged. This latch could be upsetable under bending. This latch concept does not restrain rotation except for the frictional forces which would develop when the strut is pretensioned.

A sketch of the two piece retractable radial latch (concept 2) is shown in Figure 19. The concept 2 latch is similar in design to the baseline split ring latch since both designs use a split ring to serve as both flexure and pawl which moves in the radial direction. The concept 2 pawl is part of the inner half of the latch whereas the pawl is part of the outer half of the latch in the baseline split ring design. Concept 2 uses the pawl to restrain axial motion in one direction only. A drawing of the two piece retractable radial latch is shown in Figure 20.

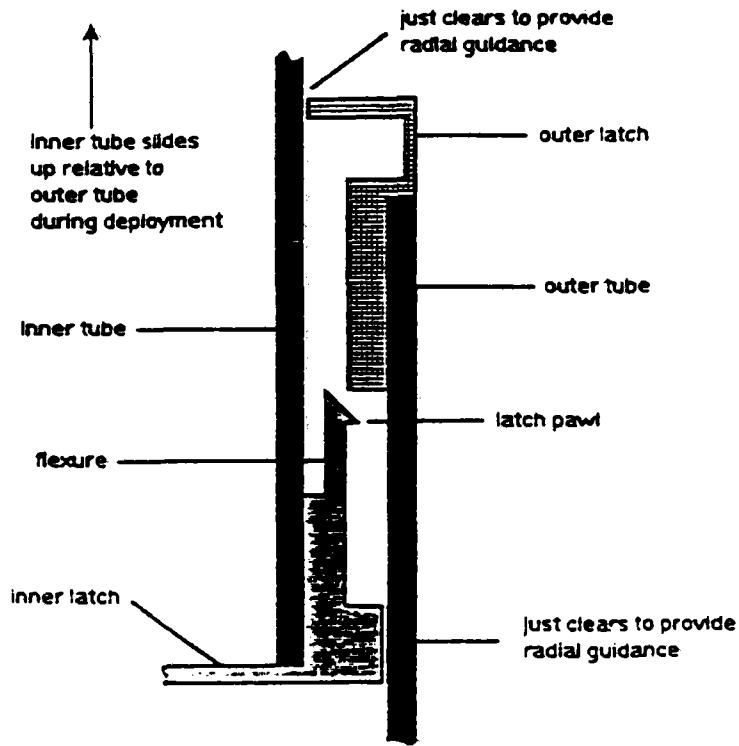


**Figure 19**  
**The two piece retractable radial latch adds radial guidance to the split ring design**

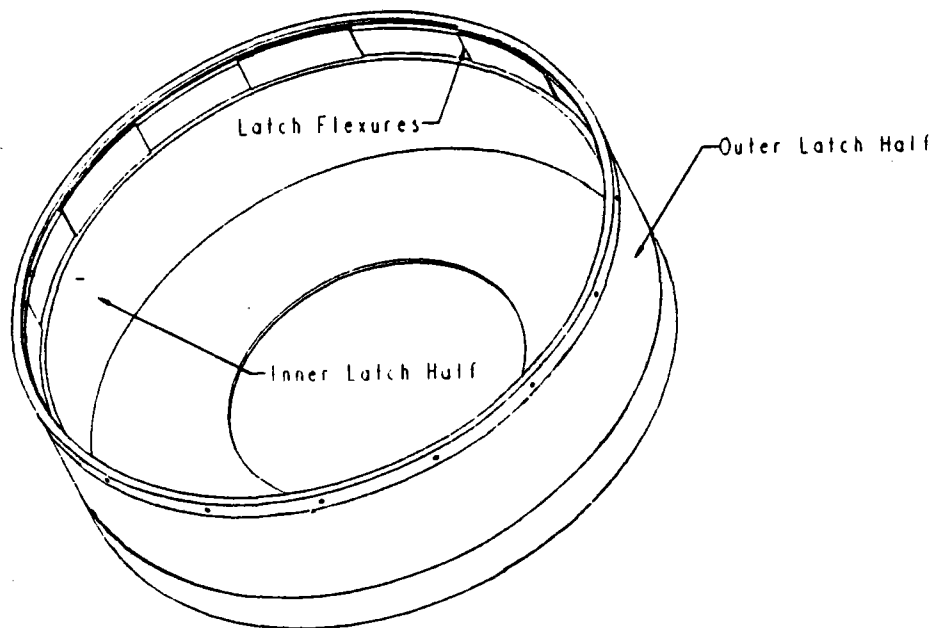


**Figure 20**  
**The two piece retractable radial latch requires 0.125 inch separation between adjacent tube faces**

An ambitious latch design would require about 0.125 inch of separation between the faces of neighboring tube segments. The drawing of the concept 2 latch shown in Figure 20 is based on this 0.125 inch dimension. It was also estimated that a 3.0 inch outer diameter was the smallest tube which could be used for the concept 2 latch. The limitation is caused by excessive geometrical stiffening of the flexure as the radius of curvature of the flexure decreases.

The concept 2 latch requires fewer components than the concept 1 latch since the inner latch half just clears the outer tube and thus does not require the guides needed for the concept 1 latch. Additionally, since the outer latch also just clears the inner tube, the concept 2 latch is radially guided. This concept also has a large amount of radial surface area with metal-to-metal contact. The top part of the outer half of this concept can be drilled to provide an access hole which will enable easy retracting of the latch once it is engaged. The concept 2 latch also is more adaptable to different deployment techniques including a cable-pulley system. Like the concept 1 latch, this latch could disengage under bending load. This latch concept also does not restrain rotation except for the frictional forces which would develop when the strut is pretensioned.

A drawing of the circumferential latch (concept 3) is shown in Figure 21. The concept 3 latch uses a pawl which engages by moving in the circumferential direction. This design is different in that the pawl is not an integral part of the latch ring but rather is a subassembly which is fastened to the latch ring. The pawl can be a flexure type pawl (like concepts 1 and 2 and as is shown in Figure 21) or it can be a rigid body pawl which is spring actuated. The concept 3 latch also requires guides on the inside of the tubes to keep the pawls lined up with the slots in the outer latch ring. The concept 3 design does have minimal staggering but would probably be somewhat thicker than other designs. This would lead to a slightly larger stowed diameter and weight. The concept 3 design is radially guided and is amenable to deployment techniques such as cable-pulley deployment. The concept 3 design can be retracted easily since the pawl would protrude above the top surface of the outer latch half. This design is less likely to disengage in bending like the concept 1 and 2 designs since ovaling of the latch would not change the circumference of the latch (whereas ovaling of the latch does change the apparent local diameter of the tube which could cause the concept 1 and 2 latches to disengage). The main disadvantage of the concept 3 latch is that it requires guides inside of the tube which must align the pawls with the outer half of the latch. These guides

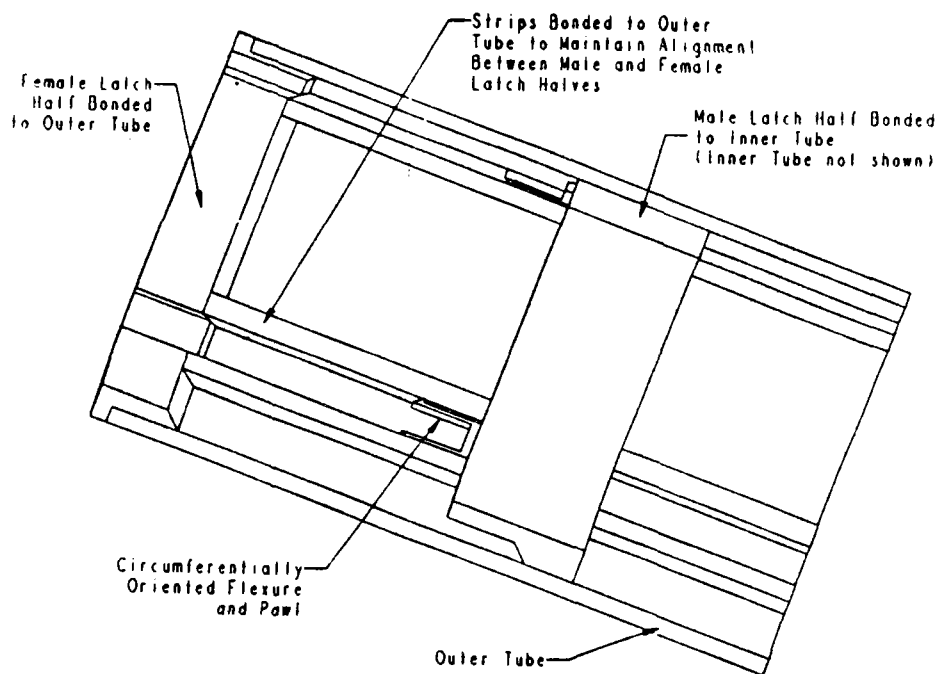


**Figure 21**

**The circumferential latch design has improved performance in bending but requires internal guides along the tube walls to assure deployment**

would significantly increase the cost of the tubes, especially since each telescoping strut is comprised of several different diameters of strut tubes which would each require fixturing. The use of such guides would also increase the complexity of the design. However, the use of guides could be advantageous for certain deployment techniques, such as cable-pulley deployment, which may require such alignment.

### **3.1.2.3 Latch Design Selection**

A trade matrix for the three latch concepts is presented in Table 9.

**Table 9. Latch concept trade matrix**

| Latch Concept                                   | Advantages   | Disadvantages   |
|---|--|---|
| <p>1<br/>Split ring latch</p>                   | <p>1 Thin and tailorable<br/>2 Minimal staggering</p>  | <p>1 Difficult to assemble<br/>2 Multipiece construction<br/>3 Limited radial metal-to-metal contact<br/>4 Pawl must restrain axial motion in two directions<br/>5 Unguided radially through most of stroke<br/>6 Limited deployment options<br/>7 Difficult to retract<br/>8 Might be upsetable in bending</p> |
| <p>2<br/>Two piece radial retractable latch</p> | <p>1 Thin and tailorable<br/>2 Minimal staggering<br/>3 Radially guided<br/>4 Ample radial metal-to-metal contact<br/>5 Retractable<br/>6 Amenable to different deployment techniques<br/>7 Simple (2 parts only)</p>      | <p>1 Might be upsetable in bending</p>  |
| <p>3<br/>Circumferential latch</p>              | <p>1 Minimal staggering<br/>2 Radially guided<br/>3 Moderate metal-to-metal contact<br/>4 Retractable<br/>5 Amenable to different deployment techniques<br/>6 Leaf springs not required<br/>7 Not upsetable in bending</p> | <p>1 More difficult to assemble<br/>2 Multipiece construction</p>   |

After the three latch concepts were evaluated against one another, the two piece retractable radial latch (concept 2) was selected over the other 2 concepts. The two piece retractable radial latch has many advantages over the split ring (concept 1) latch with far fewer of the disadvantages. The two piece retractable radial latch is simpler than the circumferential latch (concept 3), has fewer parts, occupies less stowed volume, and weighs less. If guides are not required for the two piece retractable radial latch, this design will also be less expensive and more robust since there will be far fewer sliding surfaces in contact.

### 3.1.2.4 Strut Stowed Packaging

With the tube thickness, latch thickness, and the minimum tube outer diameter defined, the stowed diameter of the struts can be calculated as follows:

$$\begin{aligned} \text{SDL} &= ( N - 1 ) * ( 2 * \text{LT} + 2 * \text{TT} ) + \text{ITOD} \\ &= 6.64 \text{ inches} \end{aligned}$$

where

|      |   |  |
|------|---|--|
| SDL  | = | stowed diameter of long strut              |
| LT   | = | latch thickness = 0.125 inch               |
| TT   | = | tube thickness = 0.125 inch                |
| ITOD | = | innermost tube outer diameter = 3.0 inches |
| N    | = | number of strut tube segments = 14         |

The stowed height of the strut is the length of one strut segment plus the total staggering (which is the staggering per segment times the number of segments). For the two piece retractable radial latch shown in Figure 20, the total staggering is 0.70 inch (0.050 inch \* 14 segments). Therefore, the total stowed length is 27.96 inches plus 0.70 inch or 28.76 inches.

### 3.1.3 Strut Deployment System Design

The telescoping strut design described in Section 3.1.2 requires a deployment system to extend the struts from the stowed position to the deployed position. This section describes the design concepts considered for the deployment of the struts and the selection process used to determine the preferred design.

Five design concepts for the strut deployment system were developed: the Bladder Concept, the Sealed Tubes Concept, the Push-Pull Concept, the Cable-Pulley Concept, and the Gear Drive Concept. Each of these concepts is described in this section.

The preferred design was determined by evaluation of each concept with respect to design simplicity, design maturity, weight, stowed volume, system reliability, cost, and scalability.

### **3.1.3.1 Bladder Concept**

The Bladder Concept (shown in Figure 22) uses pressurized gas to inflate a bladder which has been placed inside the telescoping strut. As the bladder inflates, the strut tubes are pushed to deployment. When a strut tube segment reaches its full deployment position, the latch locks the tube in place. Upon latching of all tube segments, the pressurized bladder can be depressurized as the stiffness of the strut is derived from the latches and is not dependent on the bladder.

The main advantages of this design concept are its lightweight and compact stowage. The bladder is the only large component and it is light in weight and folds easily into the internal volume of the strut. This design also takes advantage of the pressurized gas supply required to inflate the concentrator, thus minimizing additional weight and volume.

The main disadvantage of this design is the immaturity and perceived reliability concerns. There are no known systems of this kind in use in space applications (or in development for future space use) at this time.

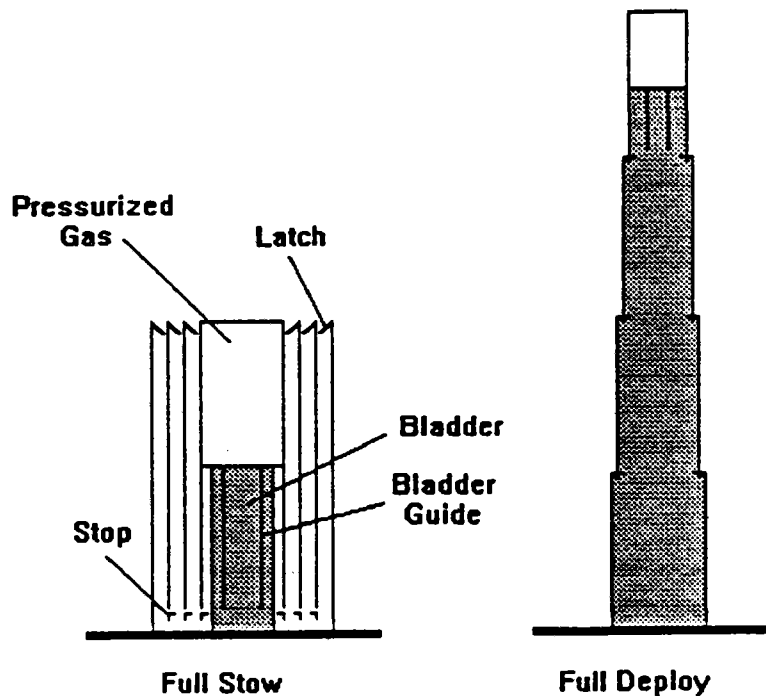


**Figure 22**  
**The Bladder concept uses pressurized gas to inflate a bladder which drives the strut tubes to deploy**

### 3.1.3.2 Sealed Tubes Concept

The Sealed Tubes design concept, as shown in Figure 23, is similar to the Bladder Concept in that they both rely on pressurized gas as the motive force behind strut deployment. However, the Sealed Tubes Concept eliminates the bladder and simply uses a seal on the inside of each nested tube to contain the pressurized gas during strut deployment. As the gas fills the strut, the strut tubes deploy until they latch in place. The pressure is only required during strut deployment since the latch stiffens the strut upon deployment.

The sealed tube design concept is even lighter in weight and requires less volume than the bladder concept. The seal does add an element of risk since any loss of pressure may result in failure. The seals may be difficult to maintain under the severe vibration loads of the launch.

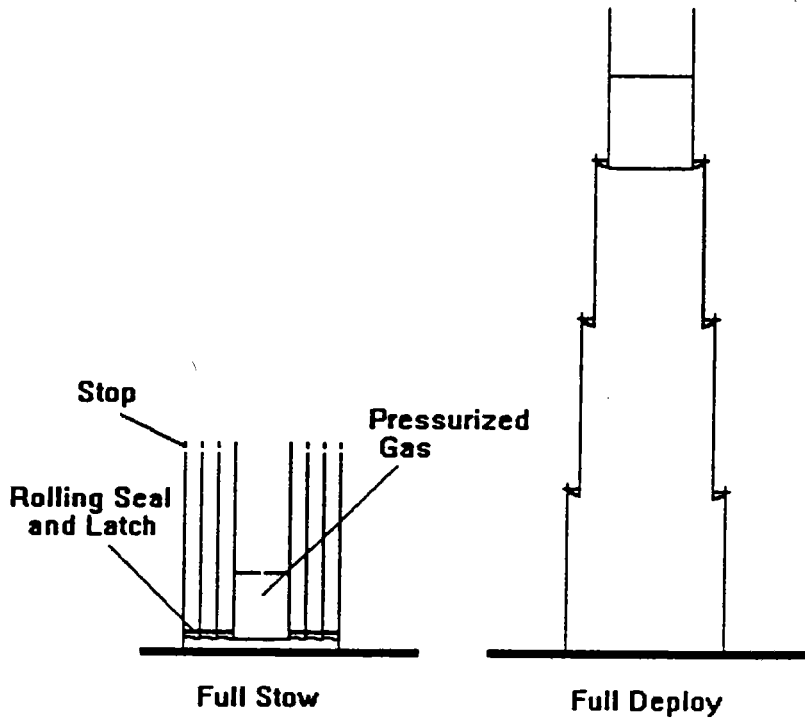


**Figure 23**  
**The Sealed Tubes concept uses pressurized gas to force the strut tubes to deploy and relies on a seal to maintain the pressure differential**

### 3.1.3.3 Push-Pull Concept

The Push-Pull design concept, shown in Figure 24, uses a motor to turn a ballscrew which drives a push-pull tube up and down the length of the nested tubes. When the deployment begins, a push fitting engages the outermost tube segment and the ballscrew drives the tube to deployment. Latches engage the tube and the ballscrew reverses to drive the push - pull tube down to engage the next tube. This process continues until all tubes are deployed and latched. The deployment in this concept is controlled and sequential to ensure latching.

The main advantage of this design is the maturity and scalability of mechanical mechanisms of this type. Mechanisms of similar complexity are routinely used in the deployment of large space structures. This design does require more weight than the inflation driven concepts since a motor, ballscrew and push-pull tube are required.

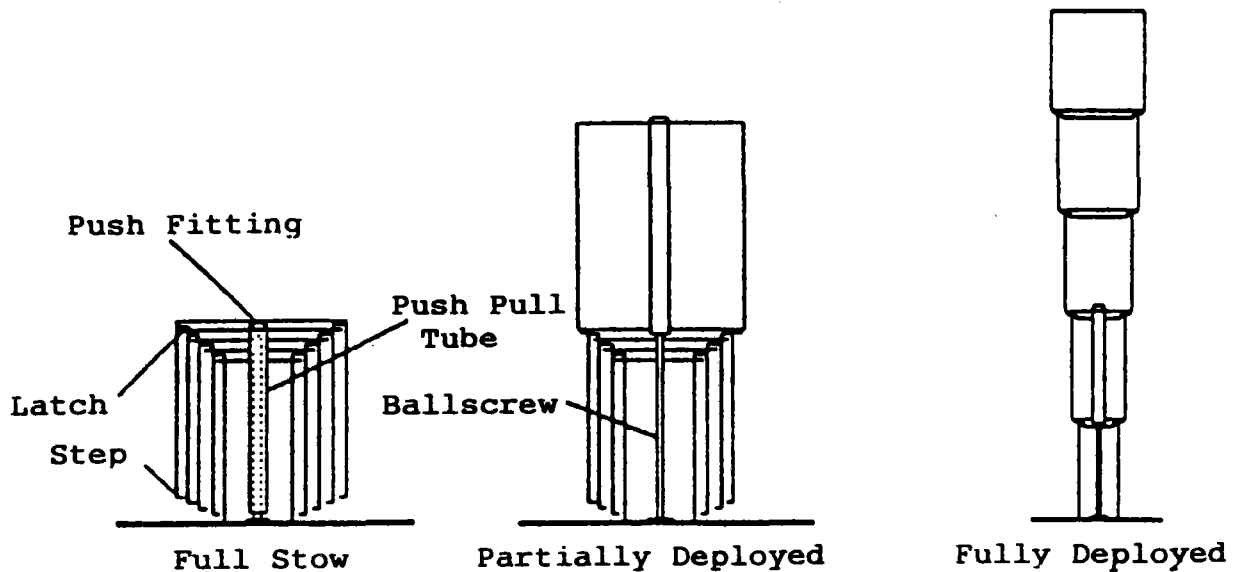


**Figure 24**  
**A ballscrew transports a tube which drives the individual strut tube segments to deployment in a synchronized fashion in the push-pull design**

#### 3.1.3.4 Cable-Pulley Concept

In the Cable-Pulley Concept, a cable (or tape) is routed inside each tube through a series of pulleys and anchored at the last tube. One end of the cable is attached to a motorized take up spool. As this spool is rotated by a motor, the tubes are pulled to deployment and the latches engage. The deployment sequence with this design concept is not necessarily sequential.

The cable-pulley design is a mechanical system with much heritage in ground based applications. Systems of this type have not been widely used in space for a variety of reasons. The reliability of such systems and the weight are the main disadvantages.

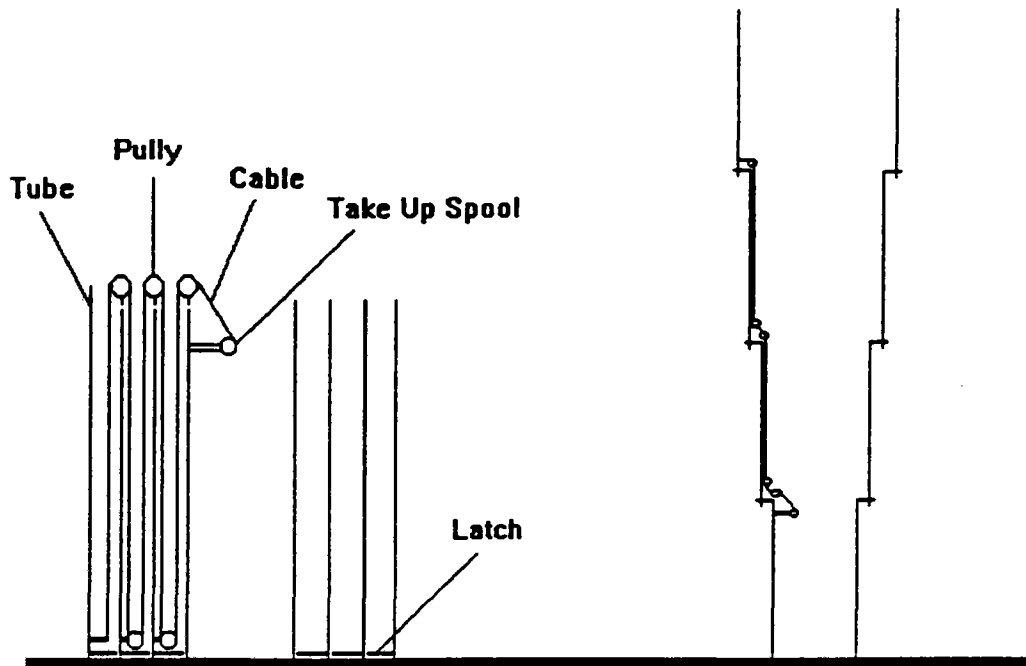


**Figure 25**  
**A rotating spool takes up a cable which pulls the tube segments to deployment in the cable-pulley concept**

### **3.1.3.5 Gear Drive Concept**

The Gear Drive design concept uses a compression spring to engage gear teeth on tracks running along the length of the strut tubes. A motor is used to drive the gears which causes the tubes to deploy and latch in place. The deployment in this concept is controlled and sequential.

This design is also a mechanical system with significant maturity. However, the lengthwise tracks in each tube add weight, complexity, and reliability concerns. This design is the least preferred of the mechanical systems.

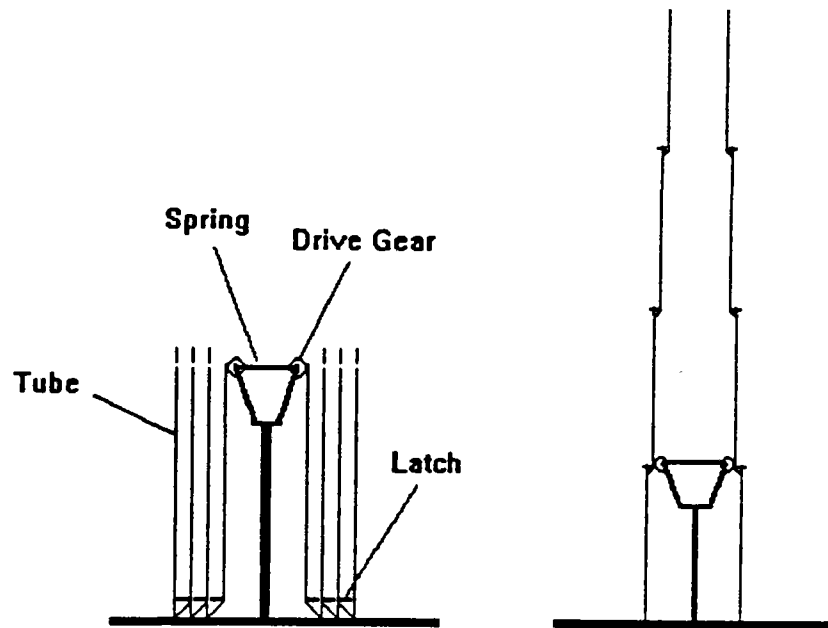


**Figure 26**  
**A motor turns gears which engage lengthwise tracks on each tube segment and deploys the segments sequentially**

### 3.1.3.6 Strut Deployment Design Selection

The five designs can be classified in two groups; inflation deployment or mechanical deployment. The inflation concepts (Bladder & Sealed Tubes) offer the advantage of less weight due to fewer parts. Also, the deployment force already exists on the spacecraft. However, the mechanical systems offer the advantages of design maturity, reliability, and testability.

The table below lists the results of the ranking of each of the design concepts considered. Each concept was ranked in each category on a scale of 1 to 5 (1= poor performance and 5= excellent performance). A weighting factor for each category was assigned based on relative importance to the program. The results of the ranking provide insight to the concept most suited for this program's application.

**Table 10. A trade matrix identifies the Push-Pull design as the most advantageous to the Solar Thermal Propulsion system**

|                         | <i>Simplicity</i> | <i>Maturity</i> | <i>Weight</i> | <i>Stowed</i> | <i>Reliability</i> | <i>Cost</i> | <i>Scaling</i> | <i>Total</i> | <i>Weighted</i> |
|-------------------------|-------------------|-----------------|---------------|---------------|--------------------|-------------|----------------|--------------|-----------------|
| <b>Weighting Factor</b> | 4                 | 1               | 2             | 1             | 4                  | 1           | 3              | N/A          | N/A             |
| <b>Bladder</b>          | 3                 | 2               | 4             | 4             | 2                  | 3           | 3              | 21           | 46              |
| <b>Sealed Tubes</b>     | 2                 | 2               | 4             | 4             | 2                  | 3           | 4              | 21           | 45              |
| <b>Push - Pull</b>      | 3                 | 4               | 3             | 3             | 3                  | 2           | 4              | 22           | 51              |
| <b>Cable - Pulley</b>   | 3                 | 3               | 3             | 3             | 2                  | 2           | 3              | 19           | 43              |
| <b>Gear Drive</b>       | 3                 | 2               | 3             | 3             | 2                  | 2           | 2              | 17           | 39              |

The results of the design trade indicate that the push-pull design was ranked the highest followed by both inflation concepts (Bladder and Sealed Tubes). The Push-Pull design is recommended.

### **3.1.4 Strut End Fittings**

The movement of the struts relative to the torus and the spacecraft is dictated by the deployment sequence of the structure. The deployment sequence described in Section 3.1.7 requires that both ends of each strut must be capable of rotation in two axes to enable the deployment.

The basic fitting design is the ball joint as shown in Figure 27. The specifics of each end fitting will vary depending on the strut (long strut or short strut) and the end (hoop end or spacecraft end). This design uses a spherical ball which is fixed in place using a support bracket. The rod end of the joint is attached to the strut which allows rotation about the spherical ball. The bushings are added to prevent contact of the rod end to the support bracket.

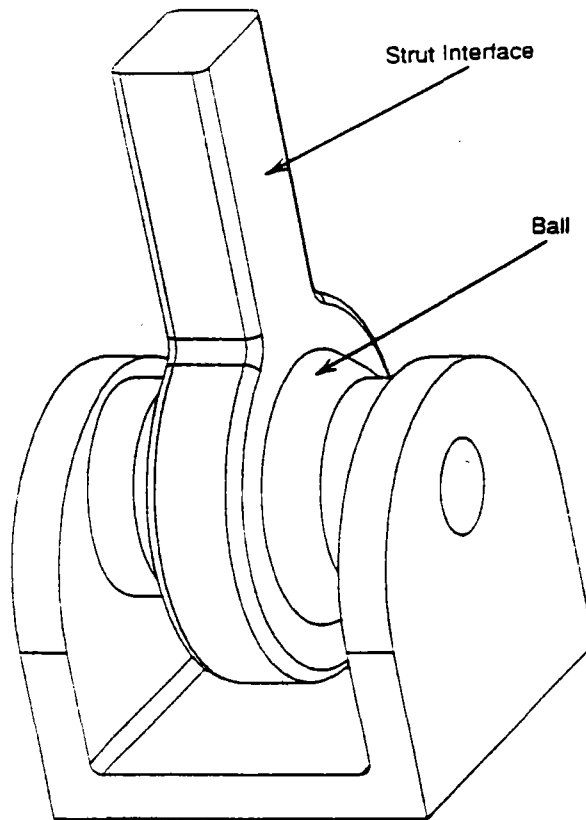


**Figure 27**

**A spherical ball joint at each end of the three struts allows the struts to rotate about three axes, a requirement for system deployment**

### **3.1.5 Torus to Concentrator Attachment**

This section describes the method by which the inflatable concentrator is attached to the deployable torus. This attachment scheme is directly related to the quality of the optical surface of the concentrator. Any uneven loading of the thin film concentrator could cause creases and reduce optical performance. The concepts considered are based on using the segmented circular deployable torus described in Paragraph 3.1.1 with an elliptical concentrator attached to the inside of the circle. Qualitative requirements for the torus to concentrator attachment are listed in Table 11.

**Table 11. Qualitative requirements for the attachment between the hoop and concentrator**

| Requirement            | Rationale  |
|------------------------|--|
| Deployable             | Design must deploy with the hoop and concentrator  |
| Even load distribution | Any uneven loads in the film can cause a wrinkle or a tear   |
| Lightweight            | Minimize system weight   |
| Adjustable             | Adjustment of the load during the manufacturing process is required to account for tolerance buildup |

Two design concepts were generated to attach the concentrator to the hoop.

The first method, shown in Figure 28, uses an undetermined number of stringers to connect the concentrator to the hoop. The stringers could be fabricated from graphite fibers which is space qualified and has a low coefficient of thermal expansion. The load would be transferred to the concentrator at distinct points around the perimeter. Previous experience with thin films dictates that stringers be placed at 1 inch increments around the circumference to avoid tears and wrinkles. Approximately 1000 stringers would be required for a flight experiment size concentrator. The individual stringers could be adjusted at any time to accommodate manufacturing uncertainties and tolerances.

A second method of attachment, shown in Figure 29, involves the use of a mesh material with low stiffness and high elasticity to provide even load distribution. The mesh material is attached continuously around the concentrator. It is also directly attached to each segment of the hoop. This design creates an even load distribution in the concentrator but is not easily adjustable during the manufacturing process.

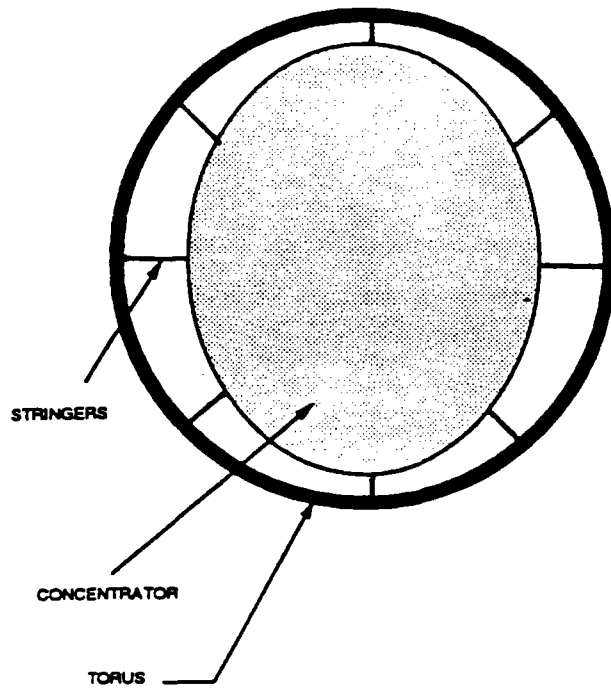


**Figure 28**  
Individual stringers could be used to transfer loads from the hoop to the concentrator

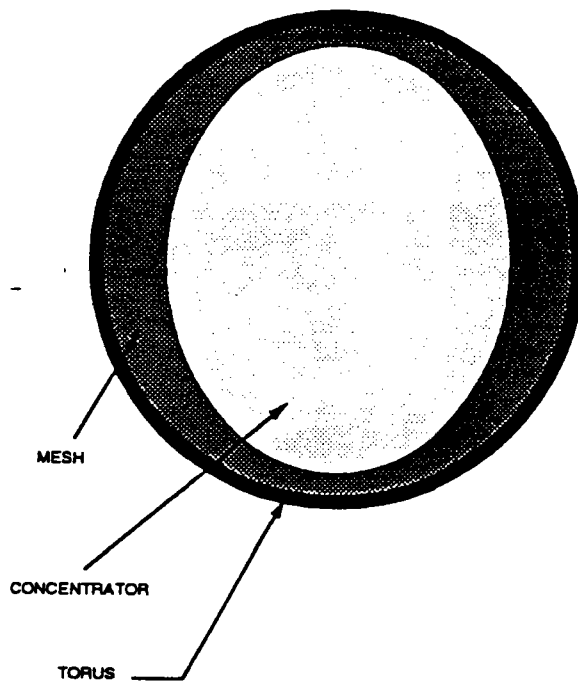


**Figure 29**  
A mesh material could be used to evenly distribute load to the concentrator

The best attachment design is a hybrid of the two methods and is shown in Figure 30. The mesh material is used to attach directly to the concentrator to provide even load distribution into the thin film. A series of stringers is attached to the edge of the mesh and then to the hoop segments. Adjustment of these stringers would provide the needed manufacturing adjustment capability. In addition, the number of stringers necessary is greatly reduced (to 100 nominally) which reduces part count.

**CONCEPT #3: STIFFENED RING**

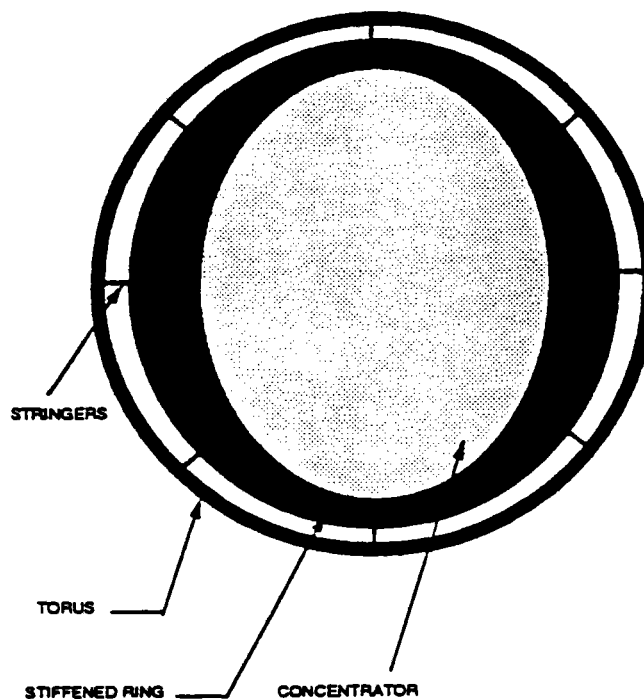


**Figure 30**

**A hybrid design capitalizes on the strong points of the mesh attachment method (even loads) and the stringer attachment method (adjustability)**

### 3.1.6 Stowed Package

The stowed volume goal for the system (see Section 2.3) is to package a flight experiment within the available volume of a Get Away Special (GAS) container. The available volume in a GAS, after accounting for the volume of NASA reserved space and the electrical, pneumatic and mechanical support equipment for the flight experiment, is 3544 cubic inches. This volume is cylindrical in shape, 12.5 inches high and 19 inches in diameter. The present design, in its current state, packages into a cylinder 28 inches high and 28 inches in diameter.

The entire system (deployable concentrator, hoop and struts) packages within the cylindrical volume of the hoop as demonstrated in Figure 31. The struts are nested and attached at approximately 120 degree increments inside the stowed hoop. The stowed height of the struts is a function of the number of strut segments. The stowed strut height is 28 inches as described in Section 3.1.2. The concentrator is folded and placed within the hoop and struts. This packaging of the system is critical to a smooth deployment since any snag could cause the deployment to stop. Harris has successfully handled similar packaging of deployable antennas where the reflective surface mesh can easily snag and disrupt deployment.

The hoop (as described in Section 3.1.1) stows into a cylindrical shape. The aspect ratio of the cylinder is a function of the number of segments in the hoop. Figure 32 shows that as the number of hoop segments increases the height of the stowed hoop decreases and the diameter of the stowed hoop increases. The stowed length of the torus is equal to the circumference of the deployed torus divided by the number of segments. The diameter of the stowed torus is given by the equation:

$$D \approx \frac{n*d}{\pi}$$

where:  $D$  = Diameter of stowed torus  
 $n$  = Number of torus segments  
 $d$  = tube diameter of torus segments  
 $\pi$  = 3.14159

Figures 33 and 34 demonstrate the relationship of stowed volume and hoop weight to the number of hoop segments. As the number of segments increases, stowed volume and weight increase due to an increase in fittings and hinges in the hoop. The system designer is able to trade off stowed height with stowed diameter and weight to meet specific available volume and weight goals.

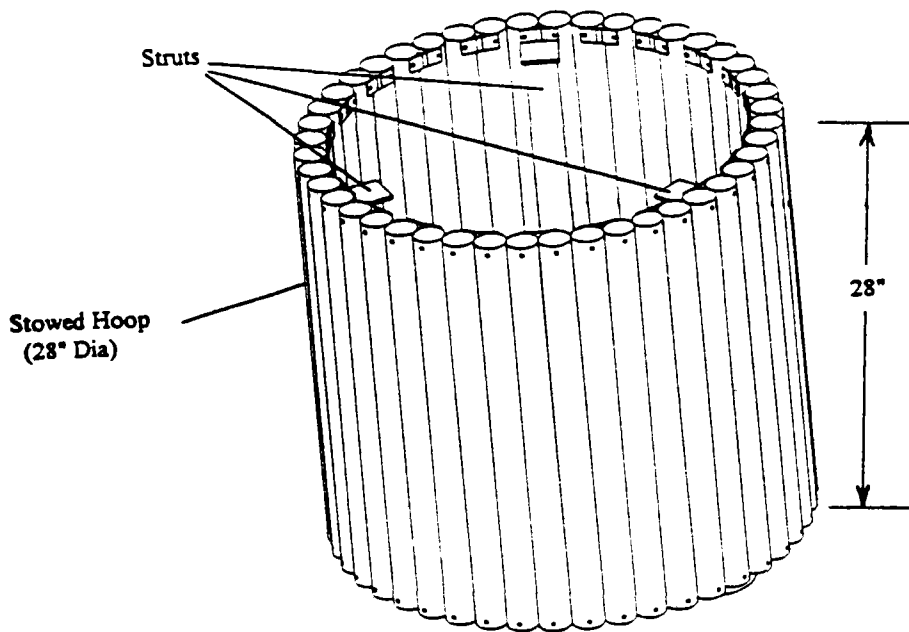


**Figure 31**  
The entire concentrator and support structure stows within the stowed hoop

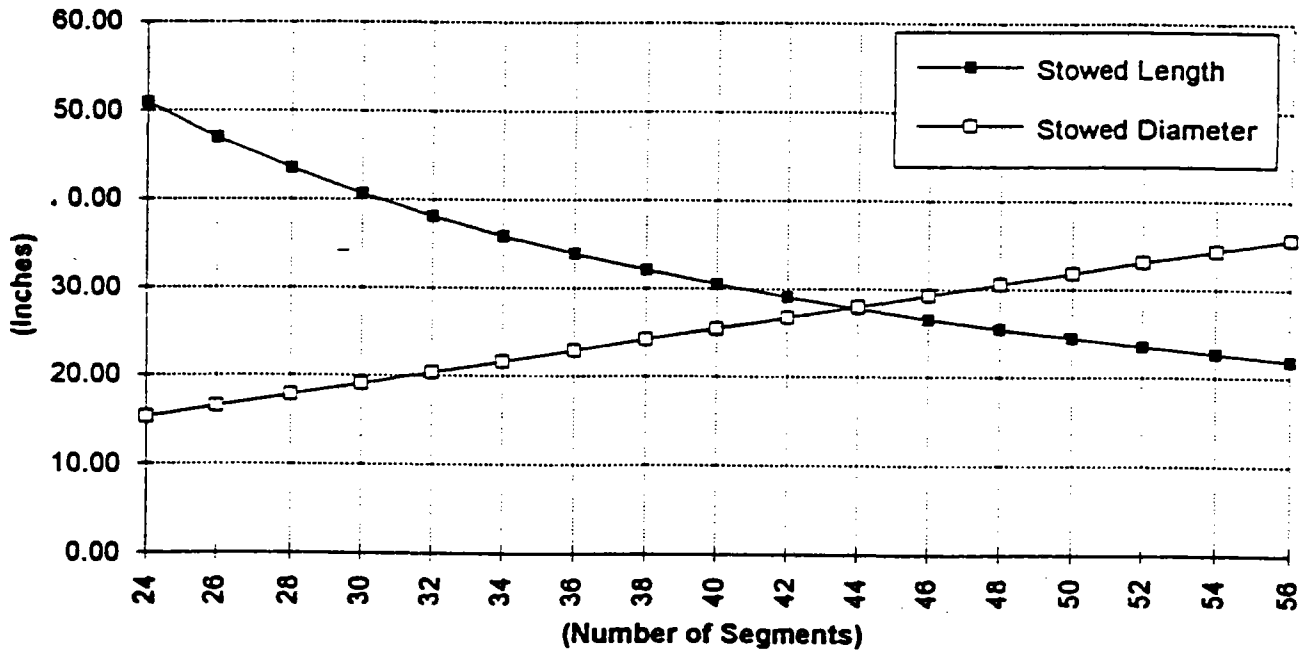


**Figure 32**  
The system designer is able to choose stowed length and stowed diameter by simply adjusting the number of hoop segments

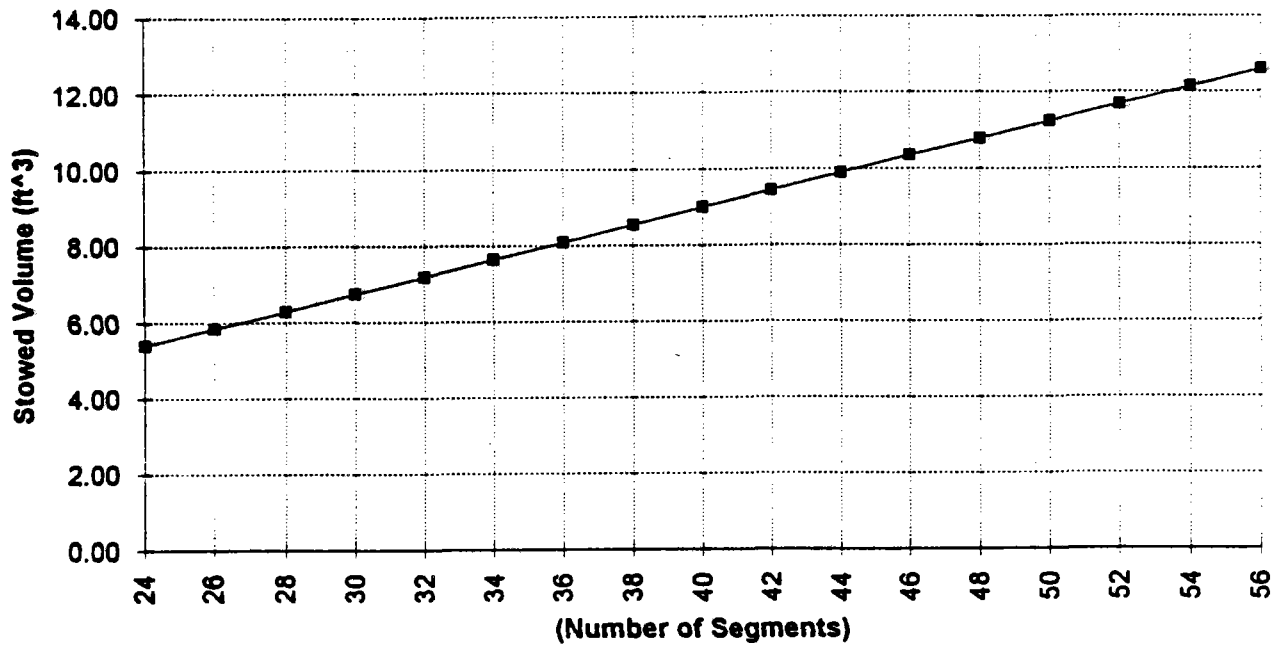


**Figure 33**  
 Stowed volume of the hoop increases as the number of segments increases

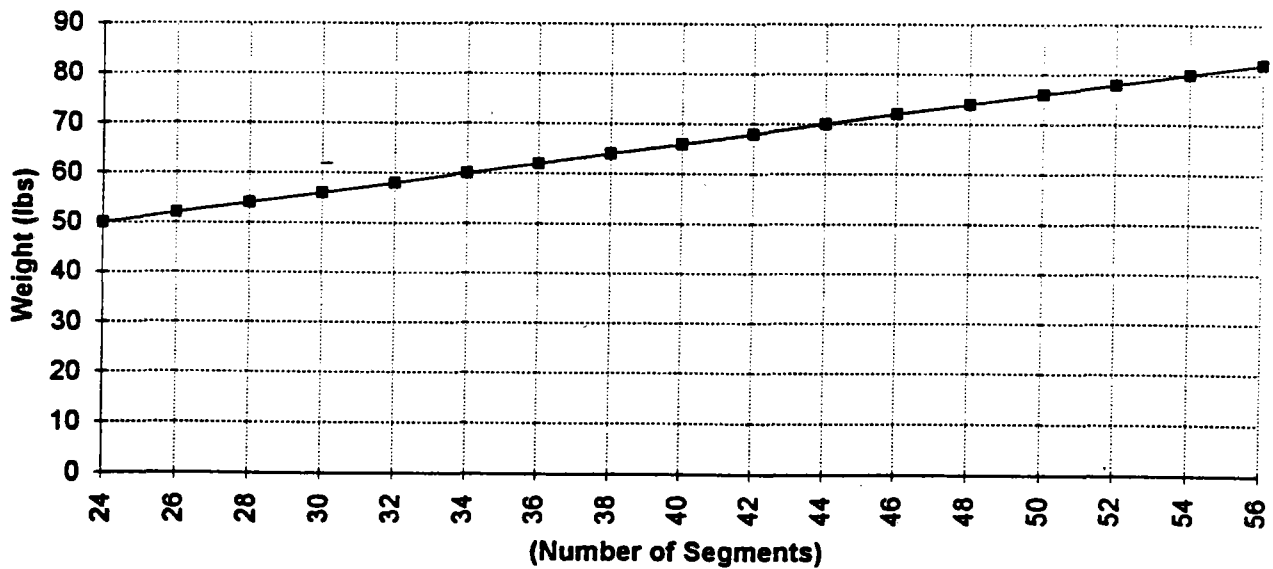


**Figure 34**  
 Hoop weight increases as the number of hoop segments increases

There is no hoop design, however, that will package within the available volume of the GAS. Therefore, in an attempt to balance volume and weight, a 44 segment hoop was chosen as a point design. This hoop yields a stowed diameter of 28 inches and a stowed height of 28 inches for the flight experiment.

A similar design has been generated for a full scale (30 meter by 40 meter) concentrator. Figure 35 displays stowed length and stowed diameter as a function of the number of segments of the hoop (segment diameter 2.5 inches). Assuming that a cylinder of aspect ratio equal to 1 is desired, a hoop of 78 segments produces a stowed height of 65 inches and a stowed diameter of 65 inches.

**Flight Model Stowed Dimensions**

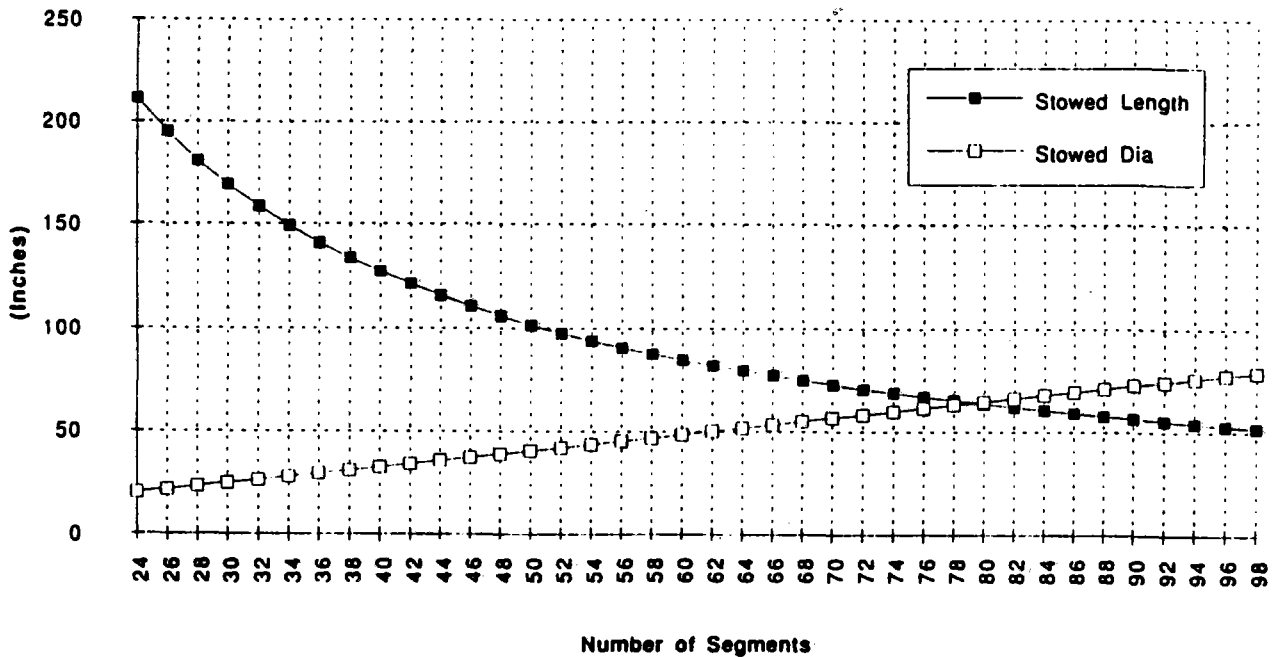


**Figure 35**  
**Stowed dimensions of the full scale system are also a function of the number of hoop segments**

### 3.1.7 System Deployment

The process by which the system articulates from the fully stowed position to the fully deployed position is extremely important to mission success. Any small error in this deployment process could lockup the structure, preventing further deployment, and render the system useless. Harris has successfully demonstrated equally difficult deployments of communication antennas in space over the last 10 years. A slow, controlled deployment is key to achieving the fully articulated structure. The difficulty of this task is amplified by the desire to package these structures into smaller and smaller volumes for launch. The stowed package for the support structure is shown in Figure 36.

The system deployment scenario for this structure can be broken down into four basic stages:

1. Deploy all three struts simultaneously to 152.5 inches. The hoop and concentrator assembly will separate from the equipment section as shown in Figure 37. The short strut is fully deployed at this point. Telemetry at the latches of the short strut can verify full deployment of the strut.
2. Deploy the torus assembly as shown in Figures 38 through 40. This will cause the two long struts to further deploy and will open the folded concentrator. Telemetry at the latches of the hoop can verify full deployment of the hoop.
3. Deploy the long struts to their full length. This will cause the concentrator assembly to tilt to the desired offset optical configuration as shown in Figure 38. Telemetry at the latches of the long strut can verify full deployment of the long struts.
4. Complete the deployment by inflating the concentrator.

Small, synchronized motors in the strut deployment system and the hoop enable a slow controlled deployment, to minimize the risk of deployment problem.

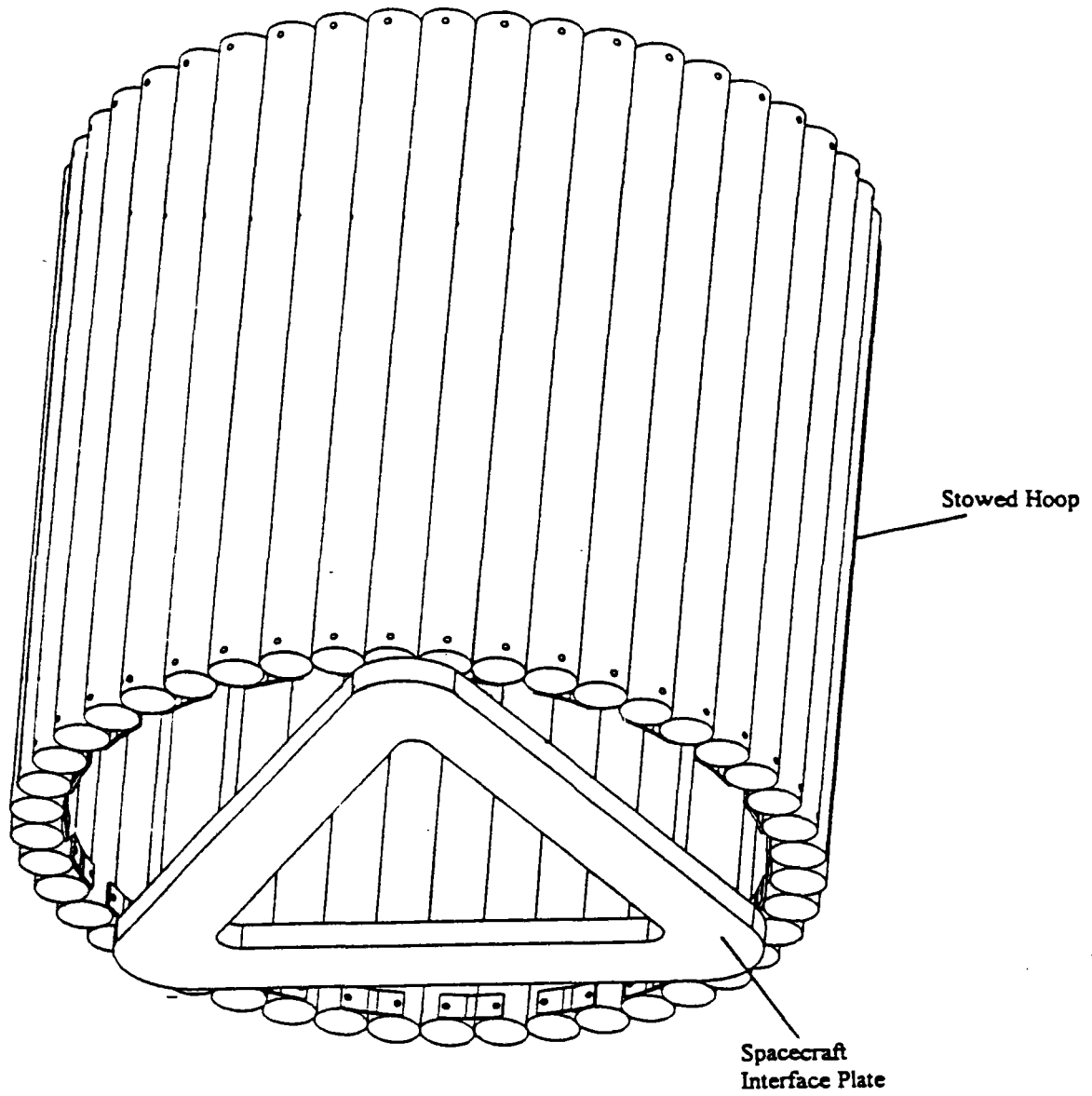


**Figure 36**  
**The support structure and concentrator begin the deployment**  
**from the fully stowed position**

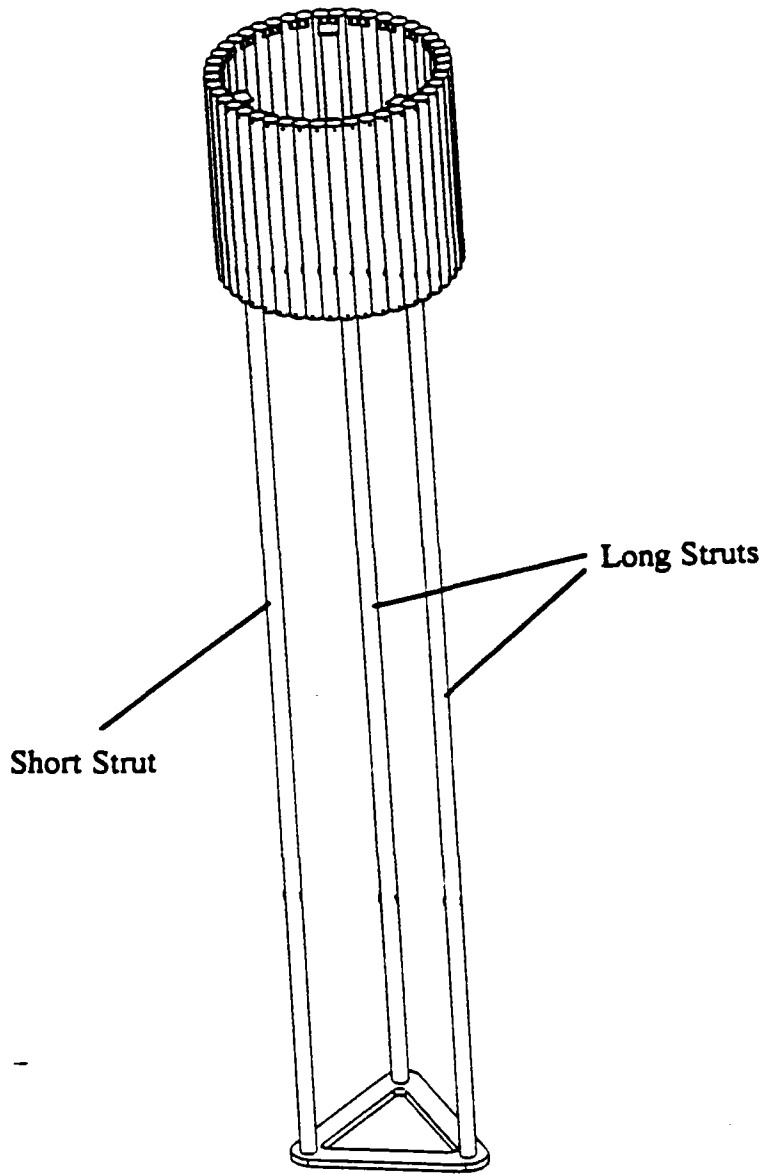


**Figure 37**  
The first deployment motion is the deploying of the three struts which moves the hoop and concentrator away from the spacecraft

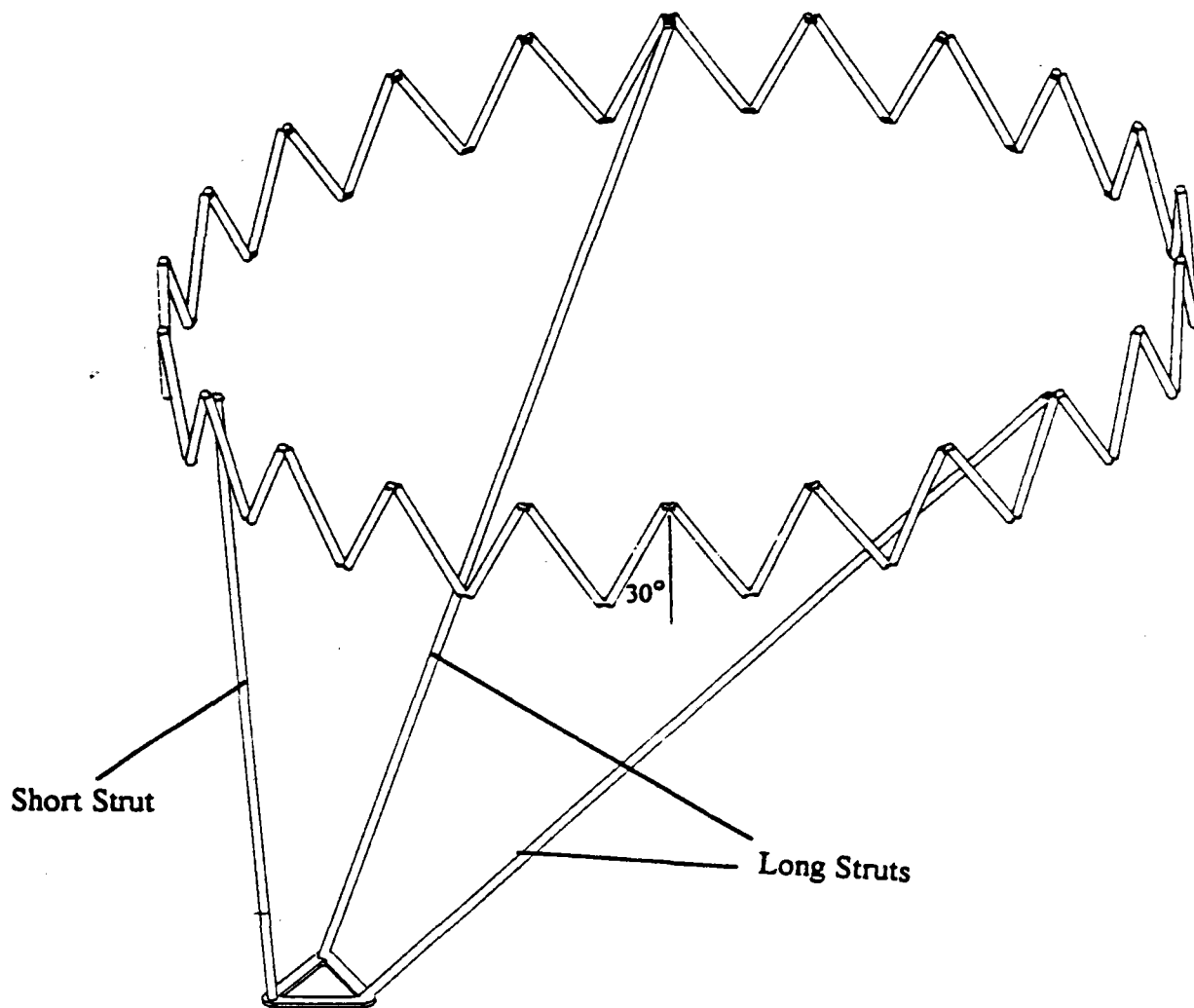


**Figure 38**  
Activation of the deployment motors begins the articulation of the hoop. In this view the hinges of the hoop have deployed 30°

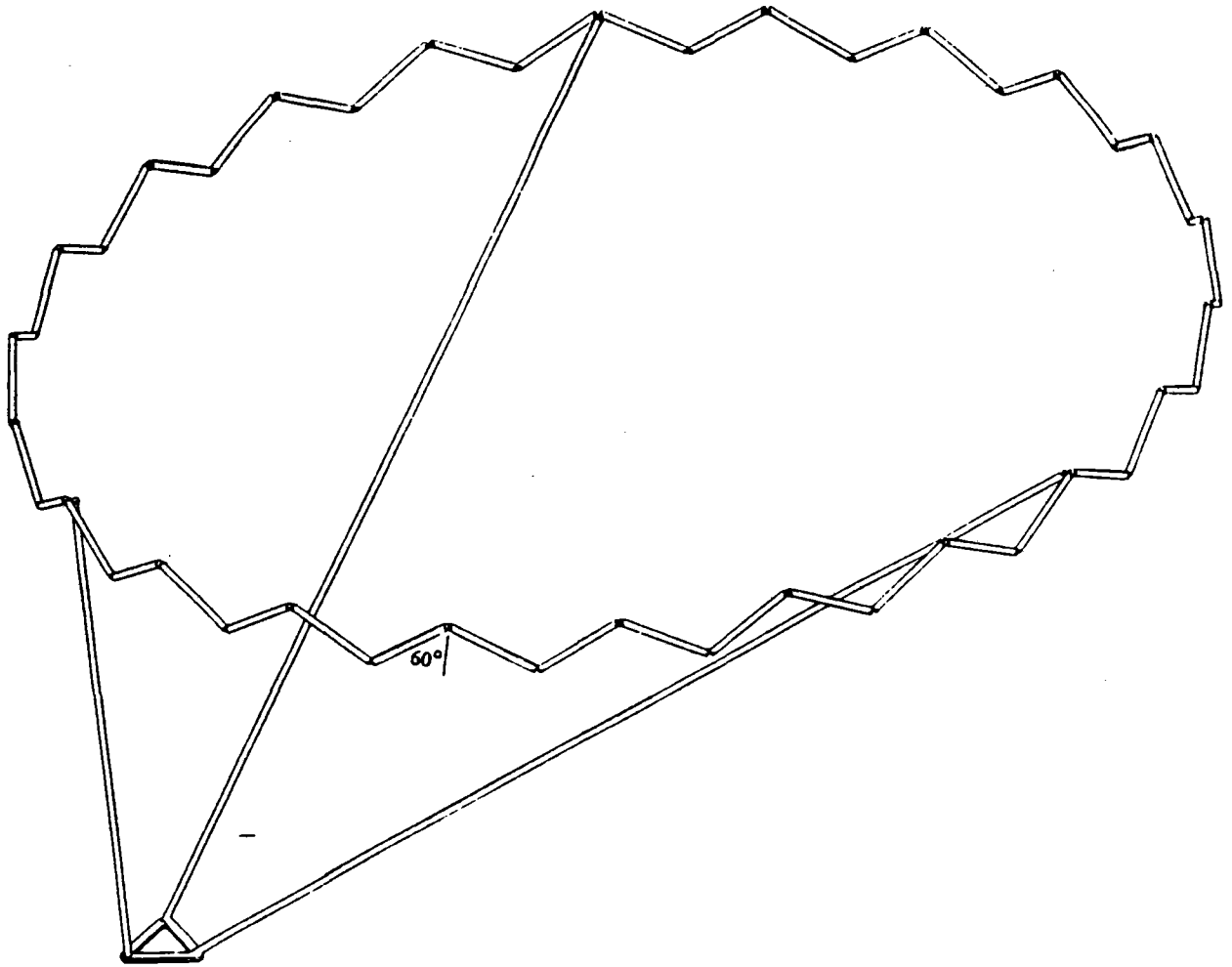


**Figure 39**  
**As the hoop deploys the long struts extend also, further**  
**deploying the structure**

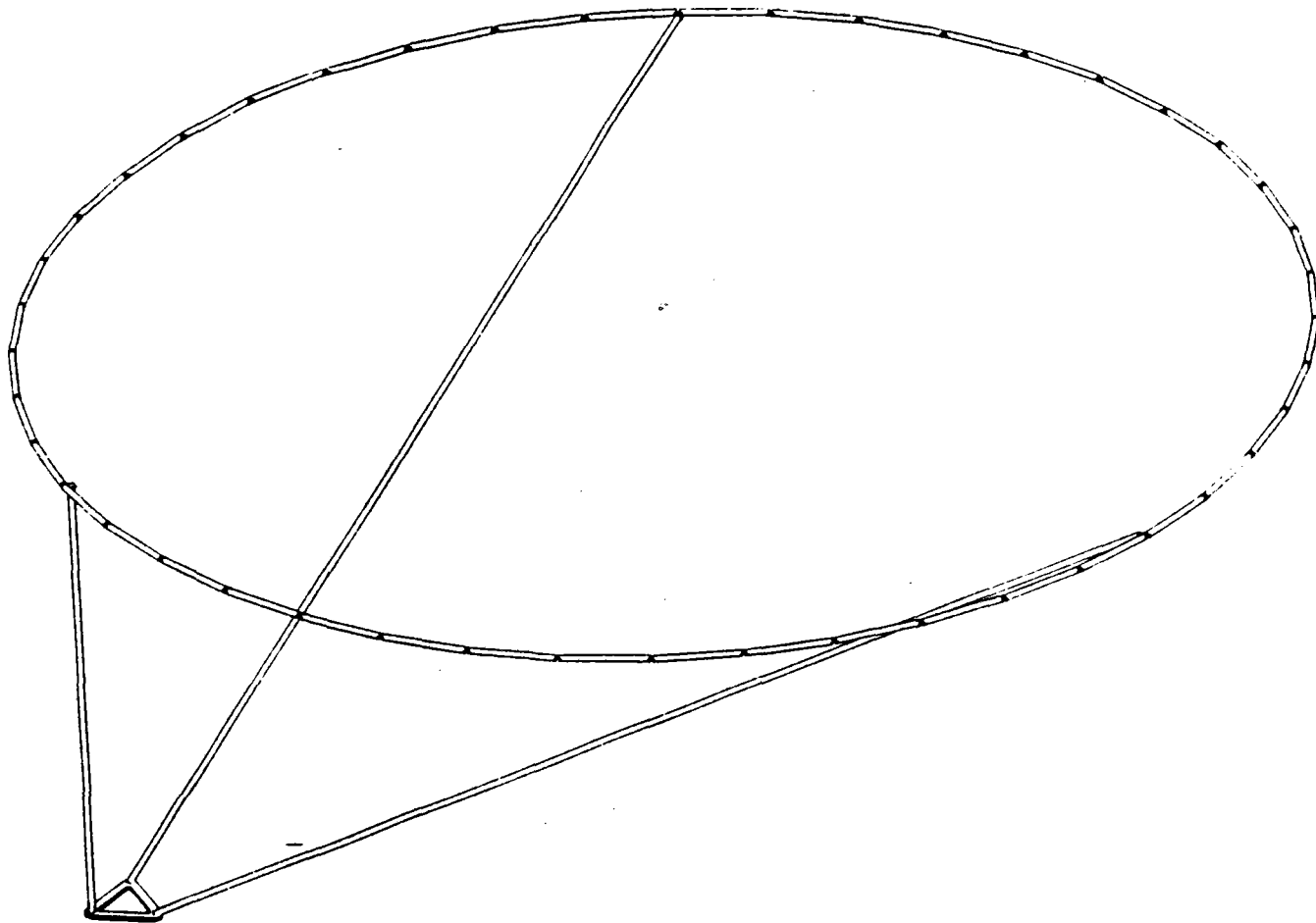


**Figure 40**  
The hoop is fully deployed when the hinges lock out. Motors are automatically shut off upon lockout

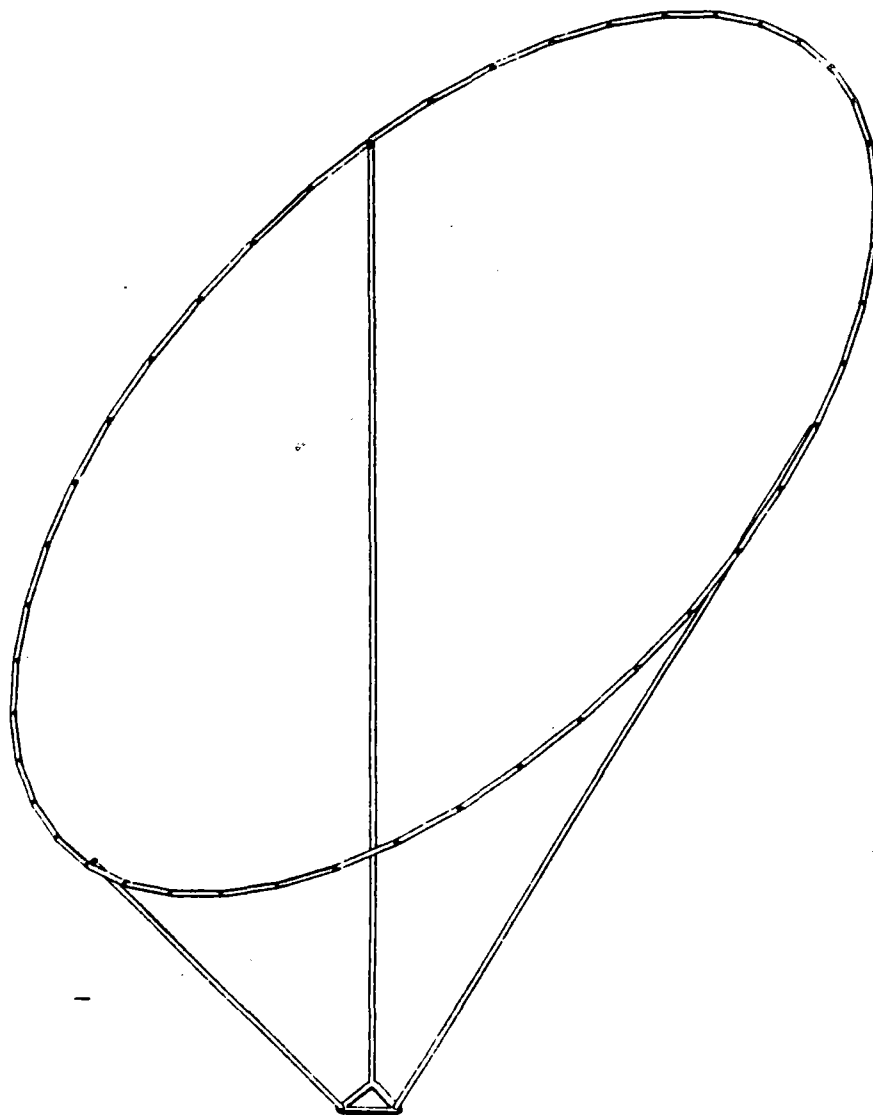


**Figure 41**  
**Deployment of the long struts to their full length sets the**  
**concentrator in the offset position**

An experiment was performed to evaluate the packaging and deployment of a thin film concentrator and a segmented torus. An existing 16 foot diameter concentrator,  $F/d=0.7$ , was integrated with a simulated segmented torus. The concentrator was made of NASA-Langley polyimide film of thickness 0.0015 inches. No canopy was used in this experiment. The simulated segmented torus was made by joining together 14, 2 foot long, 0.5 inch diameter PVC pipes. The segments were joined together by drilling holes in both ends of the PVC pipes and using string to connect the pipes together. The string allowed the pipes to be folded together by provided no rigidity. The torus did not include any locking hinges at the tube ends.

This configuration was used to investigate the packaging and deployment of the concentrator and torus and not the planarity or operation characteristics of the concentrator or torus once deployed. Figure 42 through 46 depict the packaging of the torus and thin film concentrator. This packaging method is analogous to the deployment method shown in Figure 37 through 40. The packaging of the concentrator with the torus worked well, but care had to be taken to keep the film from "snagging" the torus segments. The film and torus deployment proceeded with relative ease compared to the folding operation. Improved handling methods and hardware could be developed in a future study to aid in folding and packaging of the concentrator and torus.

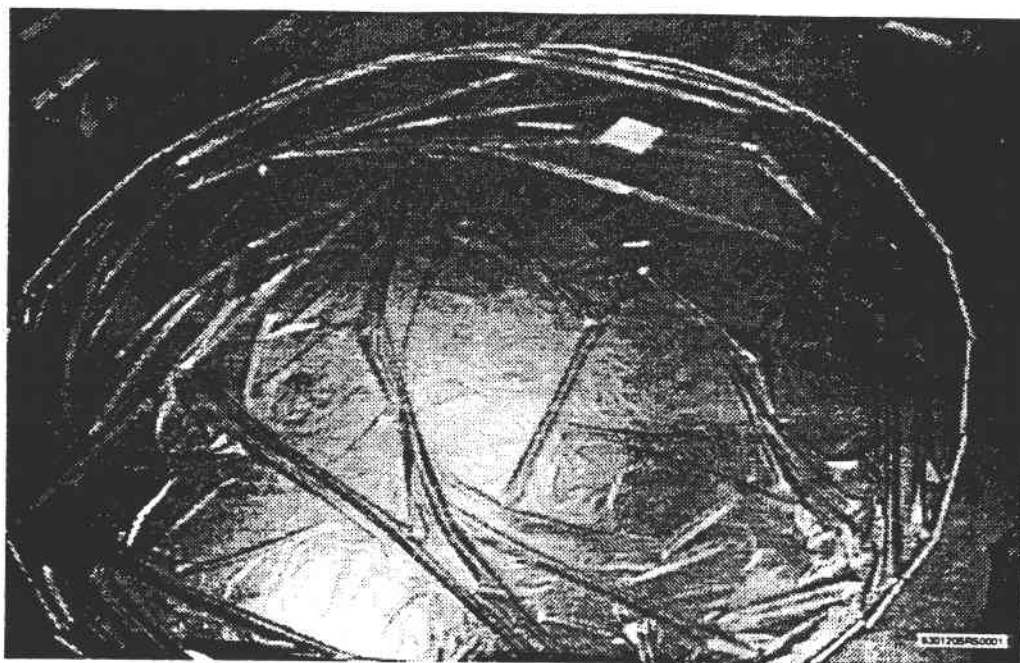


**Figure 42**  
Fully deployed torus attached to a 16 foot membrane

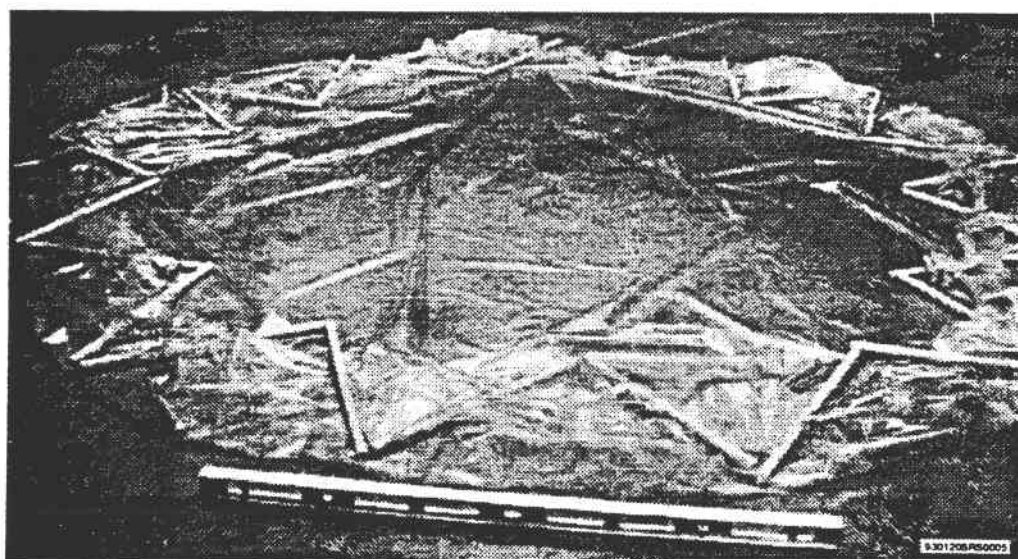


**Figure 43**  
Membrane and torus after three folding pattern. Diameter is approximately 9 feet

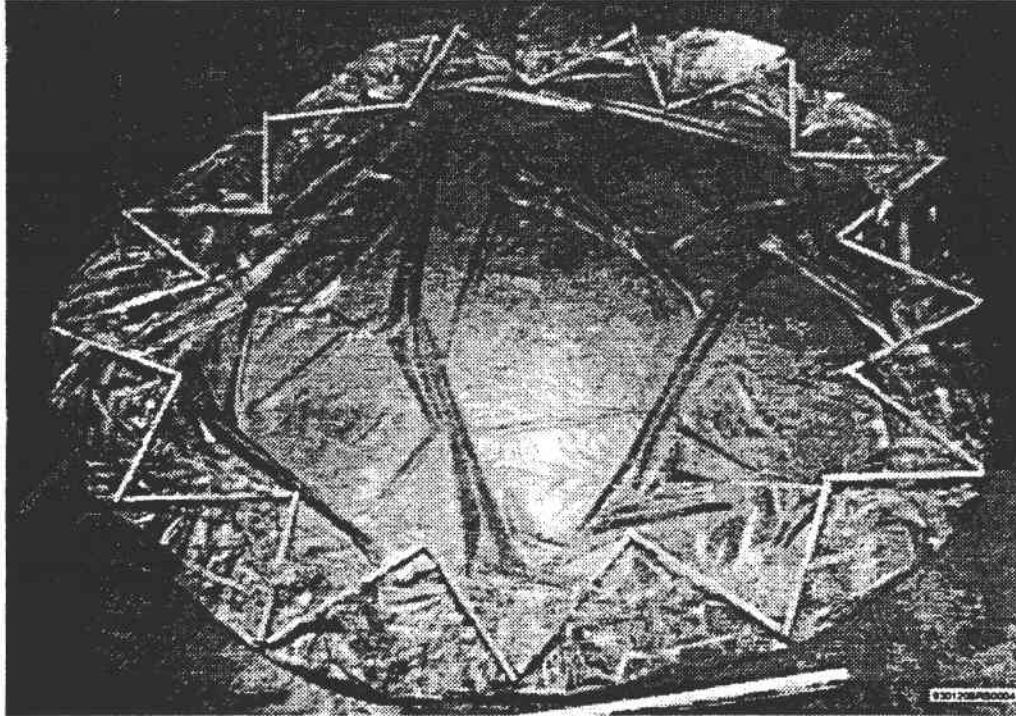


**Figure 44**  
Top view of the membrane and torus after three folding steps

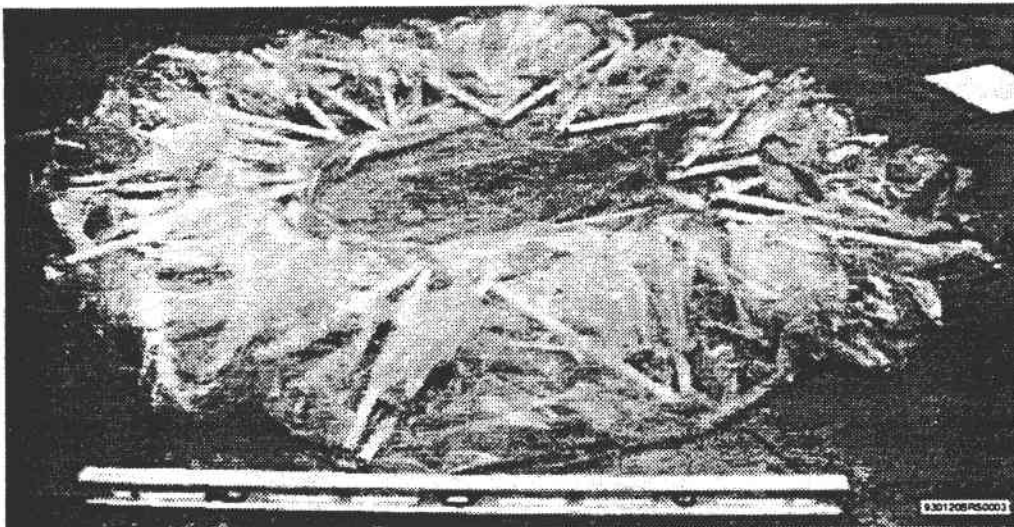


**Figure 45**  
Membrane and torus at 4-6 foot diameter. Notice the film is between some of the torus segments

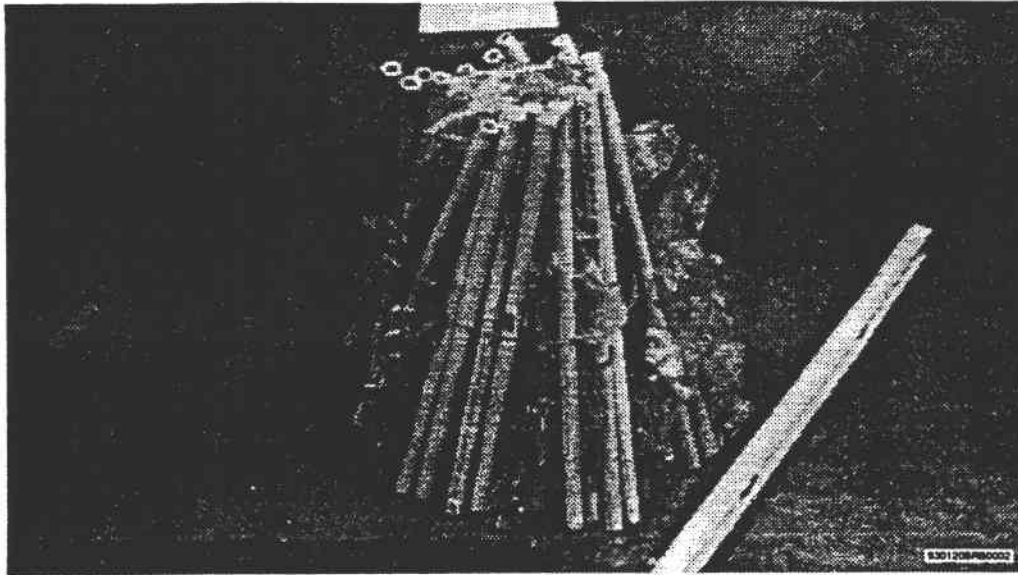


**Figure 46**  
**Membrane and torus fully packaged for deployment**

### **3.1.8 Weight Summary**

Weights were calculated for the three main components of the design; the concentrator, the hoop and the struts. The concentrator weight was calculated using the well known properties of the thin film. Inflation gas was not included in this weight. The hoop weights were calculated from design curves generated for an LSST hoop and were modified based on design changes described in Section 3.1.1. Strut and strut latch weights were determined by calculations from the CAD solid model of the latch design. The flight experiment size concentrator/support structure weight is given in Table 12. At 123.8 pounds, the weight budget does not satisfy the requirement established in Section 2.0 (85.5 pounds). The main reason is the use of the mechanical hoop assembly as described in Section 3.1.1. The mechanical hoop assembly requires significantly more weight than a comparable inflatable design. However, the mechanical design is much more mature and therefore lower in cost and risk.

A weight budget for the full scale concentrator and support structure is shown in Table 12.

**Table 12. Flight Experiment Concentrator/Support Structure Weight Budget**

| <b>Item</b>        | <b>Part</b>                       | <b>Weight (pounds)</b> | <b>Source</b> |
|--------------------|-----------------------------------|------------------------|---------------|
| Concentrator       | Reflector                         | 4.49                   | Calculation   |
|                    | Canopy                            | 4.43                   | Calculation   |
| Concentrator total |                                   | 8.92                   |               |
|                    |                                   |                        |               |
| Hoop               | tubes (44)                        | 21.1                   | Calculation   |
|                    | hinges (44)                       | 15.8                   | CAD Model     |
|                    | latches (22)                      | 5.0                    | Design Curves |
|                    | motors (6)                        | 5.5                    | Estimates     |
|                    | tapes (6)                         | 11.0                   | Calculation   |
|                    | hoop-to-strut interface (3)       | 3.0                    | Estimated     |
| Hoop total         |                                   | 61.4                   |               |
|                    |                                   |                        |               |
| Long struts (2)    | latches (26)                      | 4.8                    | CAD Model     |
|                    | tubes (28)                        | 11.2                   | Calculation   |
| Short strut        | latches (5)                       | 1.2                    | CAD Model     |
|                    | tubes (6)                         | 3.0                    | Calculation   |
|                    | stringer (9)                      | 6.2                    | Calculation   |
|                    | strut-to-spacecraft interface (3) | 3.0                    | Estimated     |
| Deployment System  | inflation gas                     | <0.01                  | Calculated    |
|                    | valves and pressure lines         | 1.0                    | Estimated     |
|                    | seals & attachment hardware (26)  | 1.0                    | Estimated     |
|                    | cable                             | 0.2                    | Calculated    |
|                    | motor (1)                         | 0.5                    | Estimated     |
|                    | winding drum (1)                  | 0.8                    | Estimated     |
| Struts total       |                                   | 32.9                   |               |
|                    |                                   |                        |               |
| Subtotal           |                                   | 103.2                  |               |
| Contingency (20%)  |                                   | 20.6                   |               |
| System Total       |                                   | 123.8                  |               |

**Table 13. Full Scale Concentrator/Support Structure Weight Budget**

| <b>Item</b>        | <b>Part</b>                       | <b>Weight (pounds)</b> | <b>Source</b> |
|--------------------|-----------------------------------|------------------------|---------------|
| Concentrator       | Reflector                         | 71.84                  | Calculation   |
|                    | Canopy                            | 70.88                  | Calculation   |
| Concentrator total |                                   | 142.7                  |               |
| Hoop               | tubes (78)                        | 107.6                  | Calculations  |
|                    | hinges (39)                       | 27.9                   | CAD Model     |
|                    | latches (39)                      | 8.9                    | Design Curves |
|                    | motors (20)                       | 10.0                   | Estimate      |
|                    | tapes (6)                         | 44.0                   | Calculation   |
|                    | hoop-to-strut interface (3)       | 6.0                    | Estimated     |
| Hoop total         |                                   | 204.4                  |               |
| Long struts        | latches (48)                      | 12.8                   | CAD Model     |
|                    | tubes (50)                        | 85.6                   | Calculation   |
| Short struts       | latches (9)                       | 3.4                    | CAD Model     |
|                    | tubes (10)                        | 22.9                   | Calculation   |
|                    | stringer (9)                      | 24.8                   | Estimated     |
|                    | strut-to-spacecraft interface (3) | 6.0                    | Estimated     |
| Deployment System  | inflation gas                     | <0.01                  | Calculated    |
|                    | valves and pressure lines         | 4.0                    | Estimated     |
|                    | seals & attachment hardware (26)  | 8.0                    | Estimated     |
|                    | cable                             | 0.8                    | Calculated    |
|                    | motor (1)                         | 1.0                    | Estimated     |
|                    | winding drum (1)                  | 3.2                    | Estimated     |
| Struts total       |                                   | 172.5                  |               |
| Subtotal           |                                   | 519.6                  |               |
| Contingency (20%)  |                                   | 103.9                  |               |
| System Total       |                                   | 623.5                  |               |

### 3.1.9 System Performance

This section will examine structural deformations due to external forces applied to the structure, and the resulting effect on optical performance. The primary requirements of the structure, as stated in Section 2.2, are to maintain pointing accuracy to within 0.5' and to obtain a first natural frequency of vibration greater than 0.1 Hertz. The satisfaction of these requirements enables the structure to maintain the supply of concentrated energy to the aperture.

Two types of external forces are of interest here. First, loading due to constant acceleration results in static deformations and allows us to assess gross structural stiffness. Second, we are interested in dynamic forces (such as firing a thruster) which cause transient deformations of the structure. The latter is considerably more complicated and involves the determination of the structures' fundamental frequencies (modes) of vibration as an intermediate step. A necessary prelude to this is to bring internal structural forces (tensions and compressions) into static equilibrium.

#### 3.1.9.1 Finite Element Model Description

The primary tool in this evaluation is a Finite element Model (FEM) of the support structure described in the previous sections. The FEM has 491 coordinates and 778 elements which result in a system of 1359 equations. A series of 158 beam, 264 membrane and 356 stringer elements are used in addition to 62 point masses, which account for latches and fittings. The stringers are graphite cords with 0.032 square inches of cross sectional area and the beams are graphite-epoxy tubes with .015 inch wall thickness, as previously described in Section 3.1.2. The tube radii vary from 1.5 inches to 3 inches, depending on function. The membranes are polyimide with 0.001 inch thickness.

A plot of the FEM geometry is shown in Figure 47. The node numbering scheme is summarized in Table 14. Of particular interest are the nodes which define the principal substructure interfaces, namely the reflector/canopy (R/C) rim nodes (44-91), and the strut attachment points at the hoop (139, 147, 155) and spacecraft (316, 348, 380). The canopy membrane elements are not shown in most of the following plots for clarity, however their effect is accounted for in the results.

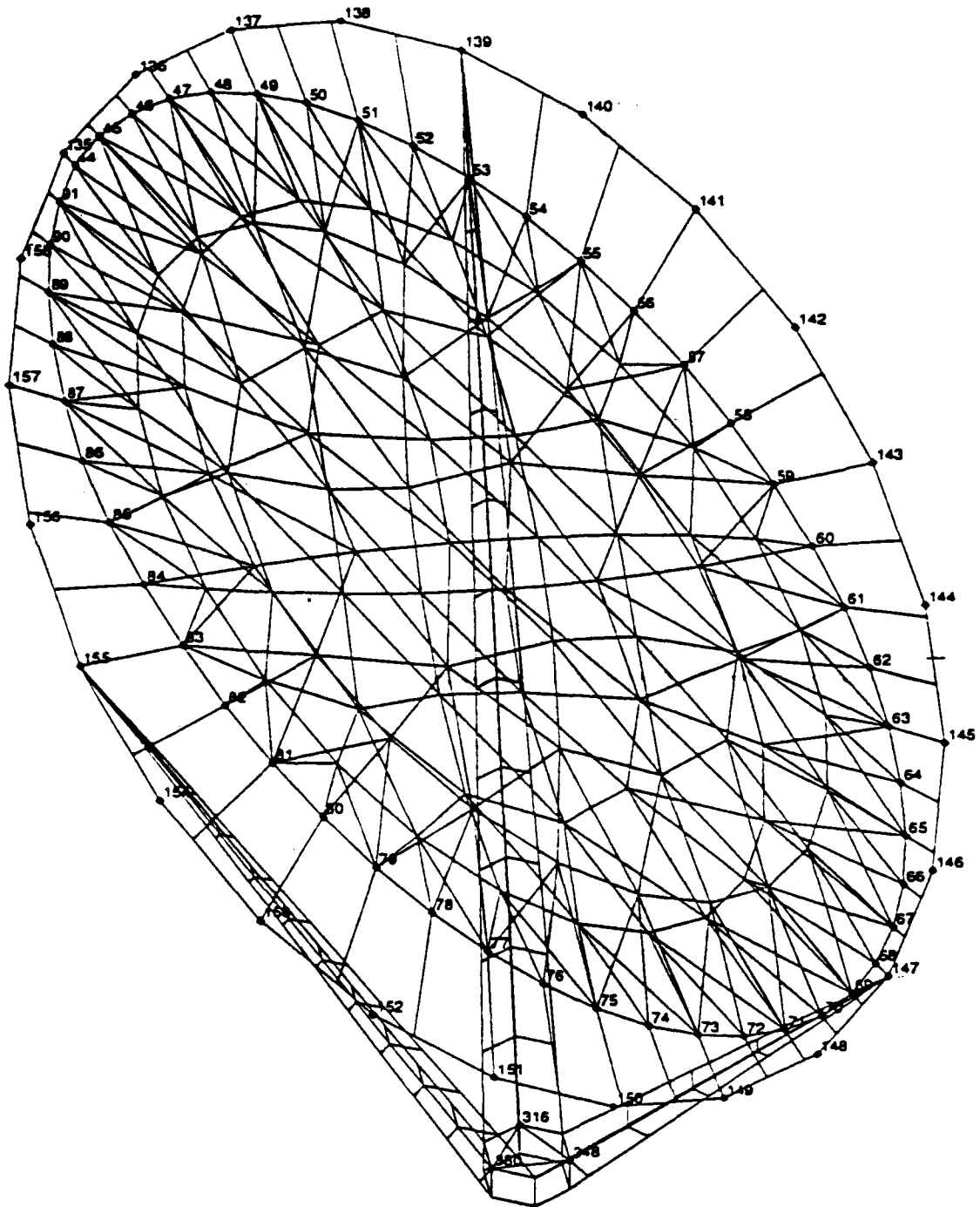


**Figure 47**  
**A finite element model of the support structure is the primary evaluation tool**

**Table 14. The node numbering scheme for the principal nodes of the support structure finite element model**

| NODES       | DESCRIPTION                             |
|-------------|---|
| 1-43        | reflector nodes                         |
| 44-91       | reflector/canopy rim nodes              |
| 92-134      | canopy nodes                            |
| 135-158     | hoop vertices (latch/fitting locations) |
| 160-226     | stringer attach points on hoop beams    |
| 317-327     | long strut #1 beams (latch locations)   |
| 349-352     | short strut beams (latch locations)     |
| 381-391     | long strut #2 beams (latch locations)   |
| 316,348,380 | strut-attachments, top of SC            |
| 331,363,395 | stringer-attachments, bottom of SC      |
| 332,364,396 | stringer-attachment, top of SC          |

The spacecraft equipment section (SC) is modeled by 12 point masses (5.5 pound weight each) arranged in two hexagons made of infinitely rigid beams. The use of infinitely rigid beams eliminates high frequency shell modes of the SC which are irrelevant to this analysis. The hexagons correspond to the top and bottom of the equipment section. For reference, the strut interface is referred to as being on the top of the SC. The total mass of the system is modeled as 201.4 pounds.

The parabolic geometry of the concentrator system is based on the HAIR Phase II reports,<sup>7</sup> scaled so that the focal length is 135.6 inches. The focal point for the parabolic reflector falls at the centroid of the strut attachment points on the top of the SC, which lies in the y-z plane of the global coordinate system. The reflector and canopy are symmetric with respect to their rim-interface plane, which forms an angle of 47.3 degrees with respect to the y-z plane. The entire structure is symmetric with respect to the global x-y plane.

### 3.1.9.2 Internal Static Load Analysis

The deployed stiffness of the support structure depends on axial compression of beams by a network of tension cords (stringers). Stringer layout was guided by the philosophy that the principal substructures should be independently self supporting. Thus if a single stringer fails, the composite structure retains some stiffness and does not necessarily collapse. This also allows substructure models to be developed and tested separately.

A web of cords between the hoop and inflatable reflector/canopy rim bears the reaction forces which maintain the proper reflector shape. These forces were determined for this geometry in the context of a continuous membrane media by Grossman.<sup>8</sup> The reaction forces of the current finite element R/C model at discrete rim nodes are shown in Figure 48. The internal pressure load of the membranes is 0.0015 psi. This results in a peak membrane stress of 520 psi. In the figure, a coordinate transformation has been applied to put the forces in the same plane used in the Grossman study. Nodes 44 and 68 define the major axis of the ellipse, while nodes 56 and 80 define the minor axis. Therefore, within the granularity limits of the current model, the reaction forces agree well with Grossman and validate the membrane portion of the FEM.

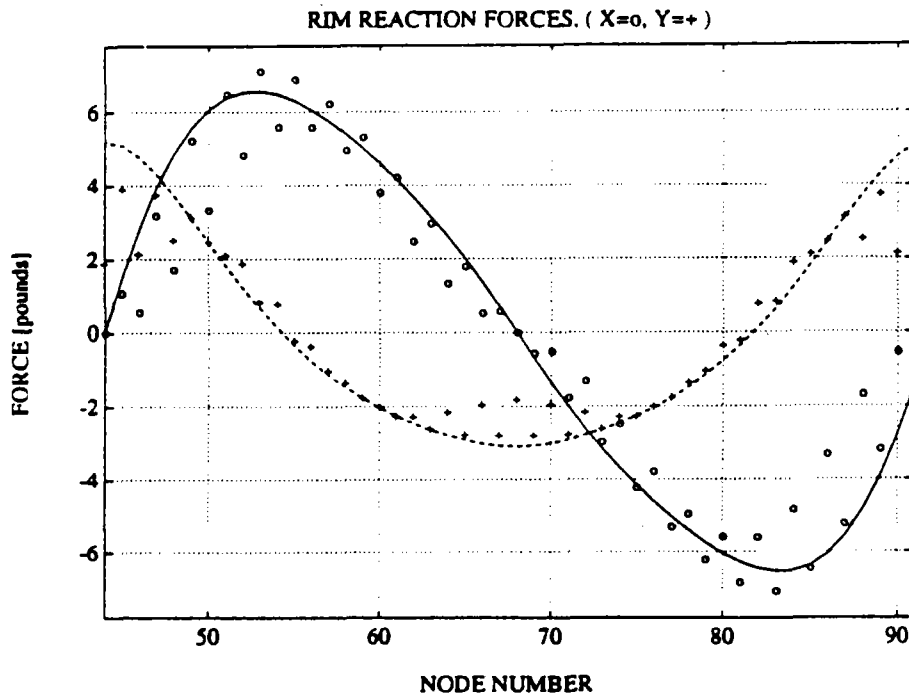


Figure 48

The reaction forces at the rim nodes agree well with continuous media predictions by Grossman<sup>8</sup> (solid line)

The baseline loading of the web cords between the hoop and R/C rim is a factor of two to four times greater than the rim reaction forces. This ensures that the structural stiffness is dominated by cord tension and beam compression rather than inflatable membrane tension and attendant reaction forces. To prevent membrane tearing, a graphite cord lines the R/C rim (external to the pressurized region) to offload excess force. Due to the cord geometry, this results in nearly uniform compressive loading of the hoop beams to 170 pounds. This makes the hoop substructure self-supporting in the event of depressurization, and also establishes the minimum loads which tube latches and fittings must bear.

Another feature of the circular-geometry hoop is that a major axis tension element (such as that described by Grossman<sup>8</sup> for a pressurized elliptical torus) is not needed to maintain rim shape. During this study it was found empirically that a tension element (cord or tape) across the minor axis could be used to improve the static figure, but the improvement was not great and the tension required was on the order of five pounds. This may not be practical due to relatively large thermal expansion of a 7 meter long cord in the varying temperature environment.

"Potato Chipping" is an out of plane deformation observed on pressurized tori which have been proposed as rim support structures for the inflatable concentrators of a solar powered rocket. A deformation of an elliptical torus FEM similar to "potato chipping" is shown in Figure 49 (undeformed torus shown as dashed lines). The phenomenon has been observed in fabrication studies and (to the best of our knowledge) has not been correlated with any detailed analysis relating this behavior to fundamental material properties or theoretical stress analysis. However it seems certain that such a relationship does exist. We speculate that "potato chipping" is a static structural instability caused by a combination of non-isotropic material properties (nonuniform thickness or randomness in the distribution of strengthening fibers) and relatively high stress levels due to the required inflation pressure.

Whether or not "potato chipping" will be a problem in a mechanical hoop rim support cannot be answered with complete certainty unless the hoop is fabricated and tested. However, the fact that an inflatable torus depends on internal pressure to produce structural stiffening, whereas a mechanical hoop has some inherent stiffness at zero stress, tends to suggest that "potato chipping" will not be as much of a problem with the mechanical approach. No "potato chipping" was noted during the FEM static equilibration exercises carried out as part of this work.

The foregoing observations consider rim supports in isolation from both the concentrator and peripheral supports. It is likely that loading an inflatable torus or mechanical hoop could aggravate the "potato chipping" problem. The construction of scale models might be the most efficient way to resolve this issue. Scale models are also useful for low-margin designs which seek to maximize the strength-to-weight tradeoff by exploiting tension stiffening.

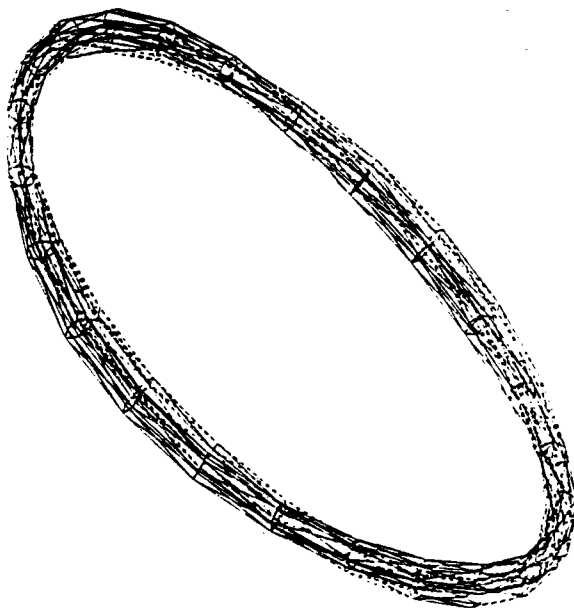


**Figure 49**  
**A deformation of an elliptical torus FEM similar to "potato chipping" (undeformed torus shown as dashed lines)**

### 3.1.9.3 External Static Load Analysis

A series of five static load cases were run to evaluate the relative strength of the support structure in orthogonal directions. The translational degrees of freedom were restrained at the spacecraft/strut interface for these tests. Due to the asymmetry of the structure, the displacements due to equal acceleration loads in the +x (+y) and -x (-y) directions will not be exactly symmetric. For small loads however, the structure should behave linearly and the deflections should be approximately symmetric in opposite directions. The degree of linear behavior is illustrated by displacements shown in Figure 50 through Figure 53, which have been magnified by a factor of 100. The load for the +x (-x) case was applied parallel to a principal axis of inertia, which is rotated about 6 degrees from the +x axis toward the +y axis. This 6 degree rotation minimizes moments in the structure for a ground test condition by placing the center of gravity on line with the support point.

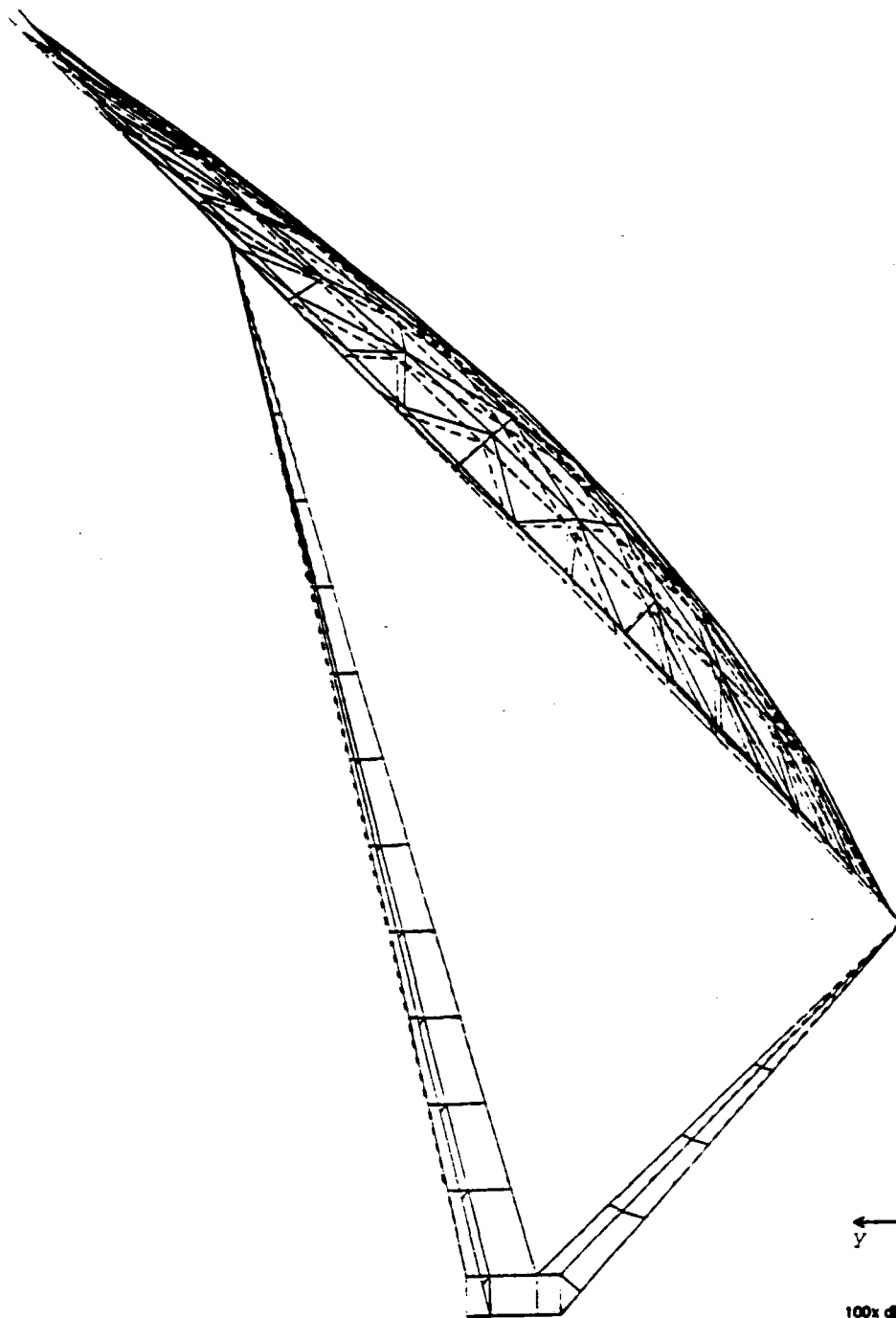


**Figure 50**  
**Case 1: 0.03g acceleration applied in the +x direction**

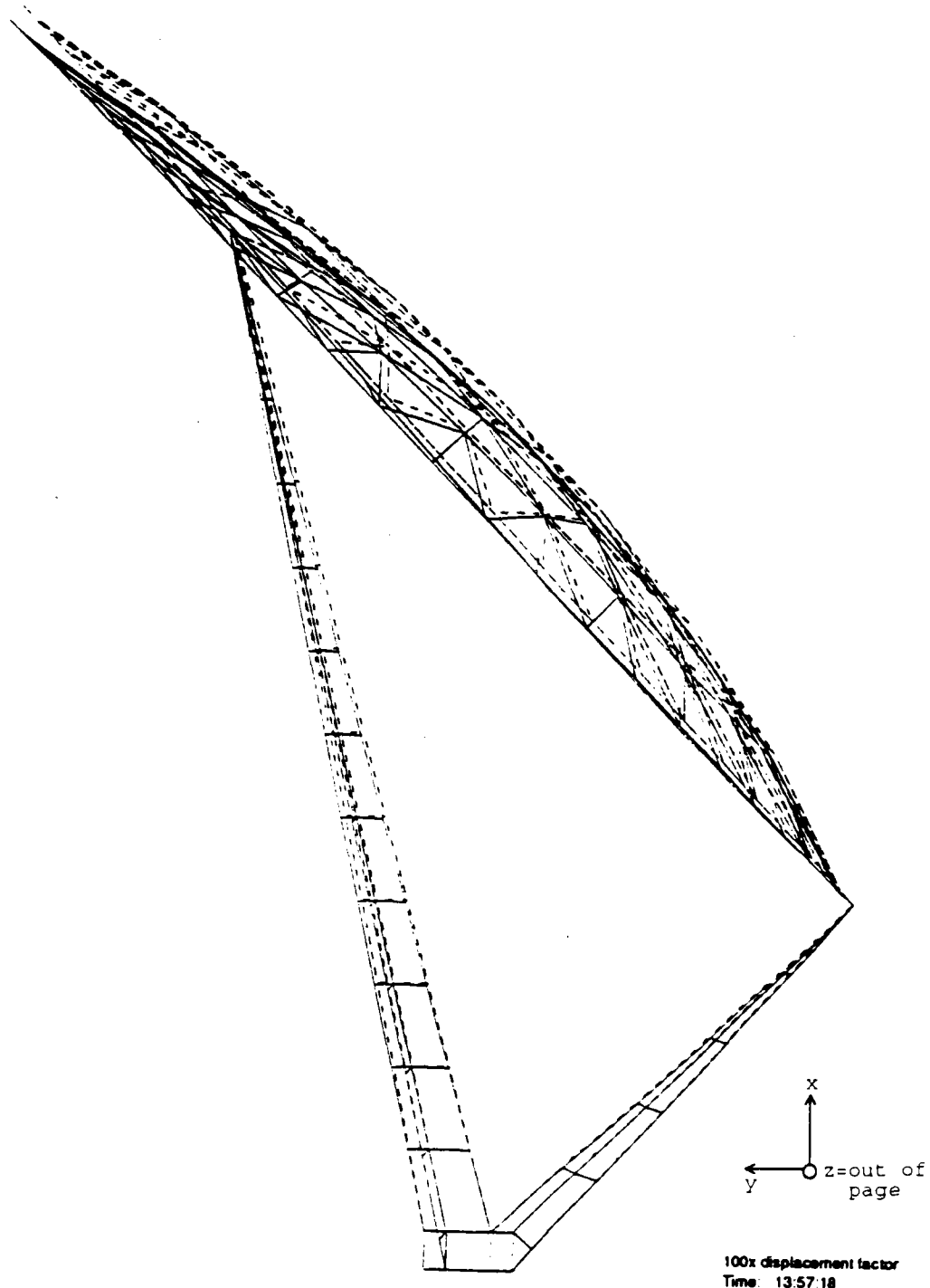


**Figure 51**  
**Case 2: 0.03g acceleration applied in -x direction**

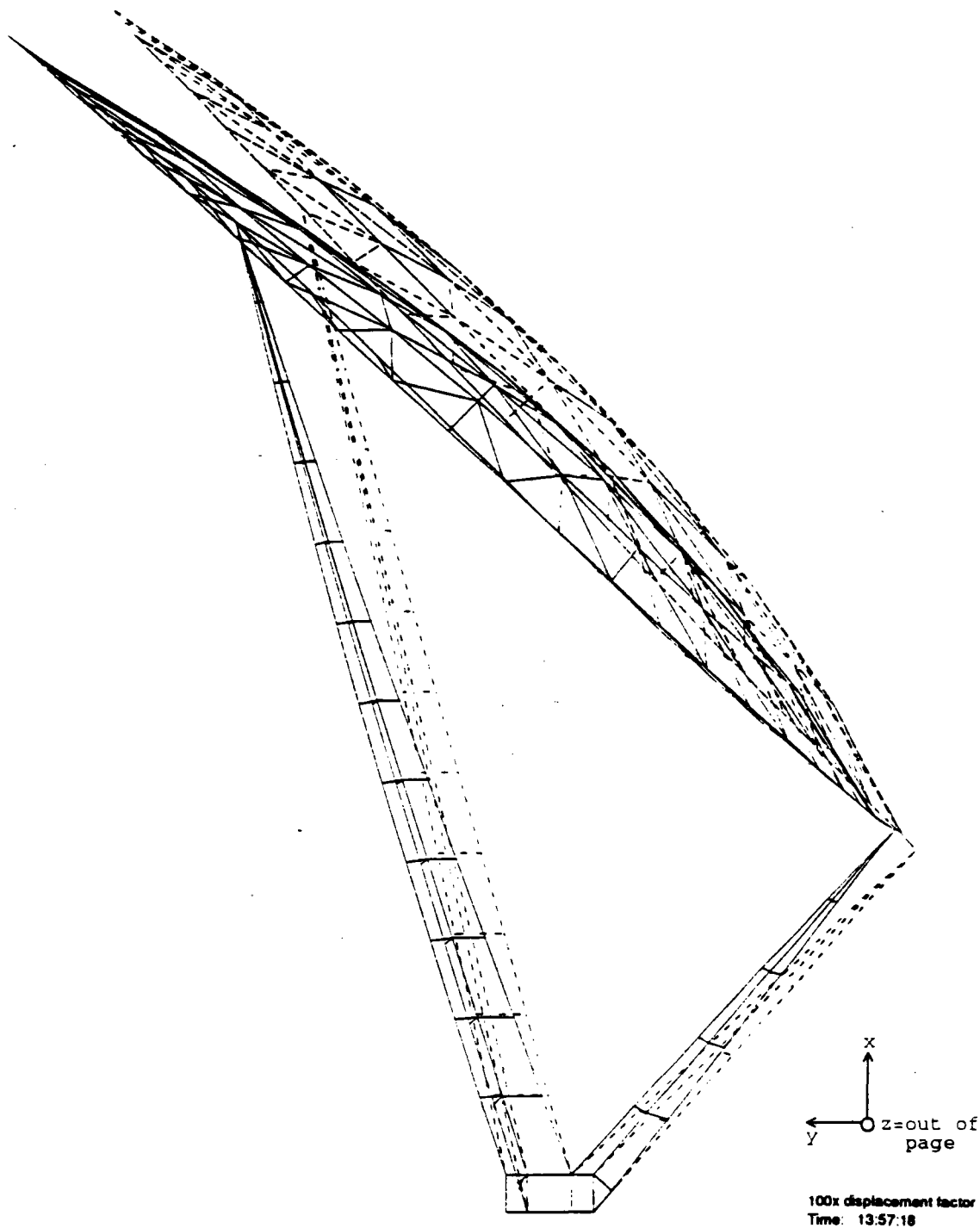


**Figure 52**  
**Case 3: 0.03g acceleration applied in the +y direction**

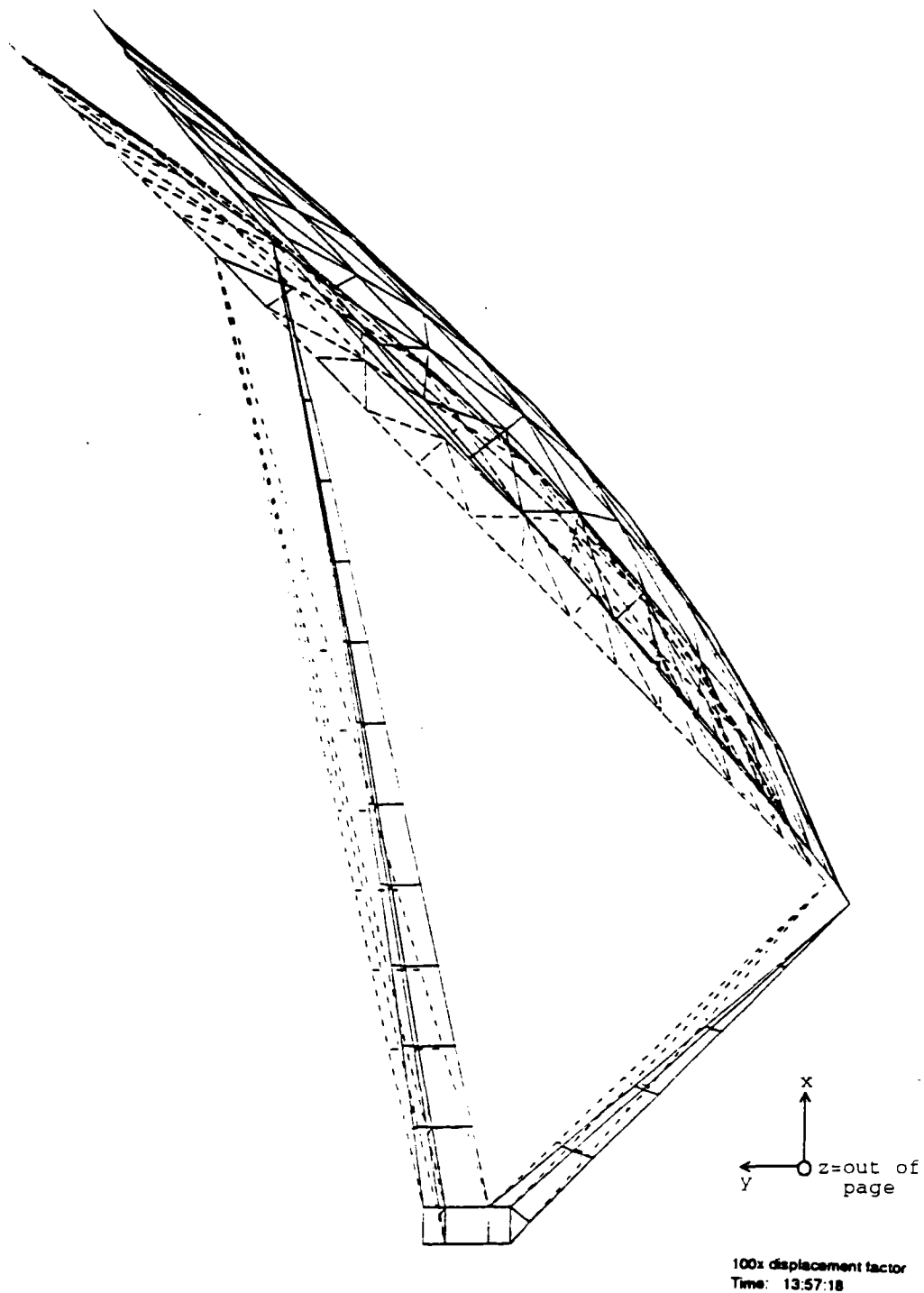


**Figure 53**  
**Case 4: 0.03g acceleration applied in -y direction**

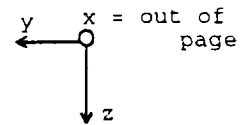
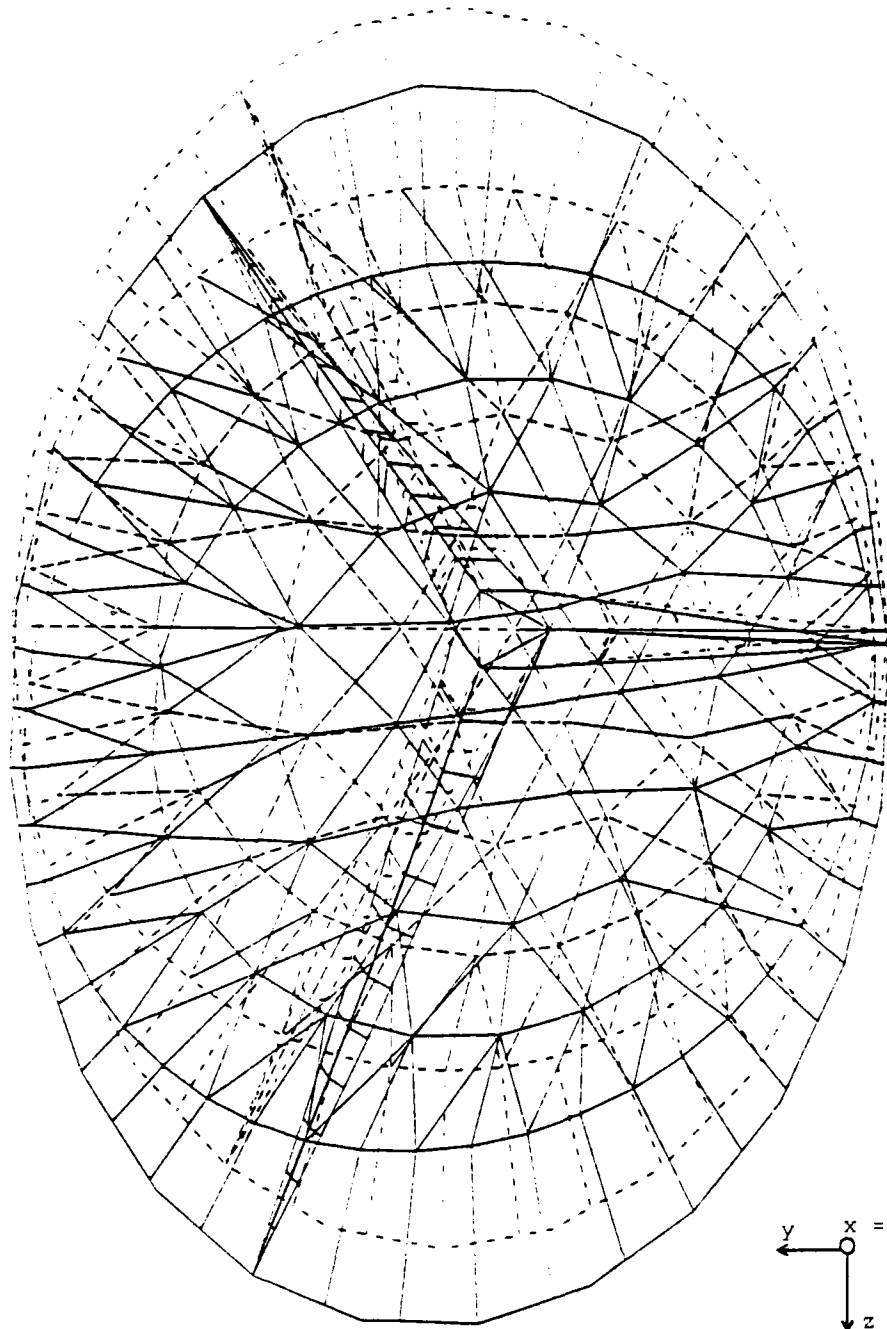
The structure is symmetric with respect to reflection across the x-y plane, so displacements due to +z and -z loads will be symmetric. For this reason a -z load case is not presented here. Displacement in the +z load case is shown in Figure 54. Peak loads in various members and parabolic rms surface fit for each case are given in Table 15.

The acceleration loading for these static cases was chosen to be 0.03g. At approximately 0.04g some of the stringers in the +z load case went slack, indicating entry into a different stiffness regime, as stringers cannot bear compressive loads. This condition does not represent a loss of structural stiffness, but it does mark the first significant change in linear behavior.

**Table 15. Static load summary with translational degrees of freedom restrained at strut/SC interface nodes (316,348,380)**

| Load Case | Desc             | Strut Tube Loads<br>Long/Short/Long | Max Strut-Stringer Load | Max Disp/Node/Dof       | RMS Surface Error |
|-----------|------------------|-------------------------------------|-------------------------|-------------------------|-------------------|
| 0         | No Load          | 130/136/130<br>pounds               | 70.2<br>pounds          | .041 inches/<br>23/x    | .035<br>inches    |
| 1         | +x,<br>.03g      | 127/132/127<br>pounds               | 70.2<br>pounds          | .041 inches/<br>111/y * | .034<br>inches    |
| 1-G       | +x,<br>.1.0<br>g | 92/117/92<br>pounds                 | 79.9<br>pounds          | 1.35 inches/<br>135/x * | 1.59<br>inches    |
| 2         | -x,<br>.03g      | 129/133/129<br>pounds               | 69.6<br>pounds          | .054 inches/<br>135/x * | .061<br>inches    |
| 3         | +y,<br>.03g      | 132/127/132<br>pounds               | 80.5<br>pounds          | .277 inches/<br>135/y * | .252<br>inches    |
| 4         | -y,<br>.03g      | 124/137/124<br>pounds               | 73.6<br>pounds          | .280 inches/<br>135/y * | .224<br>inches    |
| 5         | +z,<br>.03g      | 136/132/120<br>pounds               | 80.9<br>pounds          | .444 inches/<br>44/z *  | .054<br>inches    |

\* displacement does not include equilibration displacement (case 0).



100x displacement factor  
Time: 13.57:18

**Figure 54**  
**Case 5: 0.03g acceleration applied in +z direction**

### 3.1.9.4 Ground Test Feasibility Analysis

The foregoing analysis shows that the structure is strongest in the +x degree of freedom, which is a feasible configuration for ground testing. Such testing would be conducted in the deployed configuration. To investigate this possibility, a 1-G load case was run to determine structural loads and optical figure. For comparison, this is listed as case 1-G in Table 15. The resulting distortion is portrayed in Figure 55 with the maximum deflection (1.6 inches) occurring at node 135, located on the hoop opposite the short strut attachment point.

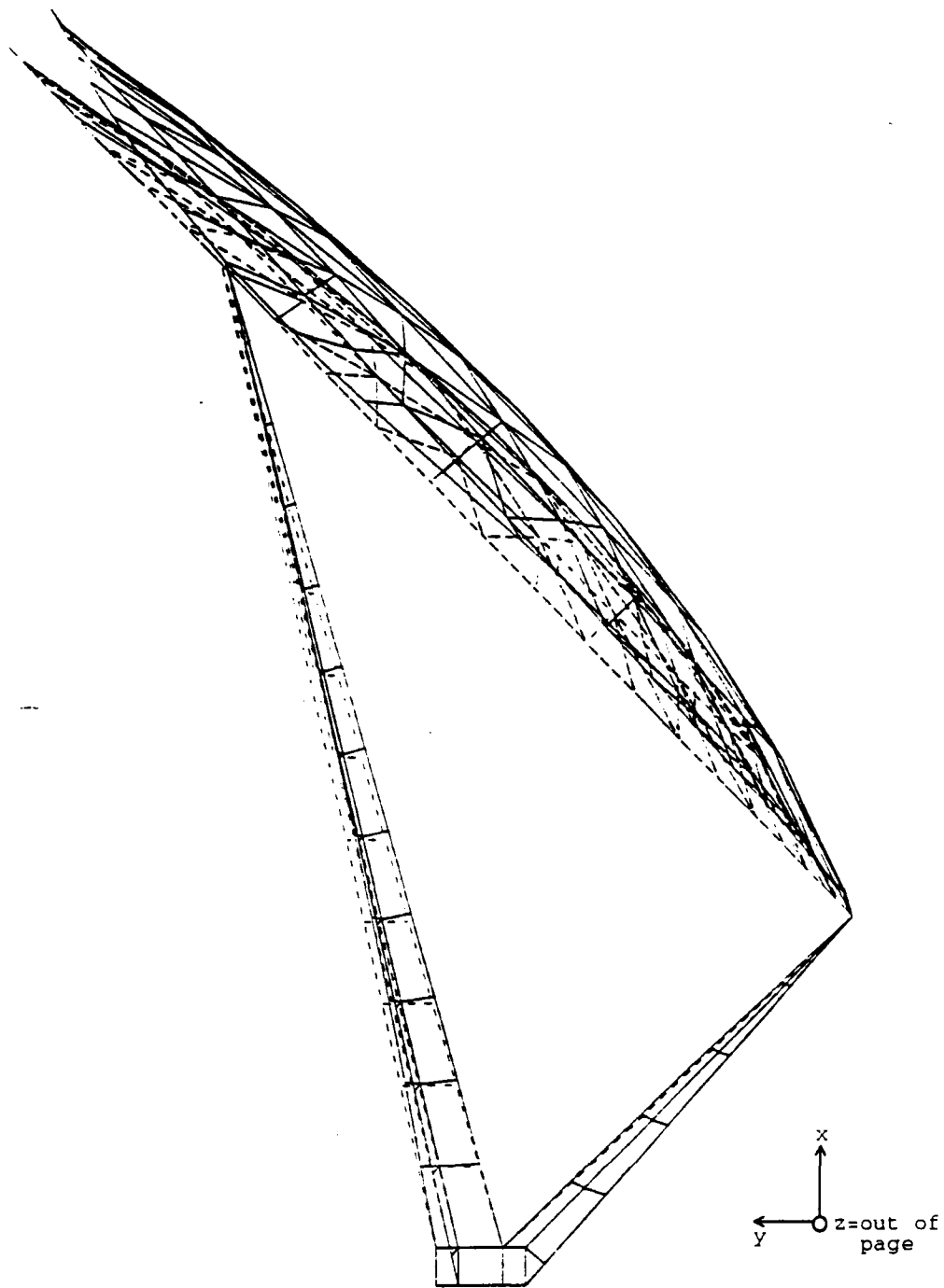
Ground testing of large, lightweight space structures generally occurs with the assistance of a counterbalance (or offload) system which minimizes the effect of the 1-G loading. Often, the design of a deployable counterbalance system can be as challenging as the flight hardware. The current structure is designed such that the 1-G loads do not cause catastrophic loads or distortions in the system. One technique to reduce the weight of the structure is the incorporation of a counterbalance system which thereby requires the space structure to carry less load during 1-G testing and allows structural members to be downsized.

The resulting distortions due to the 1-G loading were examined via a ray trace optical analysis. Two surface parameters were selected for the concentrator: a 1.0 milliradian two-dimensional randomly distributed slope error and a specular component of reflectivity of 0.9. These properties are representative of expected concentrator specifications. Figure 56 shows the intercept factor of the unloaded and 1-G loaded concentrator as a function of aperture radius. Intercept factor is defined as the amount of energy intercepted by the aperture over the amount of energy incident on the aperture plane. As the radius of the aperture increases, the intercept factor increases. The system designer must trade off increasing intercept factor for increasing radiation losses from the aperture. The figure shows that a 2.5 inch radius aperture captures 99% of the available energy in an undistorted condition and 95% in a 1-G distorted condition. An intercept factor of 95% is a "rule of thumb" goal for concentrator design.

Figures 57 and 58 show the concentrated flux contours of the undistorted and 1-G distorted system. The distortions do not cause significant change to the gross size of the image or to the peak concentration ratio. The 1-G distortions move the center of the image 1.12 inches from the center of the aperture. Thus a 2.5 inch radius aperture is required to maintain a 95% intercept factor in the distorted condition. The 1-G distortions can be greatly reduced by implementing a counterbalance system. Distortions on-orbit are the true concern and are discussed in the following sections.

While ground testing of the actual kinematic deployment sequence is generally desirable, there has been no attempt to study it in this specific case.

The +x orientation is clearly the most promising configuration for ground testing because it presents the fewest opportunities for snagging and tearing the R/C membrane during ground deployment.



x  
y z=out of page

100x displacement factor  
Time: 13:57:18

**Figure 55**  
The 1-G static load case causes a maximum deflection of 1.6 inches at node 135, a point on the hoop opposite the short strut attachment point

INTERCEPT FACTOR AS A FUNCTION OF APERTURE RADIUS  
FOR ZERO AND ONE G LOAD CONDITIONS

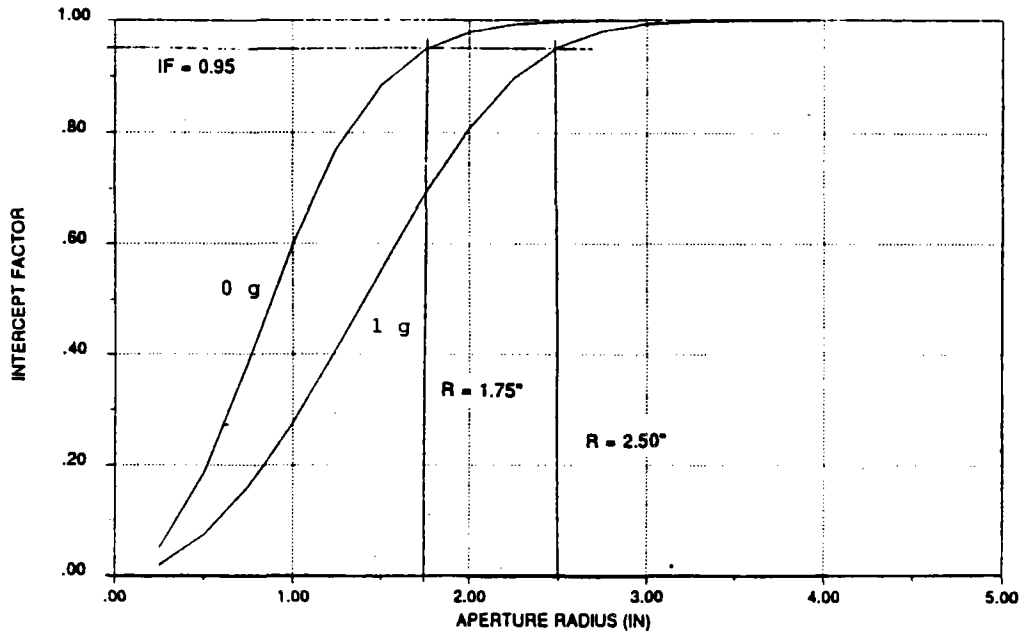


**Figure 56**  
A 2.5 inch aperture radius enables a 95% intercept factor in a 1-G distorted case

APERTURE PLANE FLUX DISTRIBUTION FOR UNLOADED GEOMETRY

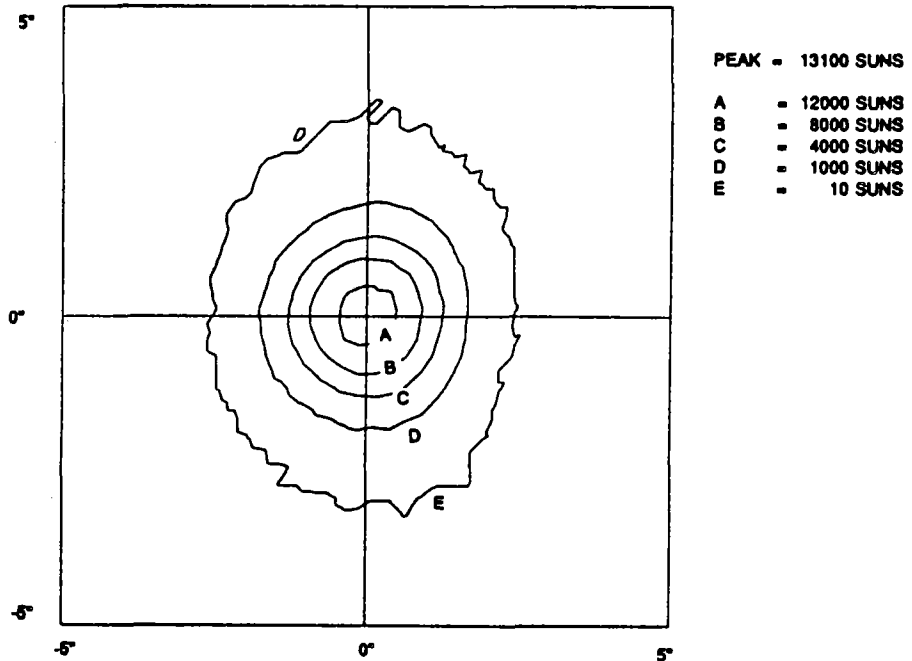


**Figure 57**  
A flux peak of 13100 suns is developed at the aperture by an undistorted concentrator

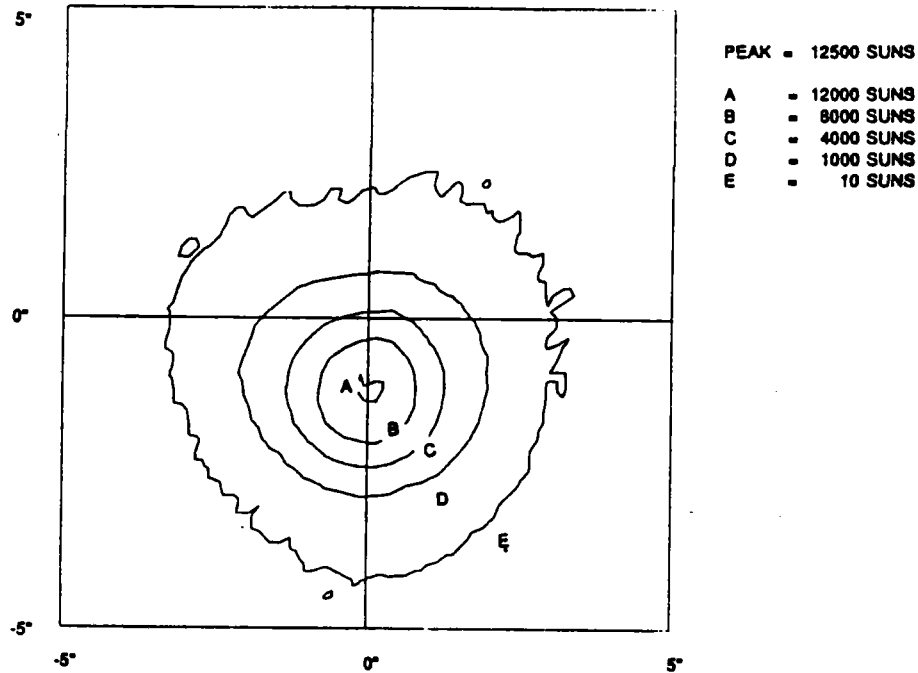


**Figure 58**  
 The 1-G static load causes the center of the concentrated energy to shift 1.12 inches on the aperture plane

### 3.1.9.5 Dynamic Analysis

As mentioned previously, determining the fundamental modes of vibration is an important step in finding the structural response to external forces. The character of a structures' mode shapes is determined by the stiffness of various elements and boundary conditions, such as fixed mounting points. The stiffness of the truss (formed by the struts and cords) and hoop depend on the balance of internal forces between beam compression and cord tension. This balance will necessarily be affected by gravity loading in a ground test configuration, such as that described in the previous paragraph. Ground testing also requires a greater degree of fixity at some nodes, than does on-orbit testing.

In general, the mode shapes observed in ground tests will be different from those found on-orbit. However, for the same (or similar) structures, one can reasonably expect them to be related. To establish traceability between ground and orbital mode shapes, eigenvectors of three configurations were computed.

The first is an on-orbit configuration with no external gravity loading. The first six modes of this "free-free" case correspond to rigid body motion of the entire structure, including the spacecraft, since no constraints are imposed on the motion of any node. Table 16 summarizes the first 20 modes of this configuration.

**Table 16. The first 20 modes of the "free-free" configuration are listed below. The first mode of significance is at frequency of 1.55 Hertz well above the 0.4 Hertz requirement**

| Eigen-vector | Frequency (Hertz) | General'd Mass | Max Disp @Node | Description          |
|--------------|-------------------|----------------|----------------|----------------------|
| 1            | 0.0000            | 0.622          | 491            | x translation        |
| 2            | 0.0000            | 0.643          | 491            | y translation        |
| 3            | 0.0000            | 0.586          | 491            | z translation        |
| 4            | 0.0000            | 0.208          | 135            | theta-x rotation     |
| 5            | 0.0000            | 0.394          | 153            | theta-y rotation     |
| 6            | 0.0000            | 0.217          | 44             | theta-z rotation     |
| 7            | 1.5466            | 0.172          | 135            | defocus, drum        |
| 8            | 1.6191            | 0.178          | 175            | mispoint, hoop twist |
| 9            | 2.9529            | 0.003          | 230            |                      |
| 10           | 2.9605            | 0.003          | 275            |                      |
| 11           | 3.1829            | 0.004          | 215            |                      |
| 12           | 3.1980            | 0.003          | 290            |                      |
| 13           | 3.6543            | 0.104          | 214            | theta-z mispoint     |
| 14           | 4.8010            | 0.003          | 486            |                      |
| 15           | 4.8027            | 0.003          | 422            |                      |
| 16           | 4.9854            | 0.210          | 141            | mispoint, hoop bend  |
| 17           | 5.1960            | 0.030          | 387            |                      |
| 18           | 5.2438            | 0.025          | 387            |                      |
| 19           | 5.3677            | 0.030          | 323            |                      |
| 20           | 5.5703            | 0.033          | 231            |                      |

The second configuration corresponds to a ground test in which the structure is constrained in translational motion at the SC/strut interface with gravity along a principal axis (approximately in the +x direction) as described in the previous section. The rotational motion of the struts is constrained only by the truss cords. Since the motion of the interface is constrained at three nodes, there is no rigid body motion in this "fixed-base" case. Table 17 summarizes the first 20 modes of this configuration.

**Table 17. The first 20 modes of the "fixed-base" case are all greater than the 0.4 Hertz requirement**

| <b>Eigen-vector</b> | <b>Frequency (Hertz)</b> | <b>General'd Mass</b> | <b>Max Disp @Node</b> | <b>Description</b>   |
|---------------------|--------------------------|-----------------------|-----------------------|----------------------|
| 1                   | 0.8382                   | 0.142                 | 44                    | theta-x torsion      |
| 2                   | 1.0950                   | 0.090                 | 135                   | theta-z mispoint     |
| 3                   | 1.1988                   | 0.133                 | 151                   | mispoint, hoop twist |
| 4                   | 1.5714                   | 0.130                 | 142                   | defocus, drum        |
| 5                   | 2.7317                   | 0.233                 | 491                   | mispoint, hoop twist |
| 6                   | 3.2915                   | 0.157                 | 143                   | defocus, drum        |
| 7                   | 3.7441                   | 0.003                 | 215                   |                      |
| 8                   | 3.7643                   | 0.003                 | 290                   |                      |
| 9                   | 4.9600                   | 0.206                 | 153                   | mispoint, hoop bend  |
| 10                  | 5.1323                   | 0.002                 | 486                   |                      |
| 11                  | 5.1332                   | 0.002                 | 422                   |                      |
| 12                  | 5.1544                   | 0.022                 | 273                   |                      |
| 13                  | 5.2676                   | 0.024                 | 228                   |                      |
| 14                  | 5.4345                   | 0.032                 | 387                   |                      |
| 15                  | 5.4872                   | 0.027                 | 323                   |                      |
| 16                  | 6.1646                   | 0.029                 | 81                    |                      |
| 17                  | 6.3529                   | 0.041                 | 117                   |                      |
| 18                  | 7.1179                   | 0.002                 | 293                   |                      |
| 19                  | 7.1186                   | 0.002                 | 218                   |                      |
| 20                  | 7.2470                   | 0.0011                | 226                   |                      |

The third configuration is similar to the second, but with the y and z translational degrees of freedom released at the SC/strut interface. This corresponds to suspending the structure from a frictionless "motion table" having the same mass and geometry as the spacecraft. The intent of this arrangement is to emulate more closely the mode shapes excitable by a spacecraft thruster oriented in the y-z plane. This configuration has precedent in Large Space Structure testing and experimentation, one example of which is the NASA/Marshall Space Flight Center ACES testbed. Two rigid body modes are present in this case, which is summarized in Table 18.

**Table 18. The modes excited by the thruster are also above the 0.4 Hertz requirement**

| <b>Eigen-vector</b> | <b>Frequency (Hertz)</b> | <b>General'd Mass</b> | <b>Max Disp @Node</b> | <b>Description</b>   |
|---------------------|--------------------------|-----------------------|-----------------------|----------------------|
| 1                   | 0.0000                   | 0.543                 | 491                   | y translation        |
| 2                   | 0.0000                   | 0.543                 | 491                   | z translation        |
| 3                   | 1.0152                   | 0.194                 | 44                    | theta-x torsion      |
| 4                   | 1.2005                   | 0.148                 | 151                   | hoop twist           |
| 5                   | 1.2403                   | 0.098                 | 135                   | theta-z mispoint     |
| 6                   | 2.0005                   | 0.187                 | 194                   | defocus, drum        |
| 7                   | 3.0000                   | 0.108                 | 292                   | mispoint, hoop twist |
| 8                   | 3.3140                   | 0.162                 | 175                   | theta-z mispoint     |
| 9                   | 3.7524                   | 0.003                 | 215                   |                      |
| 10                  | 3.7721                   | 0.003                 | 290                   |                      |
| 11                  | 4.9611                   | 0.207                 | 141                   | mispoint, hoop bend. |
| 12                  | 5.1330                   | 0.002                 | 486                   |                      |
| 13                  | 5.1338                   | 0.002                 | 422                   |                      |
| 14                  | 5.1727                   | 0.022                 | 228                   |                      |
| 15                  | 5.3356                   | 0.022                 | 228                   |                      |
| 16                  | 5.4387                   | 0.028                 | 323                   |                      |
| 17                  | 5.5413                   | 0.026                 | 387                   |                      |
| 18                  | 6.2240                   | 0.029                 | 80                    |                      |
| 19                  | 6.3591                   | 0.041                 | 117                   |                      |
| 20                  | 7.1205                   | 0.002                 | 293                   |                      |

### 3.1.9.6 Mode Shape Survey

A pervasive feature of the tabulated results is that there is a large number of "stringer" modes having generalized mass of .05 or less. The significance of these modes is not considered great, due to their low mass and relatively high frequencies (above 3 Hertz). They do not generally participate in reflector surface motion below 7 Hertz, and therefore do not affect optical performance. A typical example of this type of mode is shown in Figure 59.

Figures 60 through 63 show the mode shapes of the four dominant frequencies in the "free-free" configuration. All views are from within the plane of the hoop and are rotated to give the best view of concentrator surface distortion. The canopy members have been omitted for clarity. Dashed lines indicate the undistorted shape of the structure, while solid lines are the distorted shape. The mode shapes extracted by Finite element analysis are all displacement-normalized to 1 inch, and have been magnified by a factor of 25 in the figures.

Figures 64 through 70 show the mode shapes of the seven dominant frequencies in the "fixed-base" configuration, with the same caveats as the "free-free" case regarding display parameters. The most notable difference from the previous case is the appearance of a significant low frequency torsion mode and an additional hoop twist mode, which are directly related to the fixity of the SC/strut interface. There are also significant frequency shifts due to interface fixity and, to a lesser extent, stiffness changes due to gravity loading.

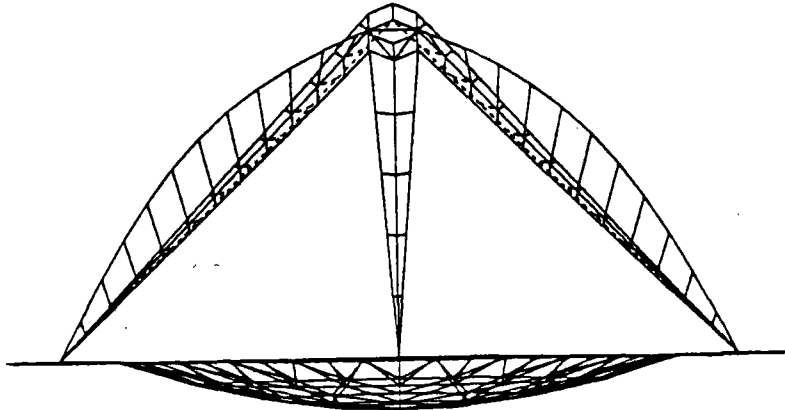


**Figure 59**  
**Fixed base mode 7 is a localized stringer motion at 3.74**  
**Hertz (displacement magnified by 25x)**

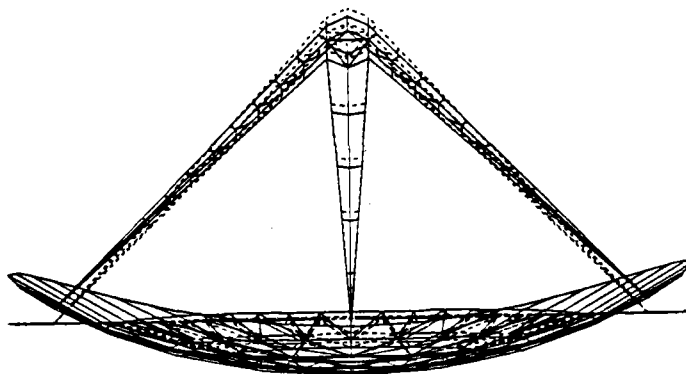


**Figure 60**  
**Free-free mode 7 is a defocus/drum motion at 1.55 Hertz**  
**(displacement magnified by 25x)**

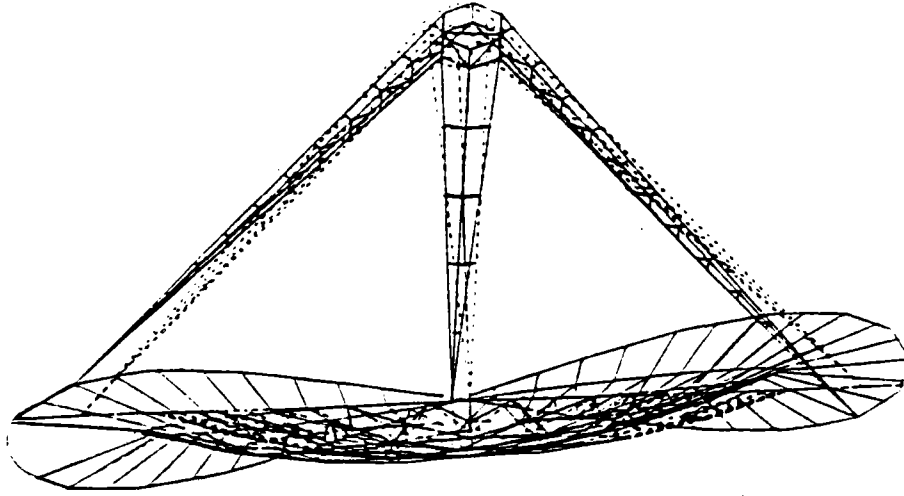


**Figure 61**  
**Free-free mode 8 is a hoop twist motion at 1.62 Hertz**  
**(displacement magnified by 25x)**

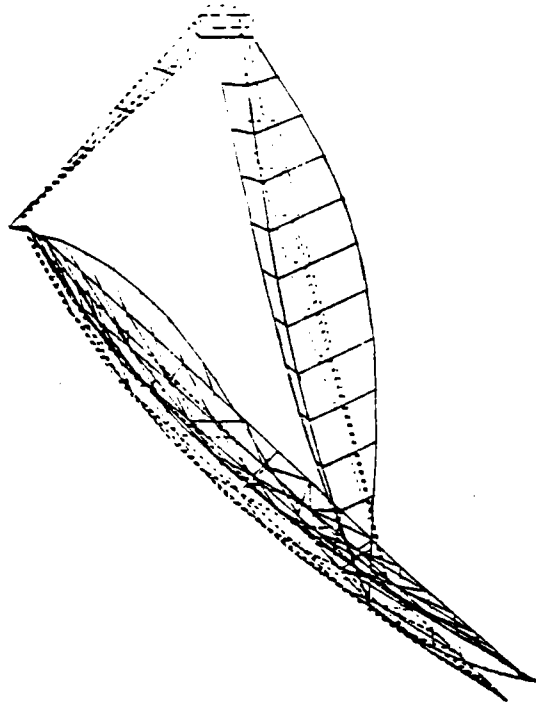


**Figure 62**  
**Free-free mode 13 involves many substructures at 3.65 Hertz**  
**(displacement magnified by 25x)**

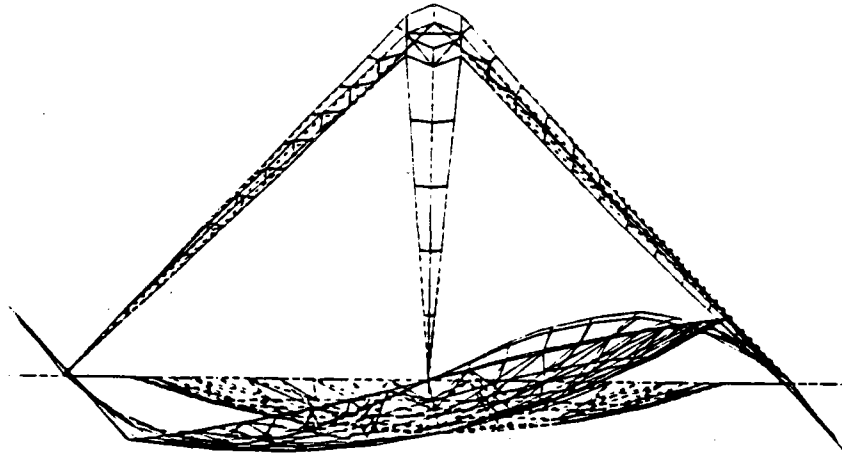


**Figure 63**  
**Free-free mode 16 is a hoop bending/mispointing motion at 4.99 Hertz (displacement magnified by 25x)**

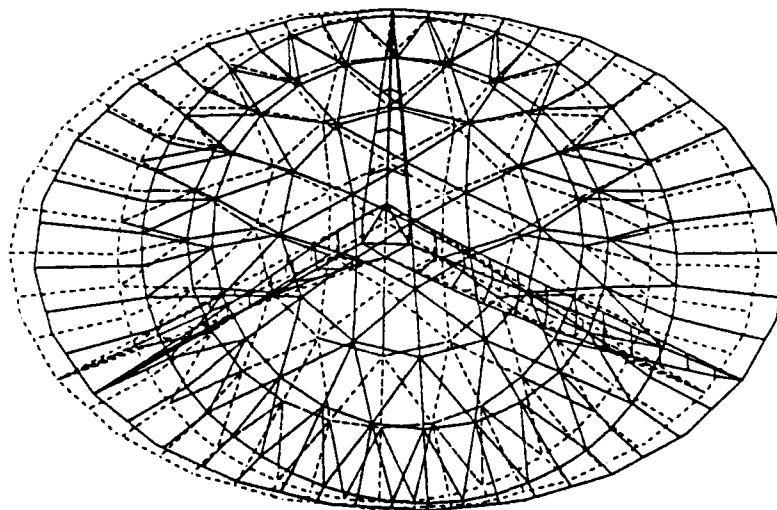


**Figure 64**  
**Fixed-base mode 1 (torsion, 0.84 Hertz) viewed from a point perpendicular to y-z plane (displacement magnified by 25x)**

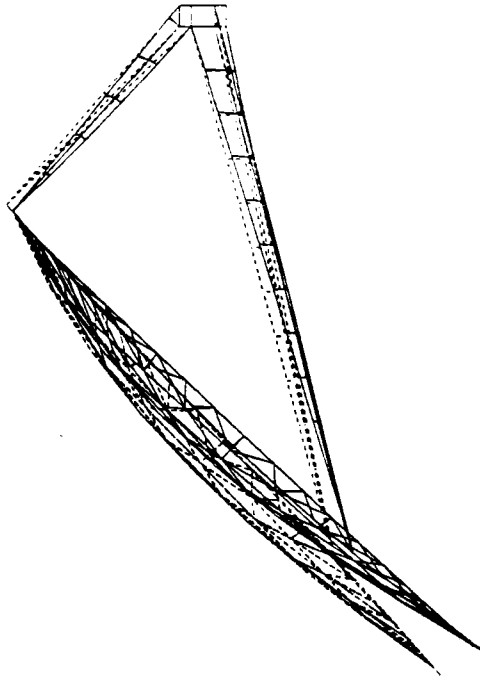


**Figure 65**  
**Fixed base mode 2 (1.1 Hertz) causes mispointing about the z axis (displacement magnified by 25x)**

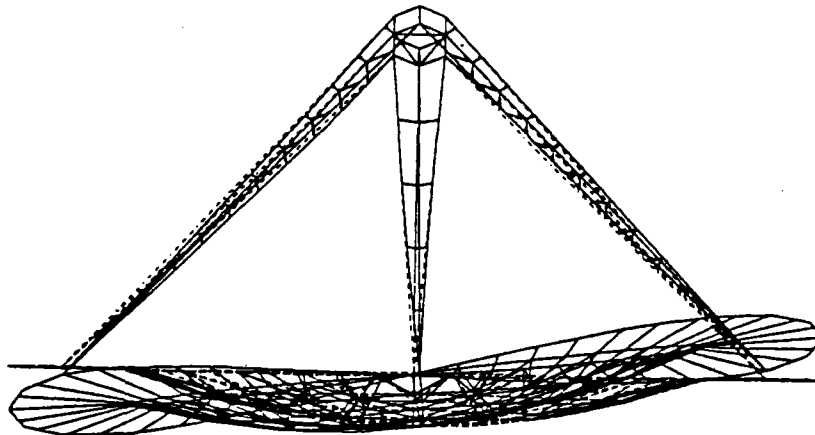


**Figure 66**  
**Fixed-base mode 3 (1.2 Hertz) is hoop twist with mispointing (displacement magnified by 25x)**

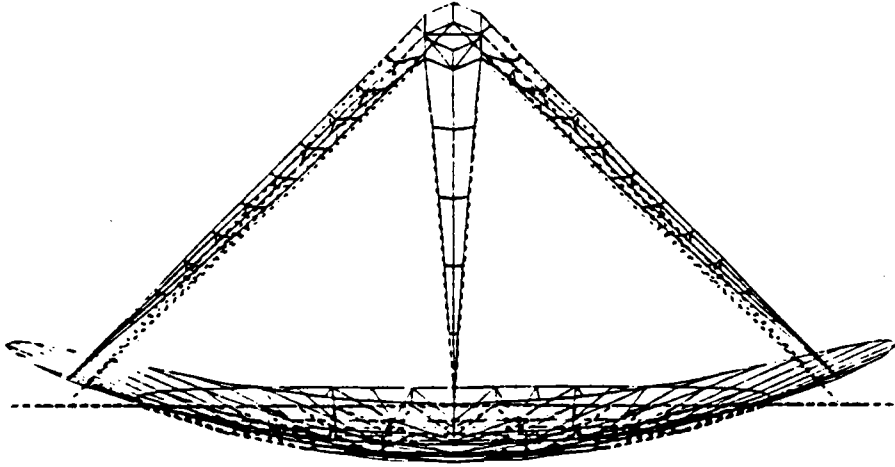


Figure 67  
Fixed-base mode 4 (1.57 Hertz) is defocus/drum shape  
(displacement magnified by 25x)

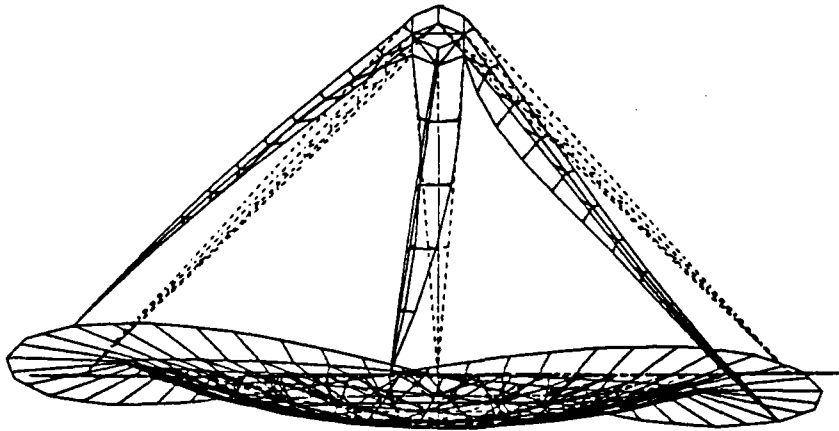
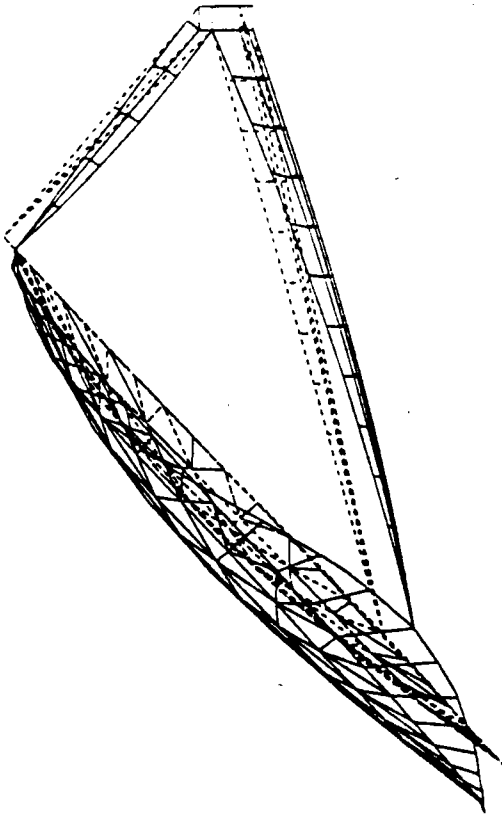
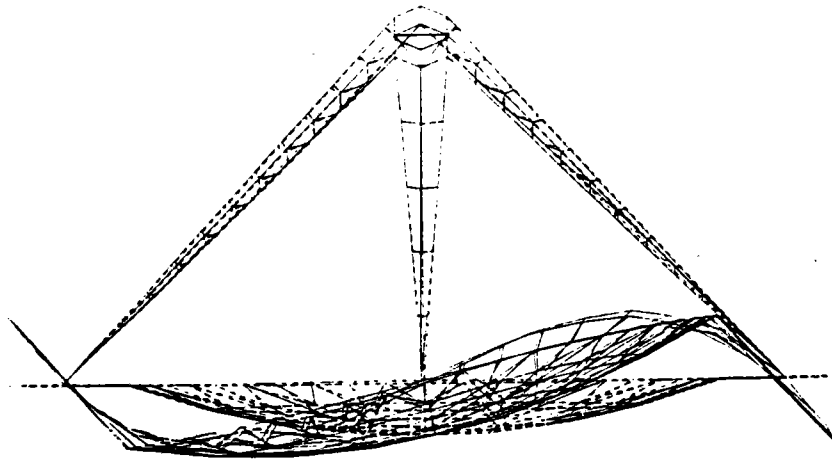


Figure 68  
Fixed-base mode 5 (2.73 Hertz) is hoop twist with strut  
motion (displacement magnified by 25x)



**Figure 69**  
**Fixed-base mode 6 (3.29 Hertz) is defocus, drum, and hoop bending (displacement magnified by 25x)**



**Figure 70**  
**Fixed-base mode 9 (4.96 Hertz) corresponds directly to free-free mode 16 at same frequency (displacement magnified by 25x)**

The mode shapes of the "motion table" case correspond very well to those of the "fixed-base" case, and are therefore not shown. The primary difference is participation of the motion table in y and z translation. Some frequency shifting of up to 30% has occurred due to the extra releases.

Table 19 summarizes corresponding mode shapes between the three configurations. The basis for the description of each mode shape is taken to be the "fixed-base" case, since there is some ambiguity in the classification of "free-free" modes. Stated another way, every major "free-free" mode shape is traceable to at least one ground based mode shape, within the frequency range of this study.

**Table 19. A mode shape summary for the ground test and orbital configurations**

| <b>DESCRIPTION</b>                              | <b>FIXED BASE<br/>freq/mass</b> | <b>MOTION-TABLE<br/>freq/mass</b> | <b>FREE-FREE<br/>freq/mass</b> |
|---|---------------------------------|-----------------------------------|--------------------------------|
| theta-x<br>torsion                              | 0.86/0.141                      | 1.02/0.194                        | - / -                          |
| theta-x<br>mispoint                             | 1.10/0.090                      | 1.24/0.098                        | 3.65/1.104                     |
| mispoint &<br>hoop twist #1                     | 1.20/0.133                      | 1.20/0.148                        | 1.62/0.178 *                   |
| defocus & refl<br>drum mode #1                  | 1.57/0.130                      | 2.00/0.187                        | 1.55/0.172                     |
| mispoint &<br>hoop twist #2                     | 2.73/0.233                      | 3.00/0.108                        | 1.62/0.178                     |
| defocus - refl<br>drum mode #2,<br>hoop bend #1 | 3.29/0.157                      | 3.31/0.162                        | 3.65/0.104 *                   |
| theta-x & -y<br>mispoint, hoop<br>bend #2       | 4.96/0.206                      | 496/0.207                         | 4.99/0.210                     |

\* Indicates approximate agreement

The low frequency torsion mode, absent in the "free-free" case for a single 7 x 9 meter reflector, can be expected to reappear in a "free-free" scenario involving two 30 x 40 meter reflectors with geometry similar to that in the HAIR Phase II Study. No attempt has been made to study this scenario in detail; it is mentioned here in relation to ground testing of a single 7 x 9 meter reflector. It is conceivable that a ground test could be constructed to emulate the expected torsion mode of a dual reflector. One approach for doing this would be to add a rotational degree of freedom about the principal x-axis on the motion table and construct a controller to project expected reaction torques into the structure.

### 3.1.9.7 Dynamic Simulation

Having identified the fundamental modes of vibration for the system with various degrees of base fixity and gravity loading, the next step is to examine their operational significance via simulation.

When a flexible structure is excited by external forces they will, in general, excite each mode to a different degree depending on the orientation of the forces with respect to the structural geometry. Eigenvectors are a matrix representation of the set of fundamental mode shapes and are displayed graphically in the previous sections. When combined with modal mass and an external force profile, enough information is present to predict the dynamic response of any mechanical node in the finite element model.

This section does not delve into the technical details of assembling the structural data into a form suitable for simulation in favor of presenting results. However, there are some baseline assumptions that must be understood. Typically the eigenvector solution neglects structural damping to simplify the extraction algorithm. The dynamics simulation presented here assumes all structural modes to have a damping ratio of 0.005. Further, all of the results presented are based on linear system theory and neglect nonlinear terms (such as coriolis and centrifugal forces) which arise in rotating coordinate systems. This is usually justified when rotational rates and beam deflection are small.

Evaluating the on orbit "free-free" case first is logical for at least two reasons. First, if we do not have confidence that the structure can perform adequately in the zero-g environment, there is no point in examining it's gravity loaded behavior. Second, the "free-free" case clearly seems to delineate which modes are significant for a single reflector flight experiment. As pointed out in the previous section, the "free-free" case appears to have four

significant modes below 5 Hertz, approximately half the number expected for the ground test configurations considered.

According to Reference 2, a small compressed gas thruster could be mounted on the spacecraft equipment section as an excitation source. The force output of the thruster decays exponentially with firing time from a maximum of one pound. Firing duration is anticipated to be 20 milliseconds. After three firings, the force available is reduced to about 1/2 pound. For simplicity, the current simulation uses a rectangular force profile with a one pound magnitude.

The thruster is directed radially outward from the equipment section cylinder at an angle of 30 degrees with respect to the +z direction (parallel to the y-z plane). Locating the thrust at four other nodes on the bottom of the equipment section was also simulated, but the results from this location are presented since they generated the largest response.

The performance measure for the simulation is the dynamic component of the line-of-sight (LOS) pointing error. This is the mispointing due to structural bending within the rigid-body reference frame of the combined spacecraft, structure and concentrator system. Mispointing due to static misalignment is not considered. The basic rigid body pointing accuracy of any onboard attitude control system is also not considered. Thus these results can be viewed as a first cut at one component of a system pointing error budget which has a goal of 0.5 degrees for a full scale system.

Construction of the LOS pointing measure is based on a combination of antenna beam theory and a least squares fit of surface nodes to a parabolic shape, rather than optical ray tracing, which would give more detailed information with respect to defocus and spot size. The interpretation of results is in terms of two "gimbal angles" ( $\theta_z$  and  $\theta_x$ ), which are parallel to the global coordinate system used to generate the paraboloid for the concentrator. Technically, the center of rotation for these angles is at the origin of the global system (vertex of the paraboloid), which is more than 100 inches from any structural node due to the off-axis geometry of the reflector. However, it is convenient to describe  $\theta_x$  as a rotation about the SC cylinder axis and  $\theta_z$  as a rotation about an axis through the long-strut attachment on the top of the SC.

Beginning with zero initial rigid body angular velocity, the rigid body rates after the thruster firing were -3, -11.5 and +7.6 milli-deg/sec about the x, y, and z axes respectively. These are the rates that would be observed at the output of a rate gyroscope mounted on the equipment section (in the rigid body reference frame). Figure 71 shows the  $\theta_z$  (solid) and  $\theta_x$  (dashed) components of

LOS error, which are almost entirely due to "free-free" modes at 1.55 and 1.62 Hertz respectively. The orthogonal phase plane plot in Figure 72 is roughly proportional to the trajectory of the focal point on the top of the SC. Taking the focal length (135.6 inches) into account, the trajectory is confined to an area approximately 10 mils in diameter, much less than the required 2.5 inch radius aperture described by Figures 57 and 58.

This dynamics simulation indicates that the dynamic response of the flight experiment support structure to a thruster of 1 pound is very small. The change in location of the concentrated energy is 0.010 inches or less and therefore little energy will be directed away from the aperture. In future studies, more comprehensive analysis of the system would be beneficial to understand the entire system pointing error budget.

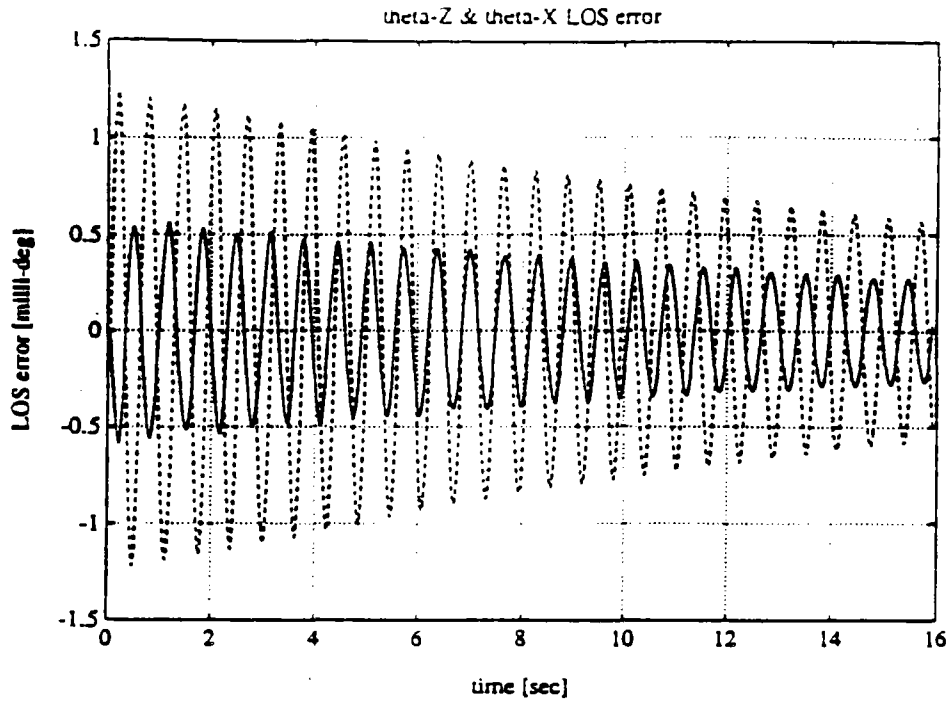


**Figure 71**  
 The theta-z (solid line) and theta-x (dashed line) components of line-of-sight error due to a 1 pound thrust are less than 1.5 millidegrees

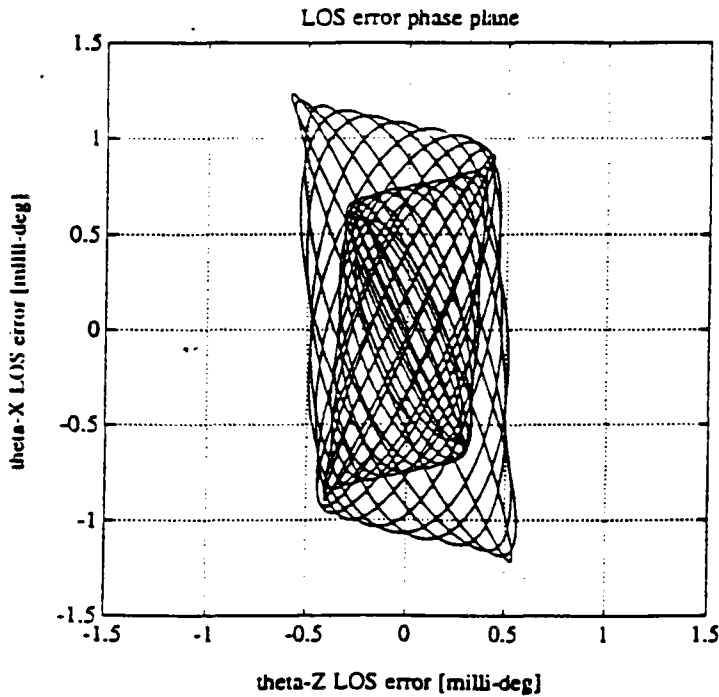


**Figure 72**  
 The trajectory of the focal point of the system due to a 1 pound thrust. This trajectory translates into focal point movement of approximately 0.010 inches

### **3.2 Single Chamber Concentrator**

The Single Chamber Concentrator (SCC) design, shown in Figure 73, is radically different from the conventional inflatable concentrators historically associated with Solar Thermal Propulsion applications. The Single Chamber Concentrator was developed by SRS Technologies.<sup>5</sup> The Single Chamber Concentrator design has the potential to reduce the complexity and weight of solar rocket systems by utilizing a self-stabilized concentrator.

In the current study, a support structure concept was devised for the SCC for purposes of comparison with the conventional concentrator and support structure designs described in Section 3.1. The SCC is connected to the spacecraft by three (3) deployable struts similar to those designed for the conventional concentrator support structure.

#### **3.2.1 Strut Design**

The struts designed for the SCC are the same basic telescoping design used for the conventional concentrator design described in Section 3.1.2. The strut tube materials and properties (see Section 3.1.2.1) and strut latches (see Section 3.1.2.2) are identical to those previously described.

The overall strut lengths used for the Single Chamber design were 228 inches for the long struts and 97.7 inches for the short strut. These dimensions were determined from a layout of the Single Chamber Concentrator design. The long struts require 8 segments of length 32.57 inches each while the short strut requires 3 segments of the same length. The struts for the Single Chamber design are somewhat shorter than those for the conventional design since the attach points on the Single Chamber Concentrator are offset from

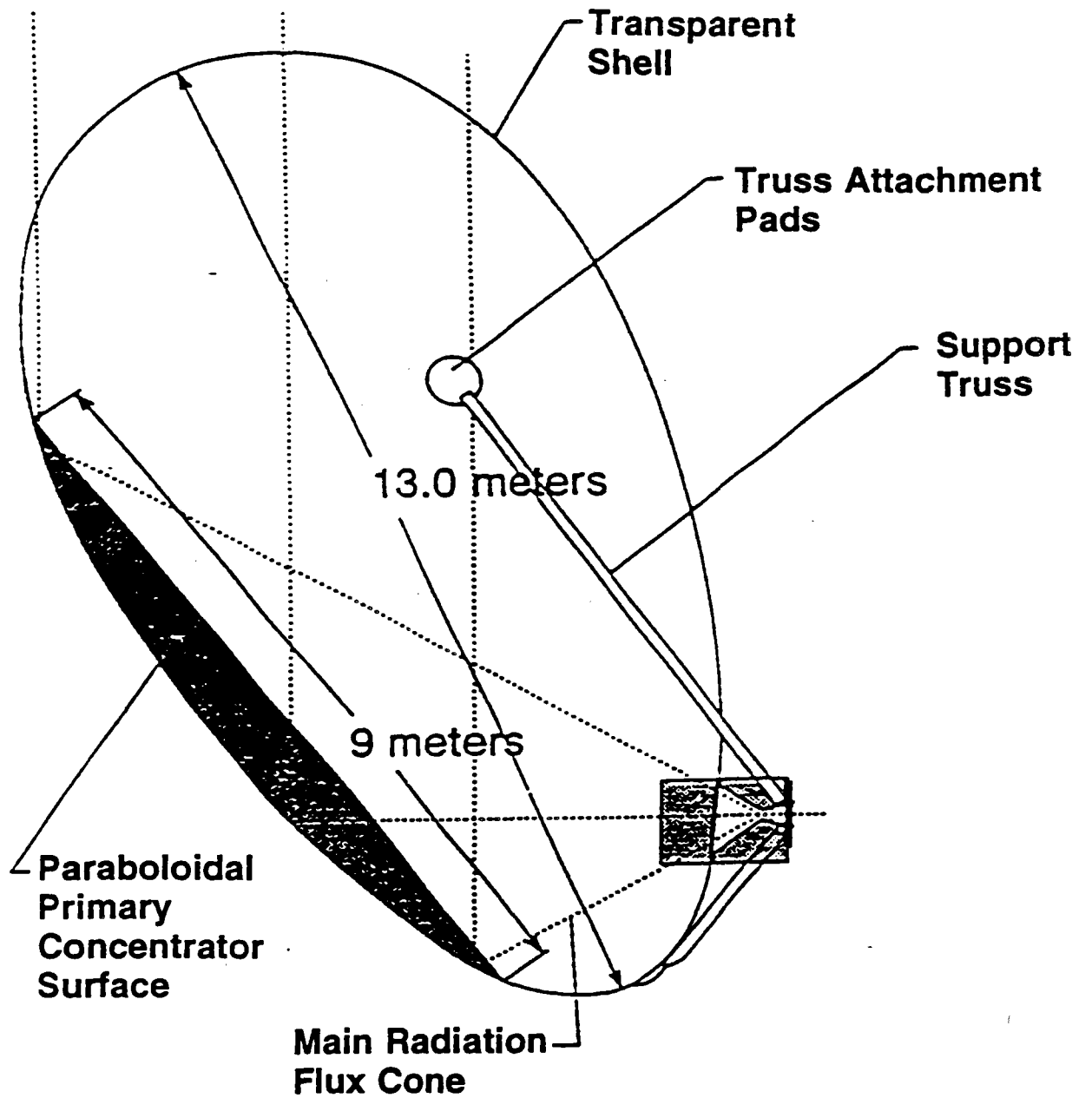


**Figure 73**  
**The Single Chamber Concentrator design provides a radical alternative to the conventional concentrator and torus design**

the concentrating surface by roughly the minor diameter of the Single Chamber Concentrator.

Also, the strut tube diameters are smaller than with the conventional design since the weight which the struts support is much lower in the Single Chamber design as compared to the conventional design. The hoop alone from the conventional design weighs almost double the SCC weight (uninflated). The long struts begin with a 3 inch diameter tube and end with a 1.4 inch diameter tube. The short strut begins with a 3 inch diameter tube and end with a 2.2 inch diameter tube.

### **3.2.2 Strut Deployment System Design**

The strut deployment system design described in Section 3.1.3 can be utilized without modification for the Single Chamber Concentrator support structure design.

### **3.2.3 Strut to Concentrator Attachment**

The attachment between the struts and the SCC is significantly different than the interface between the conventional concentrator and a hoop. The attachment points are located well away from the reflective portion of the SCC to minimize any direct effect of loading in the thin film on concentrator performance. However, deflections should still be minimized because large deflections could lead to pointing errors or dynamic instability problems.

Two design options have been reviewed and selected as candidates for further evaluation in subsequent studies. These designs are based on the 7 x 9 meter flight experiment concentrator. The preferred design, shown in Figure 74, incorporates a nylon socket with a 0.5 inch ball for a rotational pivot. A small threaded stud is shown as a means of attachment to the strut. Composite cones are used at the concentrator side to distribute the loads over the thin film. The cones are mounted to the thin film using a bonding tape or appropriate polyimide adhesive.

An alternative concept is shown in Figure 75. The design uses curved 5 inches long composite elements as opposed to a composite plate. An alternative rolling contact universal joint would be constructed using cross "ligaments".

Either of the two designs will distribute loads over the thin film and minimize distortions in the film. Both of the concepts can provide acceptable attachment at a reasonable weight.

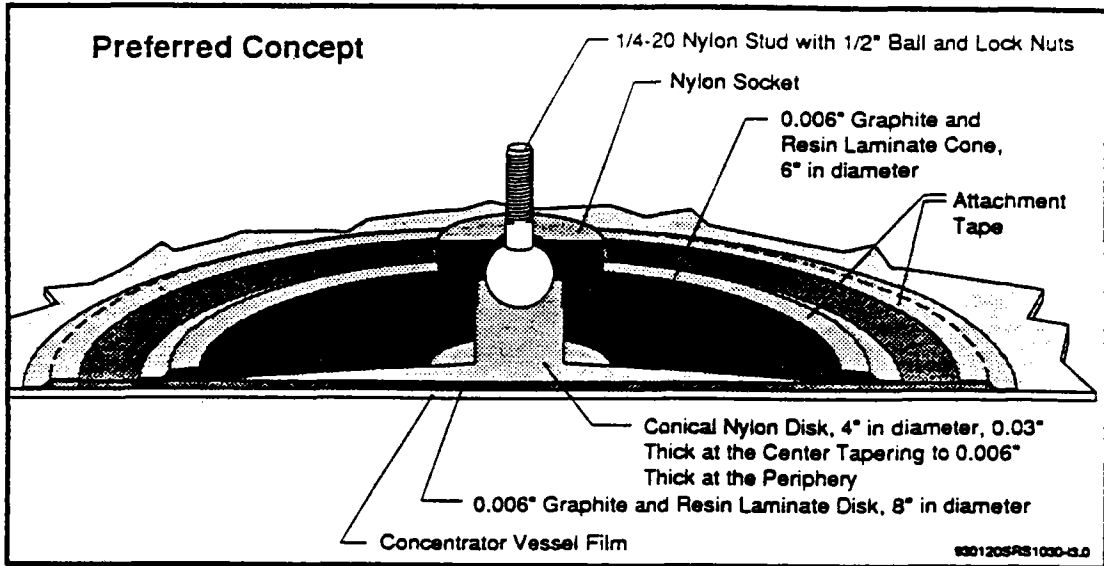


**Figure 74**  
 The preferred attachment concept uses a composite cone and a ball and socket to connect the strut to the concentrator

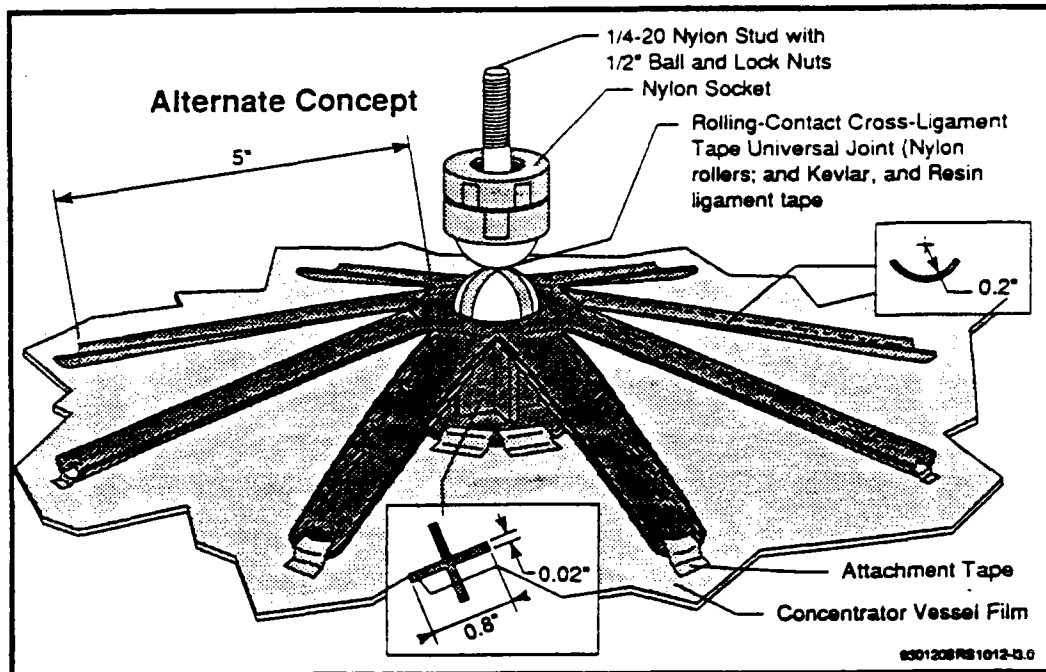


**Figure 75**  
 An alternative attachment concept utilizes composite elements and a universal joint to connect the strut to the concentrator

### 3.2.4 Stowed Package

The Single Chamber Concentrator stows into a simple package of three vertical struts and a folded concentrator. The struts and concentrator are attached only at the three attachment points.

The struts stow into three individual columns 3 inches in diameter (the outer diameter of the largest strut) and 33 inches in height. The struts are just short enough to fit in a GAS if the ejector mechanism and other electrical, pneumatic, and mechanical equipment can be designed to allow the three, 3 inch columns to extend the length of the GAS.

The Single Chamber Concentrator itself can be folded in numerous shapes to package within the available GAS volume. Experimental studies with polyimide material have determined a packing factor for concentrators of this type equal to 4.2. Packing factor is defined as the volume of the packaged concentrator over the volume of material in the concentrator. The volume of material is calculated by multiplying the surface area by the thickness. For a 7 meter by 9 meter Single Chamber Concentrator, surface area is 523,791 inches<sup>2</sup> and thickness is 0.001 inches. Therefore, the volume of the packaged concentrator is 2200 inches<sup>3</sup>, which is well within the GAS requirement of 3544 inches.<sup>2</sup>

### 3.2.5 System Deployment

The deployment of the Single Chamber Concentrator and support structure is somewhat less complicated than the conventional concentrator with a hoop and struts since there is only one mechanical subsystem (the struts, since no hoop is needed). The deployment of the Single Chamber Concentrator design can be achieved in essentially one smooth deployment operation.

The struts can be deployed using a controlled feedout rate such that each strut reaches full deployment at the same time. For example, cables wrapped around a drum could be attached to the last segment of each tube to achieve this effect. As the drum rotates, the pressure is gradually increased in the chamber and the support cones to some fraction of their final value. Then, when the struts are fully extended, a linkage on each of the support structure stringers is actuated to reduce the lengths of the stringers to their final values. The actuation of these linkages fully stiffens the support structure. The chamber can then be fully inflated.

### 3.2.6 Weight Summary

A weight estimate was formulated for the flight experiment sized Single Chamber Concentrator design for comparison to the conventional concentrator and support structure designs.

The Single Chamber Concentrator weight was calculated from the Single Chamber design finite element model. The finite element model contains representative elements for all Single Chamber Concentrator surfaces. Inflation gas was not included in this weight.

An estimate of the strut latch weights was formed by using a rule-of-thumb derived from the conventional design which showed that the latch weights are approximately 50% of the tube weights. Thus, the weights necessary for the tubes were calculated and then 50% of that value was used for the latches.

Other component weights were estimated based on the current design. A contingency factor of 20% is added to the weight to account for small parts, oversights and inaccuracies due to relatively immature designs. The SCC weight estimate is substantially smaller than the weight requirement for a GAS (85.5 pounds).

**Table 20. The flight experiment sized Single Chamber Concentrator weighs approximately 40% of the conventional design**

| <b>Item</b>        | <b>Part</b>                         | <b>Weight (pounds)</b> | <b>Source</b> |
|--------------------|-------------------------------------|------------------------|---------------|
| Concentrator       | -----                               | 27.8                   | Calculated    |
|                    | concentrator-to-strut interface (3) | 3.0                    | Estimated     |
| Concentrator Total |                                     | 30.8                   |               |
| Long struts        | latches (14)                        | 2.0                    | CAD Model     |
|                    | tubes (16)                          | 2.3                    | Calculation   |
| Short strut        | latches (3)                         | 0.3                    | CAD Model     |
|                    | tubes (4)                           | 0.5                    | Calculation   |
|                    | strut-to-spacecraft interface (3)   | 3.0                    | Estimated     |
| Deployment System  | inflation gas                       | <0.01                  | Calculated    |
|                    | valves and pressure lines           | 1.0                    | Estimated     |
|                    | seals & attachment hardware (17)    | 0.7                    | Estimated     |
|                    | cable                               | 0.2                    | Calculated    |
|                    | motor (1)                           | 0.5                    | Estimated     |
|                    | winding drum (1)                    | 0.8                    | Estimated     |
| Struts Total       |                                     | 11.3                   |               |
| Subtotal           |                                     | 42.1                   |               |
| Contingency (20%)  |                                     | 8.4                    |               |
| System Total       |                                     | 50.1                   |               |

### 3.2.7 System Performance

A finite element model was developed for the Single Chamber design. The baseline geometry for the Single Chamber Concentrator was generated by SRS and integrated into a finite element model by Harris. This geometry was subtly modified to improve its modelling characteristics without significantly impacting the overall shape. The Single Chamber model was meshed with triangular elements using film properties obtained from SRS as given in Table 21 below:

**Table 21. Film properties for the polyimide film of the Single Chamber Concentrator**

| Property | Value | Units                  |
|----------|-------|------------------------|
| E11      | .45   | Msi                    |
| G12      | .17   | Msi                    |
| Density  | .0515 | pounds/in <sup>3</sup> |

Struts were included in the model according to the design information in Section 3.2.1. of this report. The undeformed finite element model is shown in Figures 76, 77 and 78, when viewed along the x, y and z axes, respectively. Some assumptions were made in order to simplify the finite element model with respect to the Single Chamber system description given in Section 3.2. These assumptions and their effects are summarized in Table 22.

**Table 22. Single Chamber Concentrator modelling assumptions and their effects on model results**

| ASSUMPTION  | EFFECT ON ANALYSIS  |
|---|---|
| Attached struts directly to nodes; no attachment cones    | Conservative film distortions; non-conservative frequencies |
| No stringers used to stiffen struts; fixed end conditions | Conservative frequencies                                    |
| Replace secondary concentrator with fourth strut          | Conservative film distortions; non-conservative frequencies |

Pressurization of the model consisted of geometrically non-linear analysis of the chamber only under increasing internal pressure. The original estimate of 0.0050 psi internal pressure could not be achieved in the model. Despite numerous modifications in element meshing and end-cap geometry, pressure could not be applied above 0.0032 psi without the model becoming unstable. It is thought that this

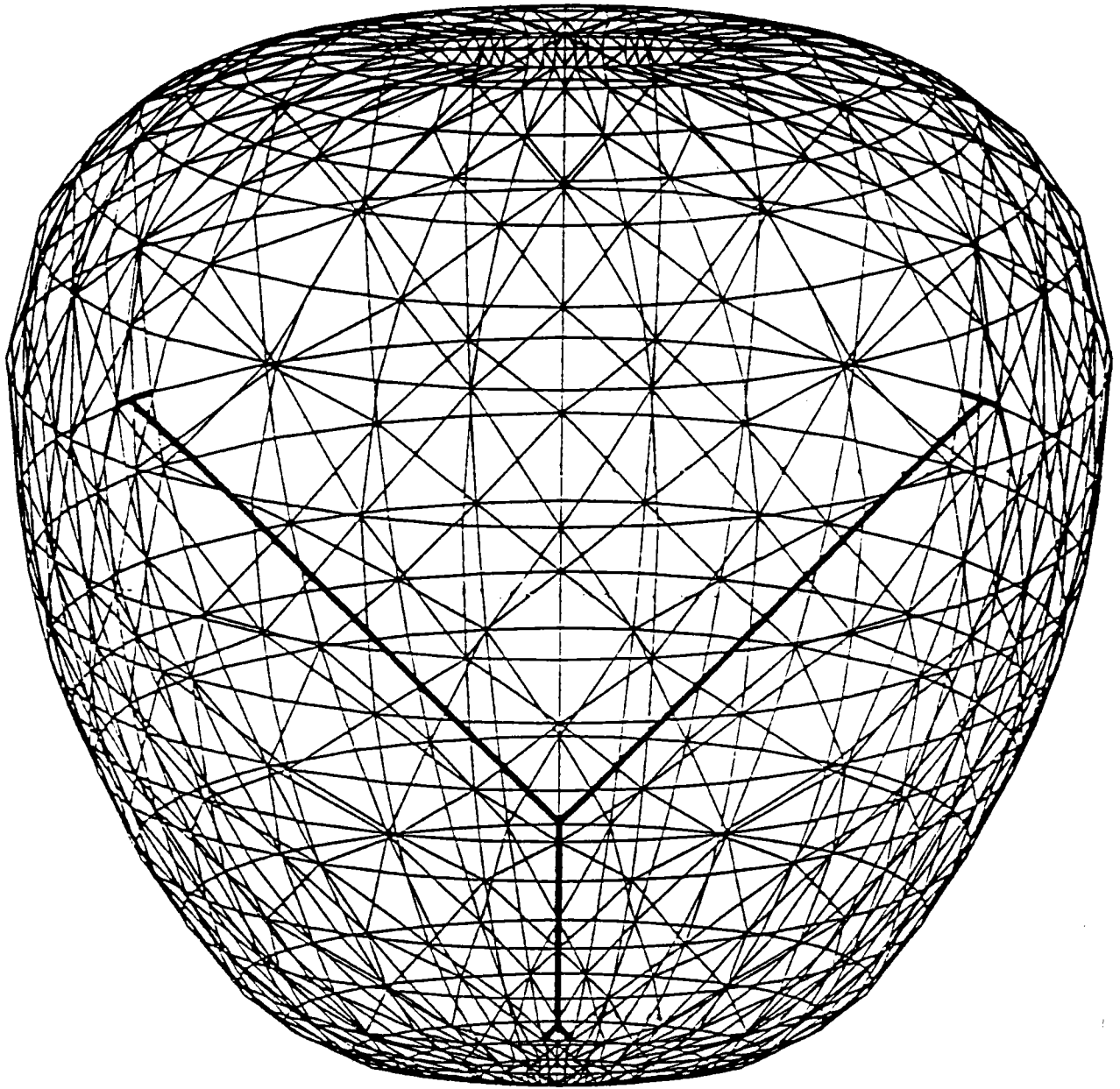


**Figure 76**  
The undeformed SCC finite element model as viewed along the  
x-axis

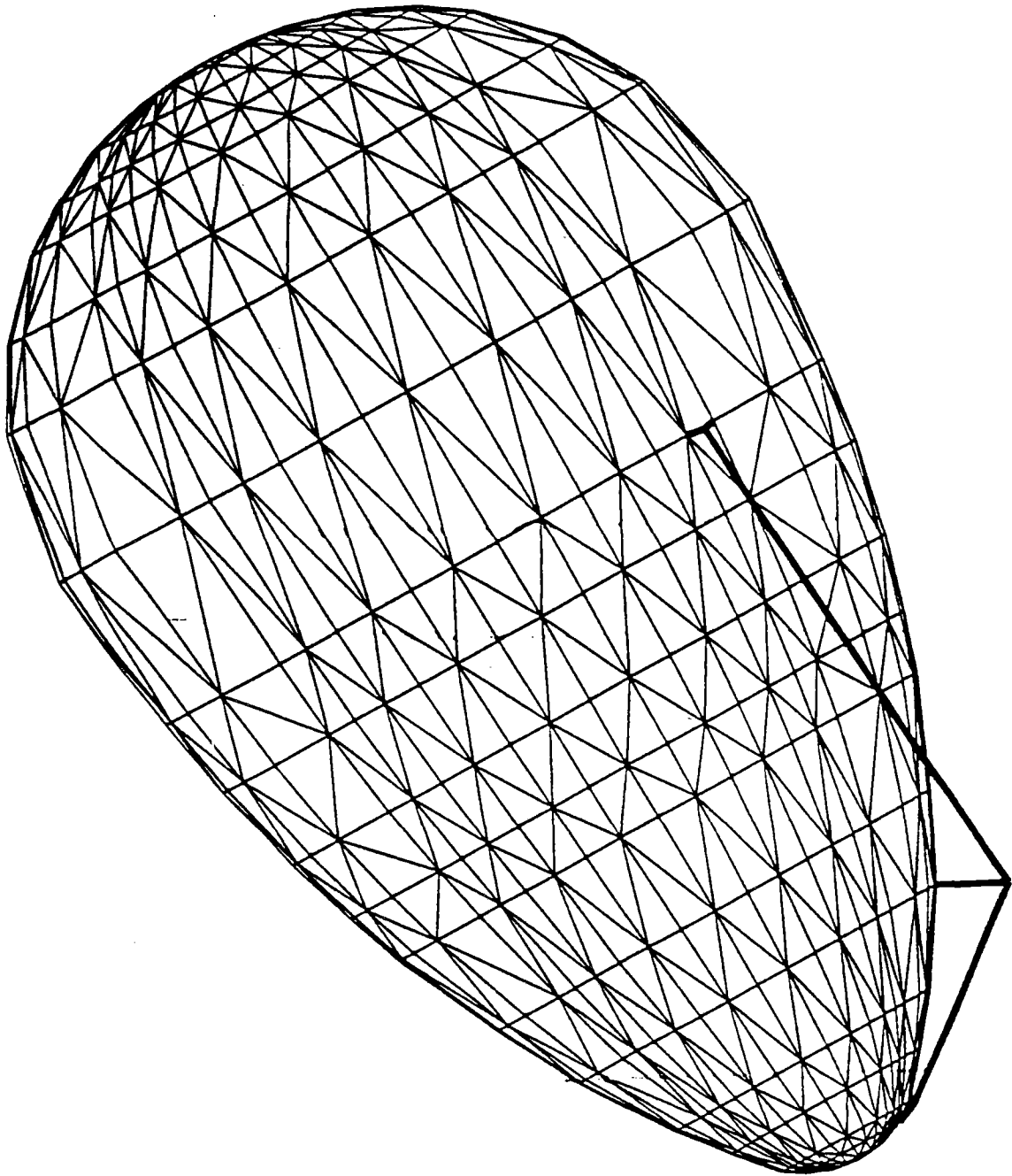


**Figure 77**  
The undeformed SCC finite element model as viewed along the  
y-axis

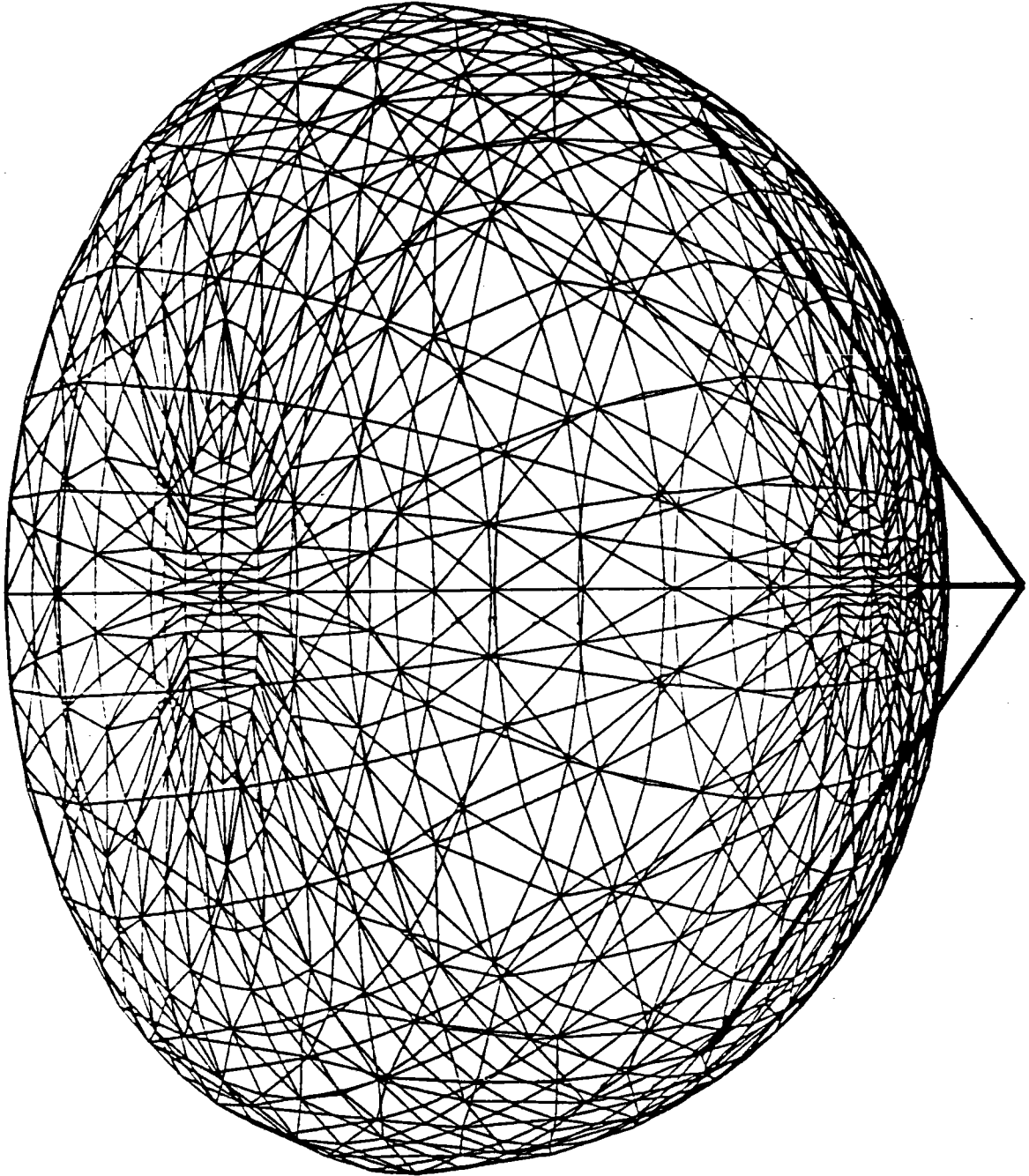


**Figure 78**  
**The undeformed SCC finite element model as viewed along the z-axis**

instability represents a real condition related to the current geometry that would physically manifest itself in wrinkling of some areas of the chamber. Future modification of the Single Chamber geometry may eliminate this problem, although no attempt was made to pursue these modifications on this program. As it turns out, the application of 0.0032 psi was more than adequate for the purpose that it was intended, namely to achieve 500 psi membrane stress in the chamber in order to eliminate wrinkles. Application of 0.0032 psi has resulted in average membrane stresses of 612 psi in the meridional direction and 582 psi in the "hoop" direction over the concentrator portion of the chamber surface.

Several iterative run cycles were made using the pressurized membrane loads with the initial undeformed geometry. This geometry is actually the final desired geometry, so this process of equilibration results in a pre-stressed membrane of the desired geometry. The undeformed geometry (membrane deflated) is not calculated.

Once the pressurization membrane loads were determined, struts representing the attachment of the chamber to the spacecraft were added to the model. The two long struts were 3.0 inches diameter tubes tapering to 1.4 inches at the far end from the spacecraft. The shorter strut going to the smaller end of the chamber tapers from 3.0 inches to 2.2 inches. All tubes used a 0.015 thick high-modulus graphite layup. The bare tube weights were doubled to account for fittings, thermal control, etc. The total model weight of 37.20 pounds included 27.74 pounds for the membrane. This weight essentially matches the final weight calculation in Section 3.2.6 if contingency and strut interface weights are eliminated. Table 3.2.7-3 shows the results of the dynamic eigenvalue analysis. Plots of the mode shapes are given in Figure 79 through 88.

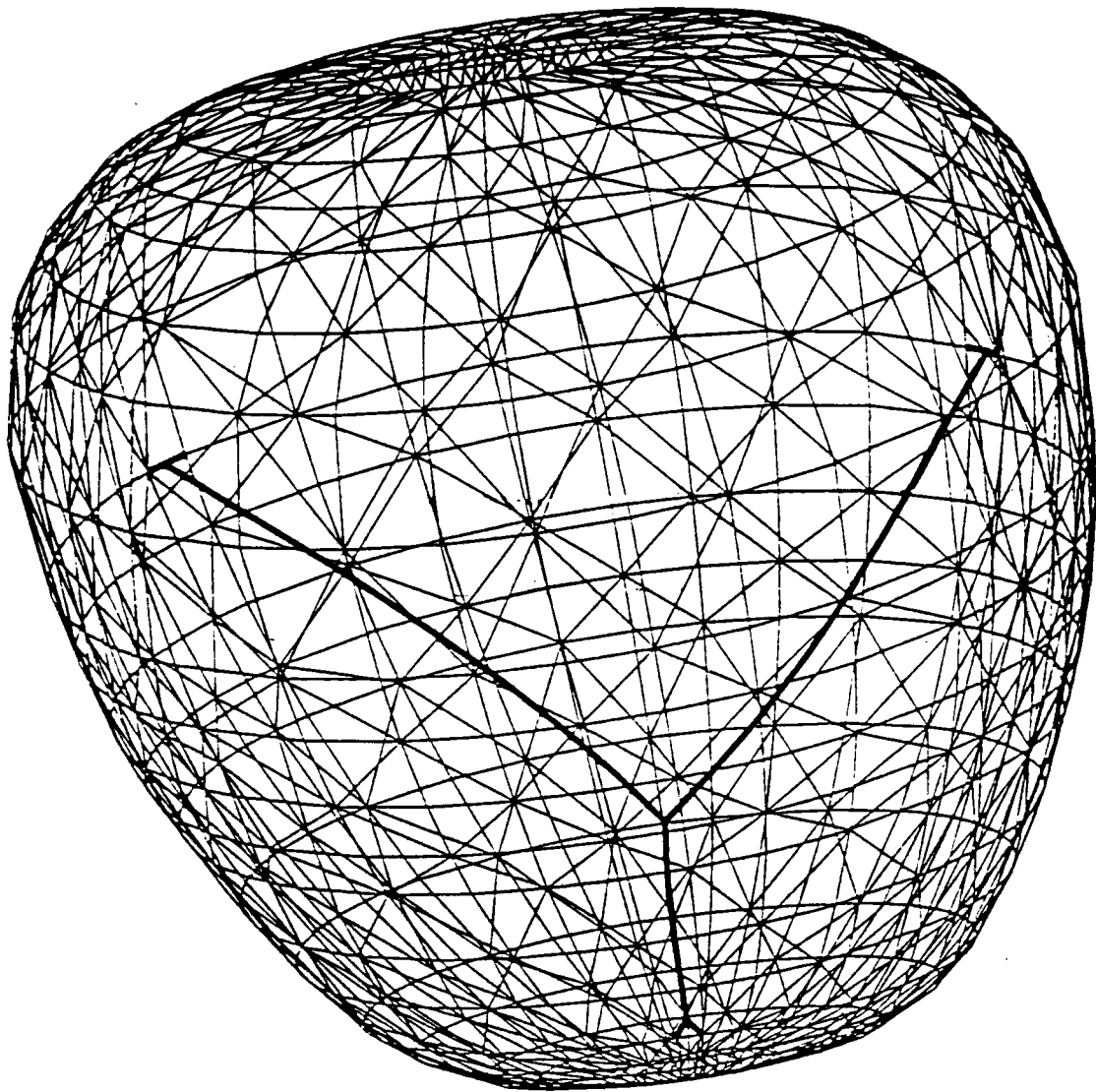


**Figure 79**  
**Mode shape 1 identified by the SCC finite element model.**  
**(Distortions greatly exaggerated for illustration)**

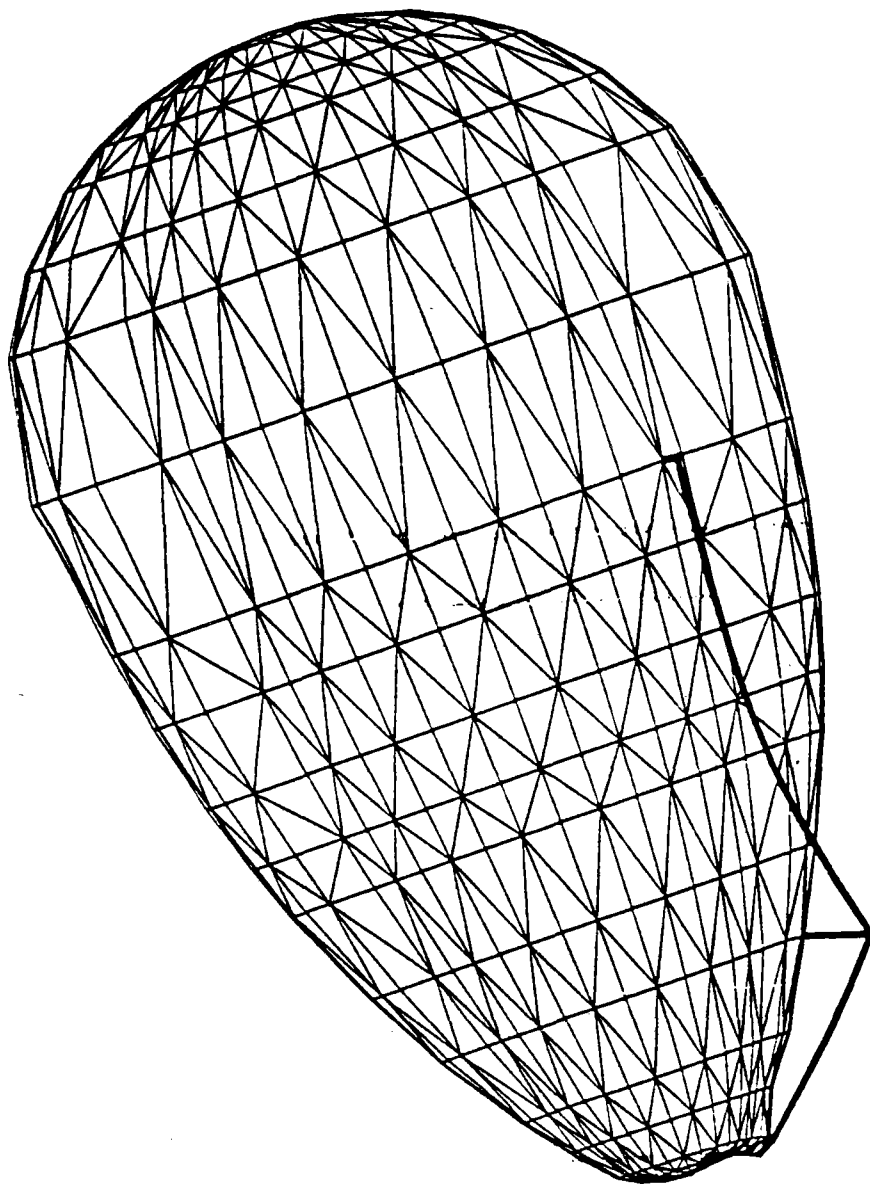


**Figure 80**  
**Mode shape 2 identified by the SCC finite element model.**  
**(Distortions greatly exaggerated for illustration)**

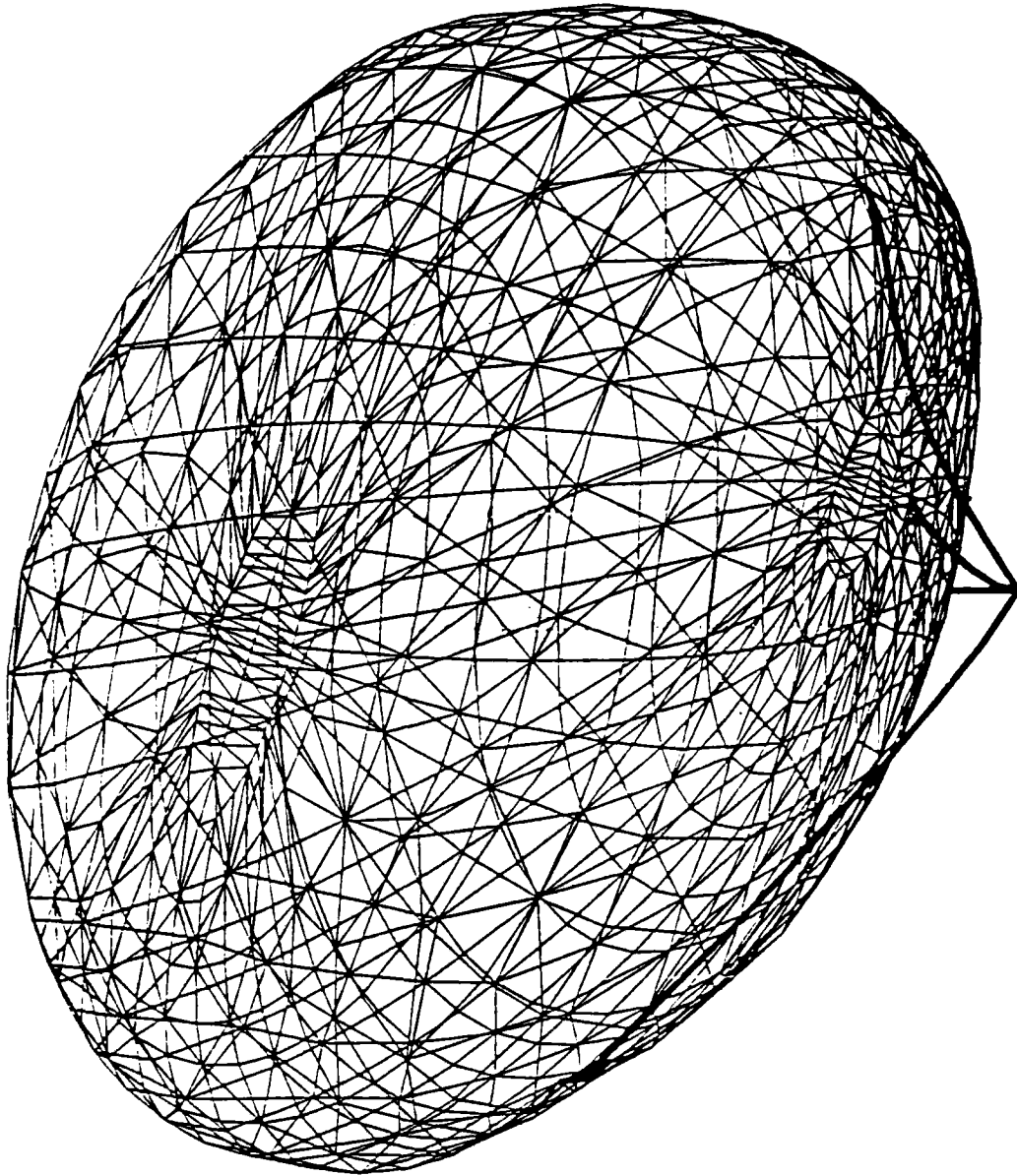


**Figure 81**  
**Mode shape 3 identified by the SCC finite element model.**  
**(Distortions greatly exaggerated for illustration)**

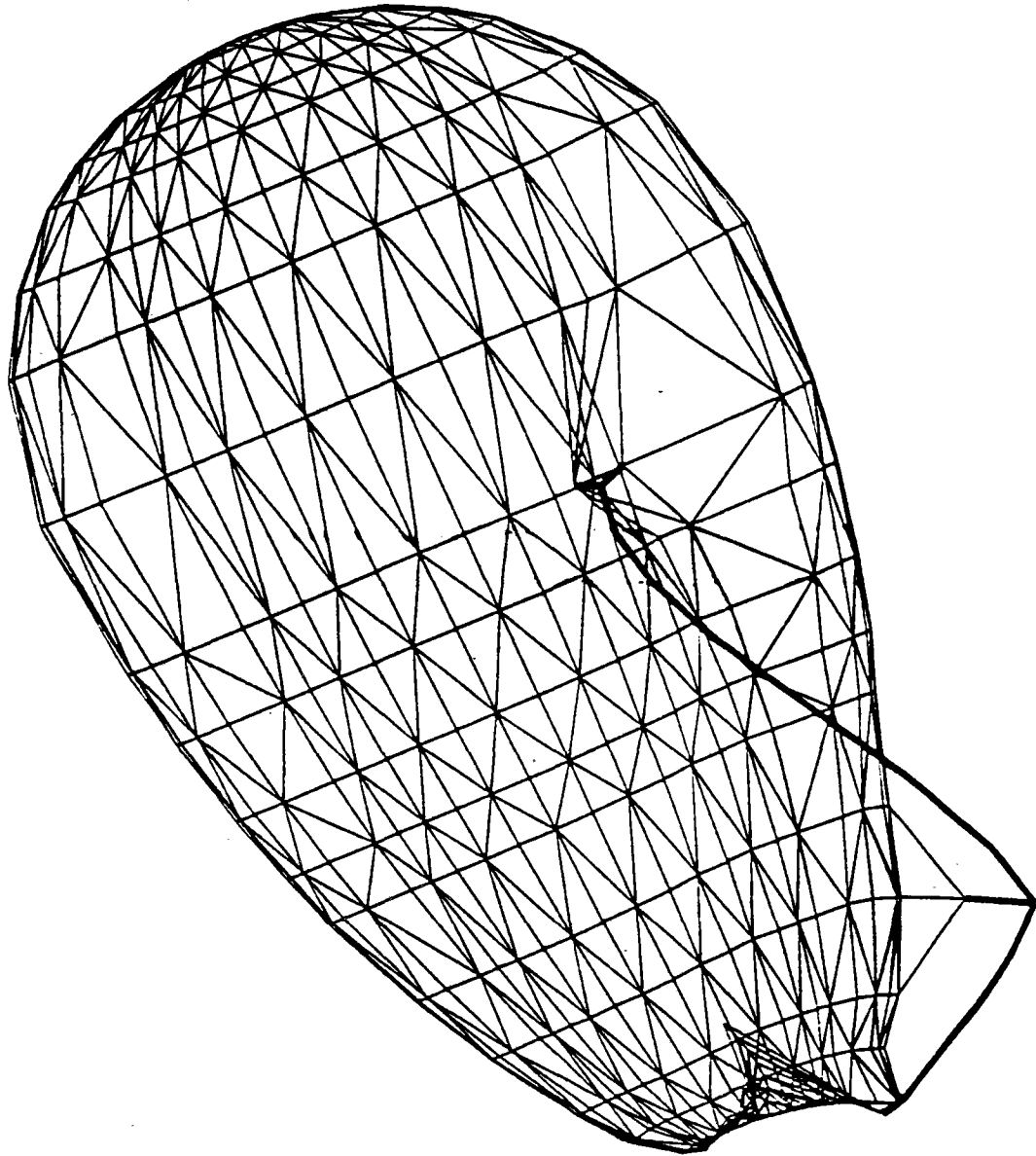


**Figure 82**  
**Mode shape 4 identified by the SCC finite element model.**  
**(Distortions greatly exaggerated for illustration)**

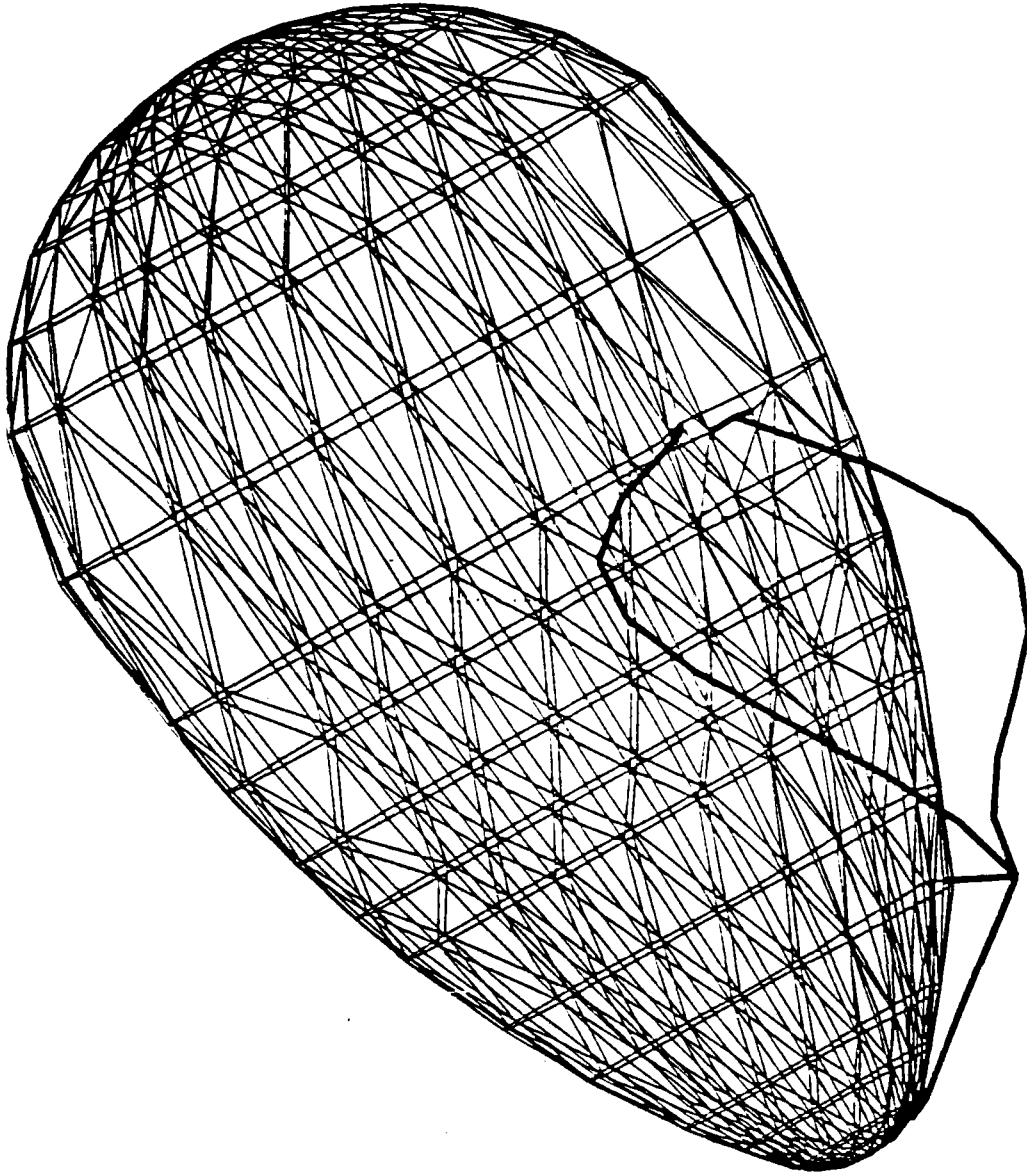


**Figure 83**  
**Mode shape 5 identified by the SCC finite element model.**  
**(Distortions greatly exaggerated for illustration)**

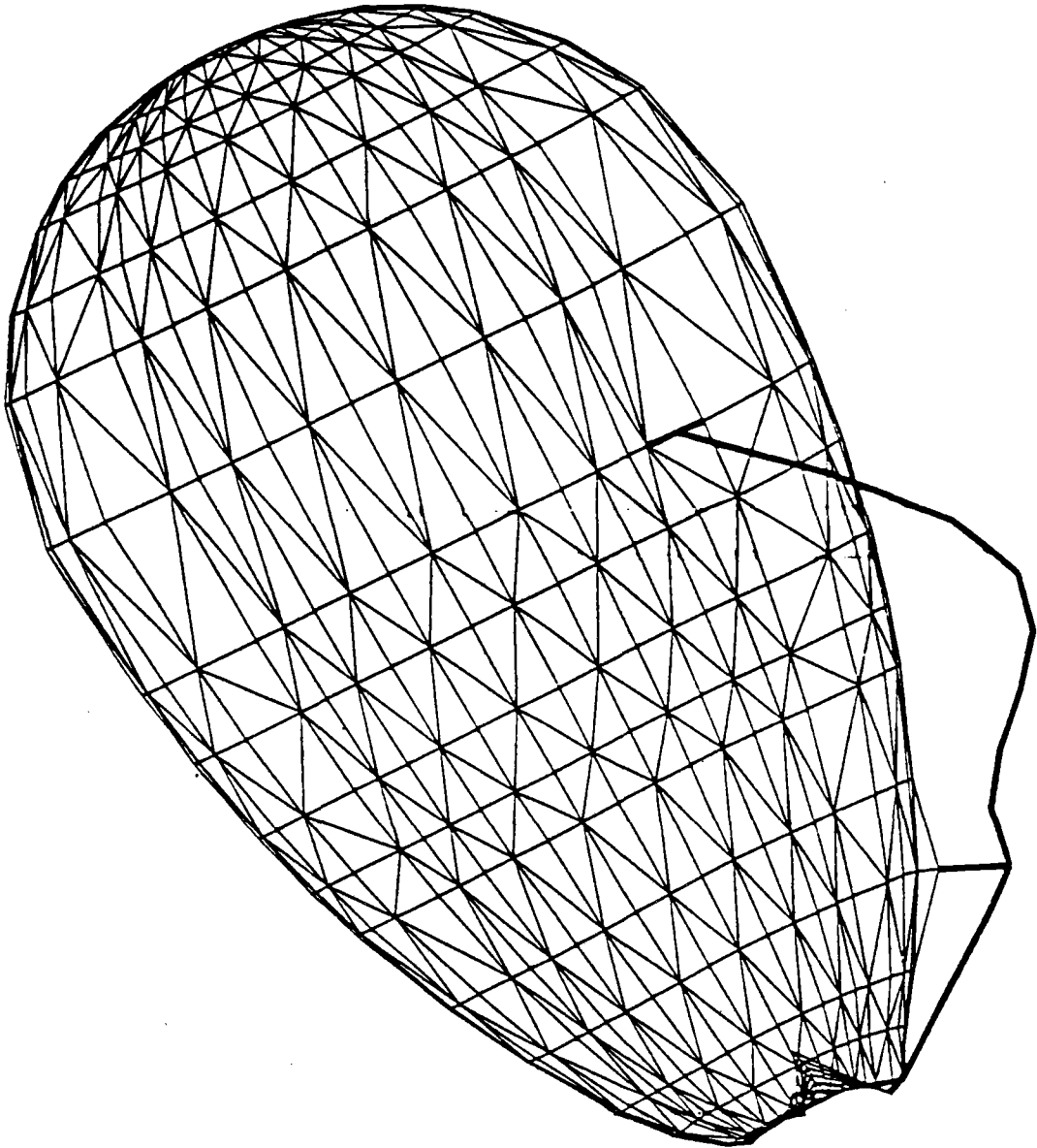


**Figure 84**  
**Mode shape 6 identified by the SCC finite element model.**  
**(Distortions greatly exaggerated for illustration)**

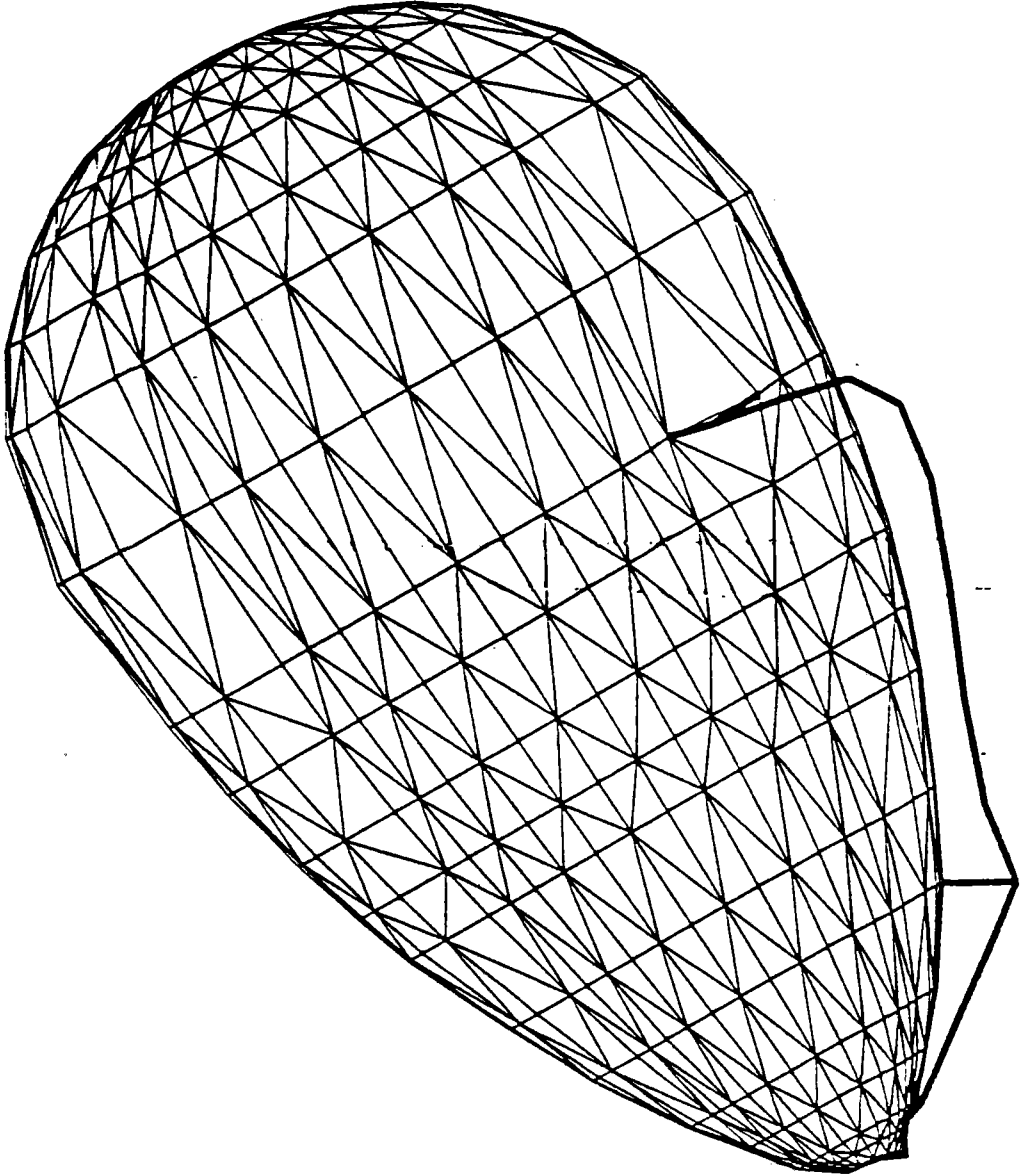


**Figure 85**  
**Mode shape 7 identified by the SCC finite element model.**  
**(Distortions greatly exaggerated for illustration)**

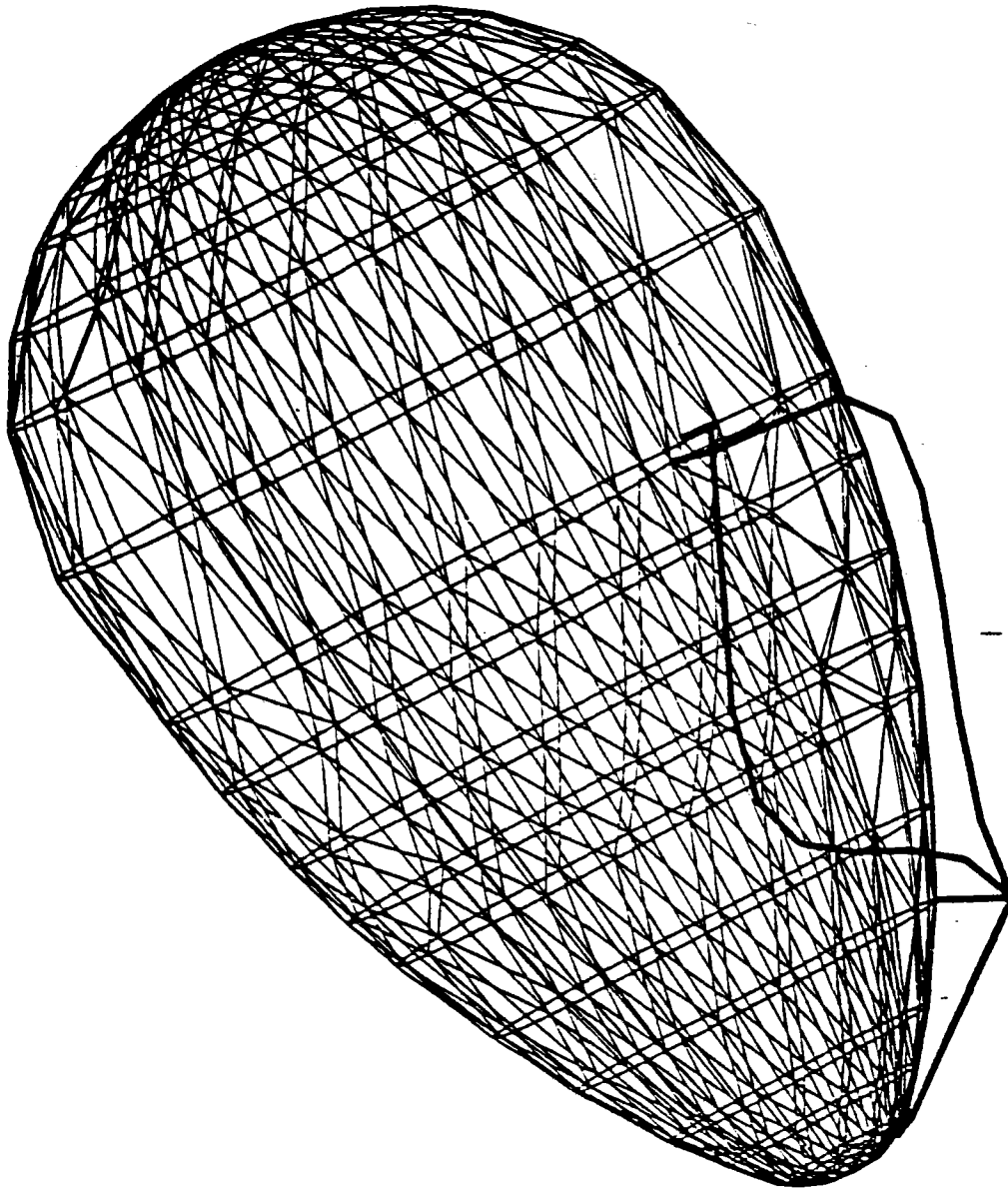


**Figure 86**  
**Mode shape 8 identified by the SCC finite element model.**  
**(Distortions greatly exaggerated for illustration)**

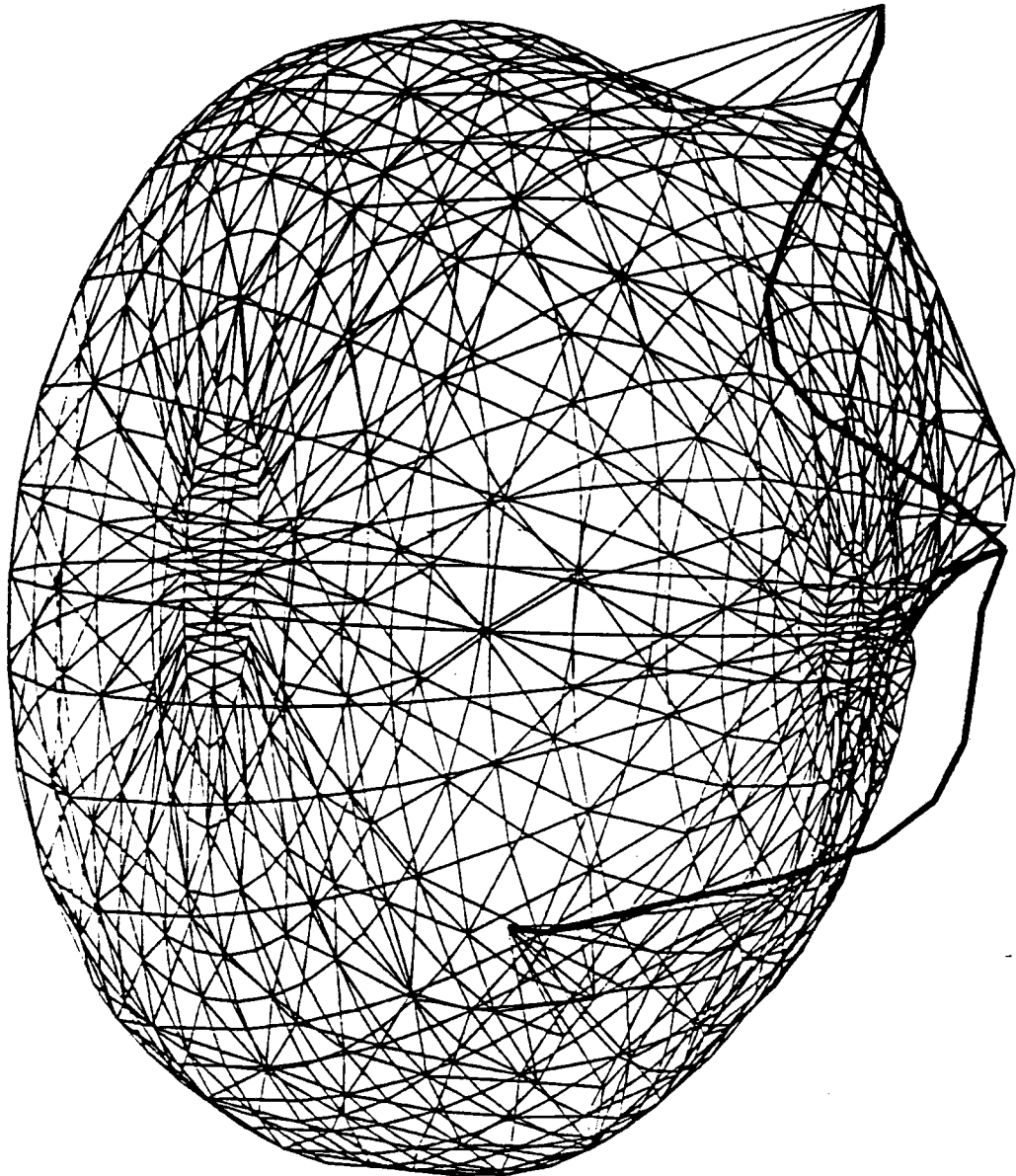


**Figure 87**  
**Mode shape 9 identified by the SCC finite element model.**  
**(Distortions greatly exaggerated for illustration)**

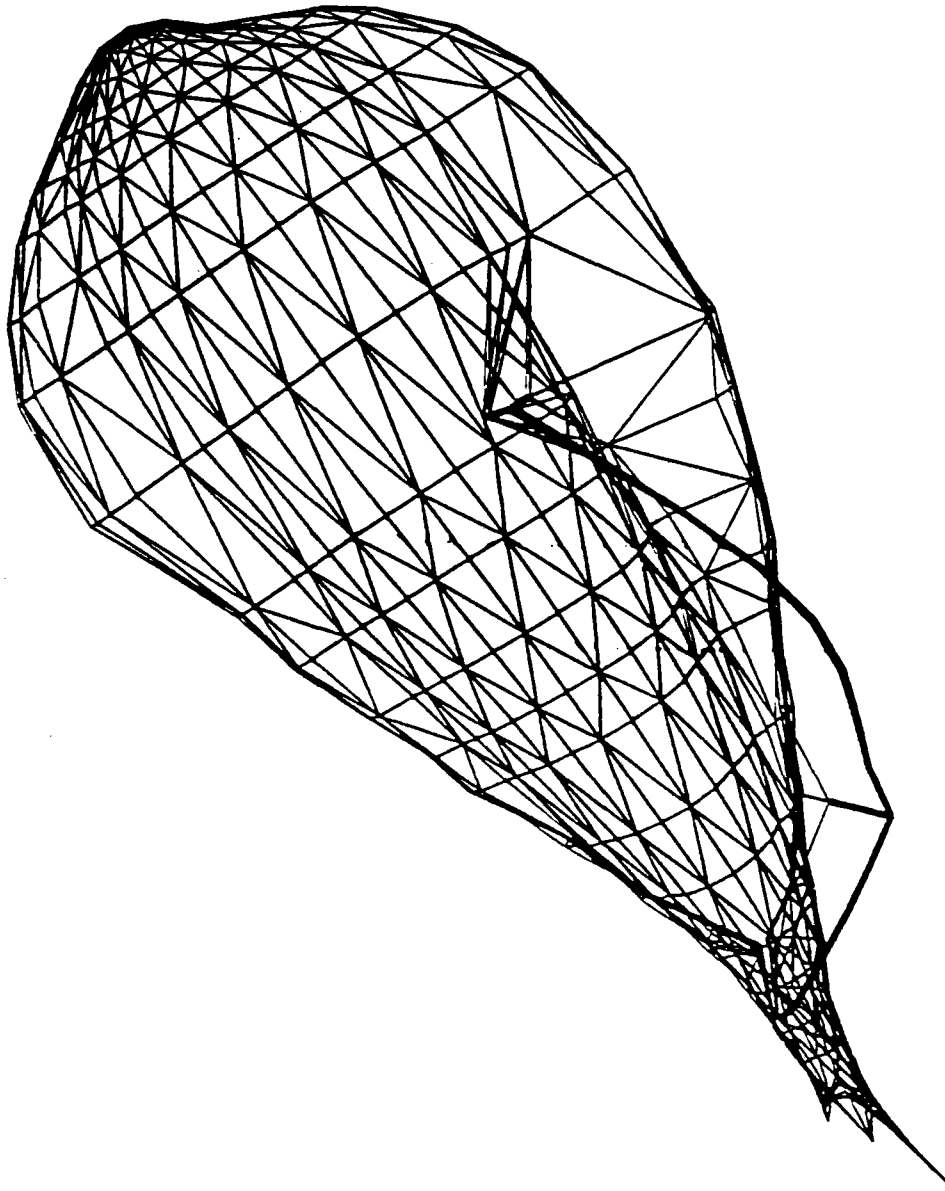


**Figure 88**  
**Mode shape 10 identified by the SCC finite element model.**  
**(Distortions greatly exaggerated for illustration)**

**Table 23. Single Chamber Concentrator (SCC) Pressurized Eigenvalues**

| 0.0032 PSI Pressure, strut-supported from Rigid I/F |             |                  |                                   |
|---|-------------|------------------|-----------------------------------|
| Mode  | Frequency   | Generalized Mass | Structural Mode Shape Description |
| 1   | 0.646 Hertz | .0326            | SCC rocking about X-axis          |
| 2   | 1.22 Hertz  | .0461            | SCC rocking about Y-axis          |
| 3   | 1.86 Hertz  | .0684            | SCC rocking about Z-axis          |
| 4   | 5.35 Hertz  | .0281            | Mast mode plus SCC X motion       |
| 5   | 7.50 Hertz  | .0101            | Mast bending mode                 |
| 6   | 8.22 Hertz  | .0126            | Mast bending mode                 |
| 7   | 8.91 Hertz  | .0129            | Mast bending mode                 |
| 8   | 9.10 Hertz  | .0133            | Mast bending mode                 |
| 9   | 13.8 Hertz  | .0106            | Mast mode plus SCC Z-rocking      |
| 10  | 14.6 Hertz  | .0144            | SCC breathing mode                |

The first three modes are the chamber rocking somewhat rigidly on the strut supports. Modes 4 through 9 are primarily strut bending modes with various small amounts of Single Chamber distortion, more so in modes 4 and 9. Mode 10 is the chamber breathing in its thinnest direction. The location of the first mode at 0.646 Hertz is promising since the initial requirement was  $>0.1$  Hertz.

To determine the influence of strut weight on the dynamic characteristics of the SCC/strut combination, the strut weights were set to zero and another dynamic eigenvalue analysis was performed. (This run, like the one summarized in Table 23, has 0.0032 psi internal pressure and has the struts fixed to a rigid spacecraft interface.) Table 24 summarizes the results of this run as compared to the baseline results. The table indicates that strut weight is not a large driver in the natural frequency of the system.

**Table 24. The sensitivity of the eigenvalues to strut weight is demonstrated in this table**

| 0.0032 PSI Pressure, Strut-Supported from Rigid I/F, Zero Strut Weight |             |                  |                                   | Table 1 Results [With Strut Wts.] |             |
|--|-------------|------------------|-----------------------------------|-----------------------------------|-------------|
| Mode   | Frequency   | Generalized Mass | Structural Mode Shape Description | Mode                              | Frequency   |
| 1  | 0.669 Hertz | .0326            | SCC X-axis rocking                | 1                                 | 0.646 Hertz |
| 2  | 1.26 Hertz  | .0461            | SCC Y-axis rocking                | 2                                 | 1.22 Hertz  |
| 3  | 1.96 Hertz  | .0684            | SCC Z-axis rocking                | 3                                 | 1.86 Hertz  |
| 4  | 6.06 Hertz  | .0281            | SCC Y motion                      | 4                                 | 5.35 Hertz  |
| 5  | 15.2 Hertz  | .0106            | SCC Z-axis rocking                | 9                                 | 13.8 Hertz  |
| 6  | 15.4 Hertz  | .0144            | SCC breathing mode                | 10                                | 14.6 Hertz  |

To determine the influence of strut stiffness on the dynamic characteristics of the SCC/strut combination, the struts were removed from the model, the chamber was rigidly held at the strut attachment points, and another dynamic eigenvalue analysis was performed. (This run, like the previous two, has 0.0032 psi internal pressure.) Table 25 summarizes the results of this run as compared to the baseline results. The results indicate that the natural frequencies are greatly influenced by strut stiffness. A reduction in strut stiffness from the current design is likely to reduce first mode frequency.

**Table 25. The sensitivity of the eigenvalues to the strut stiffness is demonstrated in this table**

| 0.0032 PSI Pressure, SCC supported from Rigid Points |            |                  |                                   | Table 1 Results [With Struts] |            |
|--|------------|------------------|-----------------------------------|-------------------------------|------------|
| Mode   | Frequency  | Generalized Mass | Structural Mode Shape Description | Mode                          | Frequency  |
| 1  | 4.99 Hertz | .0321            | SCC Z-axis rocking                | 3                             | 1.86 Hertz |
| 2  | 5.46 Hertz | .0316            | SCC Y-axis rocking                | 2                             | 1.22 Hertz |
| 3  | 9.79 Hertz | .0119            | SCC X-axis rocking                | 1                             | 0.646Hertz |
| 4  | 17.2 Hertz | .0164            | SCC Z-axis rocking                | 9                             | 13.8 Hertz |
| 5  | 17.9 Hertz | .0105            | SCC breathing                     | 10                            | 14.6 Hertz |

To determine the influence of SCC internal pressure on the dynamic characteristics of the SCC/strut combination, the membrane loads due to pressure were factored by various fixed amounts and additional dynamic eigenvalue analyses were performed. (These runs, like that for Table 23, have the SCC supported by the flexible struts.) Table 26 summarizes the results of these runs using 100%, 85%, and 50% of the baseline pressure of 0.0032 psi. The 85%

pressure brings the average membrane stress in the parabolic surface area to 520 psi in the meridional direction and 497 psi transverse to it. It should be noted that these reduced pressure runs still assume that the membrane is uniformly smooth and acts as an integral shell. Wrinkling of the surface may act to reduce the frequencies of the membrane significantly.

The results indicate that internal pressure and therefore membrane tension do not greatly affect the natural frequencies of the structure assuming the structure remains without wrinkles.

**Table 26. The effect of inflation pressure on the SCC pressurized eigenvalues is shown to be small in this table (Struts are supported from a rigid interface)**

| Mode | Frequency<br>[.0032 psi] | Frequency<br>[.0027 psi] | Frequency<br>[.0016<br>psi] | Structural Mode Shape<br>Description |
|------|--------------------------|--------------------------|-----------------------------|--------------------------------------|
| 1    | 0.646<br>Hertz           | 0.654<br>Hertz           | 0.668<br>Hertz              | SCC rocking about X-axis             |
| 2    | 1.22<br>Hertz            | 1.17<br>Hertz            | 1.05<br>Hertz               | SCC rocking about Y-axis             |
| 3    | 1.86<br>Hertz            | 1.78<br>Hertz            | 1.57<br>Hertz               | SCC rocking about Z-axis             |
| 4    | 5.35<br>Hertz            | 5.31<br>Hertz            | 5.21<br>Hertz               | Mast mode plus SCC X motion          |
| 5    | 7.50<br>Hertz            | 7.49<br>Hertz            | 7.47<br>Hertz               | Mast bending mode                    |
| 6    | 8.22<br>Hertz            | 8.21<br>Hertz            | 8.19<br>Hertz               | Mast bending mode                    |
| 7    | 8.91<br>Hertz            | 8.90<br>Hertz            | 8.86<br>Hertz               | Mast bending mode                    |
| 8    | 9.10<br>Hertz            | 9.09<br>Hertz            | 9.05<br>Hertz               | Mast bending mode                    |
| 9    | 13.8<br>Hertz            | 13.8<br>Hertz            | 13.5<br>Hertz               | Mast mode plus SCC Z-rocking         |
| 10   | 14.6<br>Hertz            | 14.5<br>Hertz            | 14.3<br>Hertz               | SCC breathing mode                   |

#### 4.0 Summary

Two support structures have been designed for use with inflatable concentrators for Solar Thermal Propulsion applications. The support structure for the conventional concentrator utilizes proven mechanical methods to deploy and support the concentrator. The Single Chamber Concentrator revolutionizes the concentrator system design and therefore a much different support structure is recommended. Components of each system were designed and analyzed and the most advantageous designs chosen for full system level weight and packaging design and performance analysis.

The support structure for the conventional concentrator design includes a torus (hoop) very similar to a hoop designed and built by Harris for NASA in the mid 80's. The LSST hoop includes 44 graphite epoxy tube segments with integral hinges at each segment end. The 9.8 meter diameter hoop deploys through a series of motors situated at the hinges. The LSST hoop design provides the highest reliability and the most mature design of the various hoop designs considered. A working model was fabricated under previous NASA funding.

The struts are 365.4 inches in length (long struts) and 148.8 inches in length (short strut). The struts are telescoping tubes with individual segments of length 27.96 inches. The struts deploy via a push-pull mechanism and latch at the fully deployed position. The latch design is a two piece radial retractable latch which provides reliable performance with minimal size and weight. The first natural frequency of the system is approximately 0.8 Hertz, well above the 0.4 Hertz requirement. Total weight of the system is 123.8 pounds as opposed to an 85.5 pound requirement. The hoop stows into a cylindrical shape and the struts and concentrator are stowed within this cylinder. The cylinder is 28 inches in height and 28 inches in diameter. The stowed package goal was a cylinder of 12.5 inches in height and 19 inches in diameter. Optical analysis shows that this concentrator design can utilize a relatively small aperture of 2.5 inches diameter at the focus. The dynamic disturbance of the thruster on-orbit has been shown to produce minimal changes to the concentrated energy.

This support structure meets the dynamic and structural requirements specified but does not meet the weight and stowed volume requirements necessary to utilize a GAS container. The weight and stowed volume of the structure are still exemplary considering the size of the deployed system. Dynamics simulation has shown the structure to be quite stiff. Further design trades could reduce weight and

stowed volume by reducing the structural stiffness until the dynamic environment begins to affect performance.

The development of the design proposed here is likely to be significantly lower in cost than development of an alternative design with lower weight and volume but less maturity (for instance inflatable torus concepts). Costs to procure launch services are low with a GAS, however it is not obvious that total program costs are minimized by using the GAS launch.

The Single Chamber Concentrator has the potential to eliminate a costly and sizable torus from the design. The Single Chamber design reduces weight to 40% and stowed volume to 20% of the conventional design and easily meets GAS weight requirements. However, significant development work on the Single Chamber Concentrator is still necessary. The development work is required in the areas of concentrator fabrication, concentrator optics (secondary concentrators) and performance simulations.

Future work in the concentrator and support structure area should focus on both fabrication issues and performance issues. Fabrication of the concentrator, either a conventional design or a single chamber design, is required to improve understanding of performance parameters such as slope error and shape error. Further work is required to perfect the concentrator fabrication process to minimize design uncertainties and bring recurring costs in line with expectations.

Performance of either system is highly dependent on the pointing and control system in use. An integrated performance analysis is necessary to define the specifications required of the various subsystems. The concentrator, support structure, pointing and control and attitude control subsystems must be modeled in a realistic scenario in order to quantify performance characteristics.

Concentrator technology shows promise for supplying energy to a thruster thus reducing cost and increasing payload size in orbit transfer applications. Further study and testing is necessary to ensure proper implementation of the technology.

## 5.0 References

1. Get Away Special (GAS) Small Self-Contained Payloads Experimenter Handbook, NASA, Goddard Space Flight Center, Greenbelt, Maryland, 1991.
2. Thompson, C. et al., Concentrator Flight Test Experiment, AL-TR-90-066, L'Garde, Inc., Tustin, California, 1991.
3. "Solar Concentrator Structure Development," Program Research and Development Announcement 91-03, Air Force STC, Kirtland AFB, New Mexico, November 14, 1990.
4. "Solar Concentrator Structure Development," Technical Proposal, Harris Corporation, Melbourne, Florida, January, 1991.
5. Gierow, P., Clayton, W., Kromis, D., Concentrator Technology, PL-TR-92-3030, SRS Technologies, Huntsville, Alabama, 1992.
6. Sullivan, M., LSST (Hoop/Column) Maypole Antenna Development Program, NASA Contractor Report 3558, Harris Corporation, Melbourne, Florida, June, 1982.
7. Veal, G., Highly Accurate Inflatable Reflectors, Phase II, AFRPL-TR-86-089, L'Garde, Inc., Tustin, California, 1987.
8. Grossman, G., "Tension Element for Reducing Loads and Deformation in Rim Support of Off-Axis Inflatable Reflectors," LTR-90-GG-007, January, 1990.